COMPUTER AIDED CHEMICAL SPECIATION IN DESIGNING METAL-BASED POTENTIAL ANTI-INFLAMMATORY AGENTS

A thesis submitted to the

UNIVERSITY OF CAPE TOWN

In fulfilment of the requirements for the degree of

DOCTOR OF PHILOSOPHY

by

SEBUSI ODISITSE
B.Sc.(UB) M.Sc.(UCT)

Department of Chemistry
University of Cape Town
Rondebosch 7701
Cape Town
South Africa

September 2006

DECLARATION

I hereby sincerely and solemnly declare that **COMPUTER AIDED CHEMICAL SPECIATION IN DESIGNING METAL-BASED ANTI-INFLAMMATORY AGENTS** is my own, unaided work, and that all sources I have used or quoted have been indicated and acknowledged by means of complete references. The thesis is submitted for the degree DOCTOR OF PHILOSOPHY, to the Department of Chemistry, Faculty of Science, at the University of Cape Town, has not been submitted before for any degree or examination at any other university.

signature removed

.....

S. Odisitse

September 2006

ACKNOWLEDGEMENTS

I would like to express my sincere gratitude and appreciations to the following;

- My supervisor, Professor Graham Ellis Jackson, for the guidance and support throughout the course of this study,
- My colleagues in the research group for their contributions,
- Members of staff and fellow students in the Department of Chemistry (UCT),
- Mr. Gerald Hesselink for the IT technical support,
- Drs. A. Hunter and R.A Hendrikse (Radiobiology Dept.) for providing space for animal experiments, J. Boniaszczuk (Nuclear Medicine Dept.), J. Visser (Animal Unit), colleagues, Dr. J.N. Zvimba and C. Jackson for their technical assistance in the animal experiments,
- Dr. J.R. Zeevart and D. Jansen of the South African Nuclear Energy Corporation (Ltd.) at Pretoria for preparing and supplying us with $^{64}CuCl_2$,
- The National Research Foundation (NRF), the Council of the University of Cape Town and Canon Collins Trust for financial support,
- My wife, Monica, family and friends for their continued support and encouragements.

CONFERENCE PROCEEDINGS

Parts of this thesis have been presented at the following conferences;

Chemical Speciation in Designing Anti-inflammatory Agents., S. Odisitse and G.E. Jackson; August 2006, 37th International Conference on Coordination Chemistry, Cape Town, South Africa.

Computer Aided Chemical Speciation in Designing Anti-inflammatory Agents., S. Odisitse and G.E. Jackson; April 2005, South African Chemical Institute Conference on Inorganic Chemistry, Pietermaritzburg, South Africa.

Thermodynamic Properties of PCUA ligand as Anti-inflammatory Agent., S. Odisitse and G.E. Jackson; July 2004, 37th National Convention of the South African Chemical Institute, Pretoria, South Africa.

ABSTRACT

The objective of this study was to develop copper based anti-inflammatory agents for the treatment of inflammation associated with Rheumatoid Arthritis.

Four low molecular ligands, N,N'-di(aminoethylene)-2,6-pyridine dicarbonylamine (PrDH), Bis-(N,N-dimethylethyl)-2,6-pyridinedicarboxamide (PrDM), N,N'-bis[2(2-pyridyl)-methyl]pyridine-2,6-dicarboxamide (PrDPr) and 3,5-bis[(aminoethyl)ethanediamide]-4-oxahexacyclo-dodecane (PCUA) were designed and synthesised. The formation constants of these ligands with H^{+}, Cu^{2+}, Ni^{2+}, Zn^{2+} and Ca^{2+} were determined potentiometrically at 25°C and 0.15 mol dm^{-3} $Na^{+}Cl^{-}$. The Cu(II) formed relatively more stable complexes than other three metal ions.

The structures of the different Cu(II) species formed with these ligands were investigated using nuclear magnetic resonance(NMR), infrared (IR) spectroscopy, ultraviolet-visible (UV-visible) spectroscopy as well as molecular mechanics calculations. For the NMR spectroscopy, results showed that the central pyridyl nitrogen and amide nitrogen(s) as well as the terminal amino/pyridyl groups coordinate to the Cu(II) ion in solution. The IR results indicated that an amide nitrogen is coordinated to the Cu(II). The UV-visible study gave the smooth deconvoluted spectra of the individual species for the Cu(II)-PrDH, Cu(II)-PrDM and Cu(II)-PrDPr systems in support of the potentiometric results. The three studied ligands form tetragonally distorted octahedral MLH_{-1} and MLH_{-2} species with Cu(II). The molecular mechanics was used to calculate the internal strain energies of the different possible geometries of related complex species. A comparison of these energies was used to rationalize the different stabilities of these structures.

The speciation modelling of Cu(II) using a computer model of blood plasma indicated that the *in vivo* Zn(II) and Ca(II) are good competitors of Cu(II) for PrDH, PrDM and PCUA whereas PrDPr is relatively selective for Cu(II). The IC_{50} values recorded for the Cu(II) complexes suggest that they are poor mimics of the Cu-Zn-SOD enzyme. The study also considered the determination of the octanol-water partition coefficients ($logP_{oct/aq}$) as a measure of hydrophobicity. It was observed that the ligand system with bulky groups as well as these forming neutral complex species had an enhanced extraction into the organic phase.

The *in vivo* verification of the modelling results was carried out by performing bio-distribution and dermal absorption studies on mice using radioactive $^{64}Cu(II)$ as a tracer. The biodistribution results showed that the [^{64}Cu]Cu(II)-PrDH, [^{64}Cu]Cu(II)-PrDM, [^{64}Cu]Cu(II)-PCUA and [^{64}Cu]Cu(II)-PrDPr complexes had improved absorption and retention over 24 hours in the body. The dermal absorption results also showed that at least 3 %dose of the applied dose on the enclosed skin was absorbed over a period of 24 hours.

Overall, these results are encouraging and merit further evaluation for the possible use of these Cu(II) complexes in chemotherapy and diagnosis.

LIST OF SYMBOLS

δ	-NMR chemical shift (ppm)
d	-doublet
t	-triplet
m	-multiplet
Hz	-hertz
$Log\beta_{pqr}$	-logarithm of the overall stability constant
δ_{pqr}	-denotes standard deviation in $log\beta_{pqr}$ for species pqr
T_H	-total proton concentration (mol dm^{-3})
T_H*	-calculated total proton concentration (mol dm^{-3})
T_L	-total ligand concentration (mol dm^{-3})
T_M	-total metal concentration (mol dm^{-3})
[L]	-free ligand concentration (mol dm^{-3})
pH	-(-Log H^+) -a measure of acidity or alkalinity
K_W	-dissociation constant of water
E_{cell}	-electrode potential (volts)
E^o	-electrode response intercept (volts)
R	-universal gas constant (J $K^{-1}mol^{-1}$)
T	-absolute temperature (Kelvin)
F	-Faraday constant
$[H^+]$	-hydrogen ion activity
s	-electrode response slope
G^o	-Gibbs free energy
H^o	-enthalpy change energy
a_i	-activity
c_i	-concentration of i^{th} ionic species
γ_i	-activity coefficient
z_i	-charge of i^{th} ionic species
U_{obj}	-objective function
N	-total number of experimental points

LIST OF ABBREVIATIONS

PrDH	-N,N'-di(aminoethylene)-2,6-pyridine-dicarbonylamine
PrDM	-Bis-(N,N-dimethylethyl)-2,6-pyridinedicarboxamide
PrDPr	-N,N'-bis[2(2-pyridyl)-methyl]pyridine-2,6-dicarboxamide
PCUA	-3,5-bis[(aminoethyl)ethanediamide]-4-oxahexacyclo-dodecane
TTDA	-3,6,9,12-tetra-azatetradecanedioic acid
DTDA	-3,6,9-triazaundecanedioic acid
5UM	-N,N'-*bis* [2(dimethylamino)ethyl]ethanediamide
5UH	-N,N'-bis[aminoethyl] ethanediamne
6UM	-N,N'-*bis* [2(dimethylamino) ethyl]propanediamide
BID	-1,13-*bis*(N,N-dimethyl)-5,9-dioxo-7-N-benzyl-1,4,7,10,13 -pentaazatridecane
DME	-1,13-*bis*(N,N-dimethyl)-5,9-dioxo-7-phenethyl-1,4,7,10,13-pentaazatri decane
EDA	-1,4,7,10,13-pentaaza-5,9-dioxo-7-N-phenethyltridecane
ZDA	-1,13-*bis* (N,N-dimethyl)-5,9-dioxo-1,4,7,10,13-penta-azatridecane
PrAO	-3,3,9,9-tetramethyl-4,8-diazatridecane-2,10-dione dioxime
H_2PAP	-N,N'-*bis* (2-hydroxyiminopropionyl)propane-1,3-diamine
BIDPAP	-(1,15)-*bis*(N,N-dimethyl)-5,11-dioxo-8-(N-benzyl)-1,4,8,12,15-pentaazapentadecane
L^{3a}	-2,6-dioxo-1,4,7,10,13,-pentaazacyclopentadencane
L^{3b}	-2,6-dioxo-1,4,7,10,14,-pentaazacyclopentadencane
L^{3h}	-2,6-bis(1-propanecarboxamido-3-amino)pyridine
EDTA	-ethylenediamine tetraacetic acid
RA	-Rheumatoid Arthritis
NSAIDs	-non-steroidal anti-inflammatory drugs
DMARDs	-disease modifying anti-rheumatic drugs
l.m.w	-low molecular weight

n_p	-number of parameters being optimised
n_e	-the total number of electrodes
w_{nq}	-the weight of the q^{th} residual at the n^{th} point
y_{nq}	-electrode emf of q^{th} residual at n^{th} point
R^H	-Hamiltonian R-factor
$R_{lim}{}^H$	-Hamiltonian R limit
Δ_o or 10Dq	-ligand field splitting
g	-gerade
u	-ungerade
I_o	-intensity of incident radiation
I	-intensity of transmitted radiation
ε	-the molar absorption coefficient
λ_{max}	-frequency of maximum absorption
U_{total}	-total strain energy
$\sum E_b$	-total bond deformation energy
$\sum E_\theta$	-total valence angle deformation energy
$\sum E_\phi$	-total torsional (or dihedral) deformation energy
$\sum E_{nb}$	-total non-bonded (van der Waals) interaction energy
K_b	-force constant or spring strength
r_0	-ideal bond length
K_θ	-strength of the spring holding the angle at its ideal value θ_0
K_ϕ	-height of the barrier to rotation about the torsion angle ϕ_{ijkl}
m	-periodicity
ϕ_{offset}	-offset of the minimum energy from a staggered arrangement.
IC_{50}	-concentration of drug required to reduce diformazan formation by 50%
mCi	-millicurie
MeV	-milli electron volt

ECCLES	-Evaluation of Constituent Concentrations in Large Equilibrium Systems
p.m.i	-plasma mobilization index
ESTA	-Equilibrium Simulation for Titration Analysis
OBJE	-task to calculate objective function
ZBAR	-task to calculate the complex formation function
Z-bar	-complex formation function
Q-bar	-deprotonation function
SPEC	-task to calculate the speciation as a function of pH
BETA	-task for initial estimates of formation constants values
KHP	-potassium hydrogen phthalate
TMS	-tetramethylsilane
NMR	-nuclear magnetic resonance
IR	-infrared
UV	-ultraviolet
MM	-molecular mechanics
SOD	-superoxide dismutase
NBT	-nitroblue tetrazolium
$\log P_{oct/aq}$	-logarithm of partition coefficient determined in an octanol-water mixture

CONTENTS

CHAPTER 3: GLASS ELECTRODE POTENTIOMETRY

CHAPTER 4: SPECTROSCOPY AND MOLECULAR MODELLING

CHAPTER ONE

INTRODUCTION

1. INTRODUCTION

1.1 RHEUMATOID ARTHRITIS

Rheumatoid Arthrtis (RA) is a chronic, debilitating disease for which there is no cure.[1,2] It is characterized by joint pain and swelling, joint destruction and pannus formation.[2,3] RA remains a medical challenge because it affects about one percent of the general population[4] and so far the exact cause of the disease is still not known. However, it is known that RA is an autoimmune disease.[2] The body's natural immune system does not operate as it should resulting in the immune system attacking healthy joint tissue and causing inflammation and subsequent joint damage.

RA is properly considered a disease of the joint. However, the inflammation response is a normal and essential response of the body to a harmful stimulus and may vary from a localized reaction in an affected tissue or joint to a more generalized whole-body reaction.[5] At the early stages of inflammation in RA perivascular aggregates of lymphocytes in the synovium are seen along with increased thickness of the synovial lining layer.[3] Chronic inflammation results in the destruction of normal connective tissue due to the activities of catalytic enzymes and cytokines. This destruction is due to activation of immune response, the release of hydrolytic enzymes, for example; collagenases, proteases, gelatinases, matrilysin, and the subsequent degradation of collagen and other extra-cellular components found in the body joints and connective tissues.[5] The situation of a joint affected by RA is well represented in Figure 1.2 and can be compared to that of a normal healthy joint in Figure 1.1.[36]

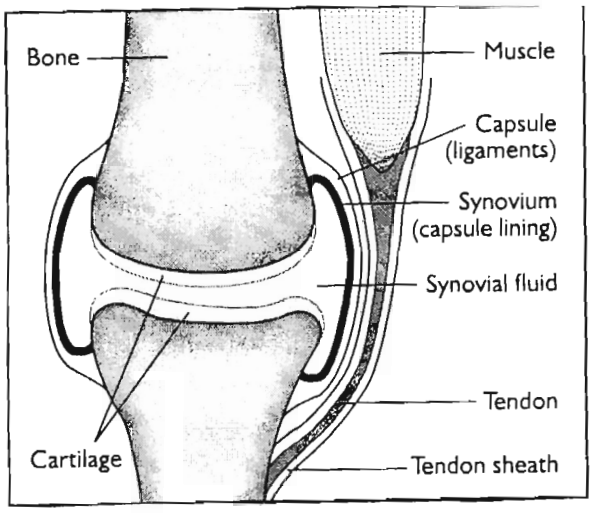

Figure 1.1: Schematic representation of a normal healthy joint

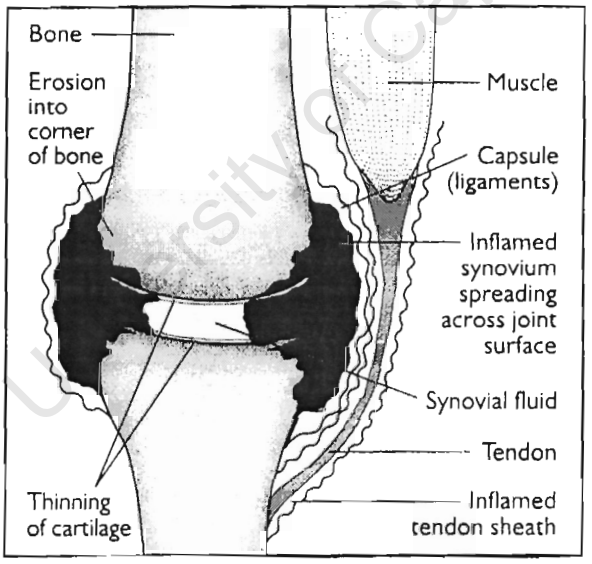

Figure 1.2: Schematic representation of a joint affected by Rheumatoid Arthritis

Further more, it is important to recognise that RA can exhibit a variety of extra-articular manifestations. These manifestations clearly show that RA has features of systemic disease capable of involving a variety of major organ systems such as lungs, blood vessels, heart, or eyes.[6] Histological studies

show that within rheumatoid synovium, there is hyperplasia of synovial lining cells and development of an extensive network of new blood vessels.[4]

Despite many decades of investigation, the etiology of RA remains unknown and its specific pathogenic mechanism is poorly understood.[3,4] However, the diagnosis is based on the clinical manifestations or findings. The symptoms associated with the disease can be alleviated by the use of anti-inflammatory drugs.

1.2 THERAPY FOR RHEUMATOID ARTHRITIS

The uses of drug therapy for RA are the relief of pain, the inhibition of inflammation and the restoration of normal immune mechanisms.[7] Highly effective drug treatments exist but early treatment is critical for relief of pain, reducing inflammation, stopping or slowing joint damage, and improving patient function and wellbeing. Ideally, a treatment should be efficacious, free of side effects, affordable and acceptable to the patient. Medication used in the treatment of RA can be divided into three categories; non-steroidal anti-inflammatory drugs (NSAIDs), glucocoticoids and disease modifying anti-rheumatic drugs (DMARDs).

1.2.1 Non-steroidal anti-inflammatory drug

NSAIDs help reduce joint pain, stiffness and swelling in RA but do not modify progression of the disease.[3] Traditional examples of NSAIDs are Ibuprofen and Diclofenac sodium. These drugs including salicylates such as aspirin possess analgesic, antipyretic and anti-inflammatory properties. Although NSAIDs are effective fighters of both pain and inflammation, renal insufficiency and failure, gastrointestinal ulceration, bleeding or perforation, exacerbation of hypertension and congestive heart failure have become important complications of chronic RA therapy with NSAIDs.[5,9]

Because ulcers are potentially dangerous side effect of NSAIDs use, a new option of NSAIDs was recently brought to the market. These are called cyclooxygenase-2 (COX-2) inhibitors and are thought to function by inhibition of cyclooxygenase pathway of prostaglandin (PG) synthesis.[8] A variety of free radicals derived from molecular oxygen, including superoxide, hydroxyl, and perhydroxyl radicals, are involved in the biosynthesis of prostaglandins and can provoke cell injury. The NSAIDs may act as free radical scavengers (antioxidants) in addition to inhibiting the formation of free radicals in the arachidonic acid pathway.[8,10] By impairing the activity of various mediators of inflammation such as bradykinins, prostaglandins and oxygen radicals, NSAIDs partially impair the final expression of inflammation. If patients with RA do not have a spontaneous remission with reasonable period of time, a slow-acting anti-rheumatic drug should be added to the continuing maximal NSAIDs therapy.[10]

1.2.2 Disease modifying anti-rheumatic drugs

DMARDs apparently affect the rheumatoid disease process and the mechanism of action for this group of drugs is diverse. Included in this broad group are methotrexate, leflunomide, D-penicillamine, sulfasalazine, gold therapy, minocycline, azathioprine, hydroychloroquine (and other anti-malarials) and cyclosporine. Although DMARDs actually stop disease progression before it causes irreparable joint damage, instant results should not be expected hence they are also called slow-acting anti-rheumatic drugs (SAARDs).[3,4,6-11] The DMARDs differ from NSAIDs in their delayed onset of action and lack of analgesia. They appear to act more proximally on the inflammation process, perhaps on the immunologic initiators of tissue injury but without actually removing the basic cause of the disease.[10]

Gold compounds are used most commonly for the treatment of RA although they have been used in the therapy of other inflammatory diseases as well. A potential mechanism of action of gold compounds in the treatment of erosive synovitis is their inhibition of enzymes such as elastase, collagenase and

hyaluronidase which are capable of degrading connective tissue components.[8] Another effect of gold compounds is that they may protect against oxygen-derived free radicals. Rash and mucous membrane ulcers are among the most common side effects in patients treated with gold compounds.

Among the anti-malarials, hydroxychloroquine has been suggested to be as effective as gold, D-penicillamine and azathioprine. It is said to be probably the least toxic DMARD.[10] Chloroquine has been shown to decrease antigen processing and presentation by both macrophages and lymphoid dendritic cells.[8,10]

A widely used, effective DMARDs which was specifically developed for RA is leflunomide (Arava). It is a novel DMARD that inhibits pyrimidine synthesis and is approved for treatment of active RA. In addition, leflunomide has been shown to slow radiographic progression of RA. It can be used in combination with metrotrexate or in place of it.[12]

1.2.3 Glucocoticoids

Glucocoticoids are sometimes referred to as corticosteroids or simply steroids. Therapeutic administration of these drugs produces rapid, potent and reliable suppression of inflammation. They have short-term effects on inflammation. The dramatic effects of cortisone and adrenocorticotropic hormone (ACTH) on the signs and symptoms of active RA were first reported by Hench and his associates in 1949.[4] For many symptomatic rheumatic diseases, these drugs simply work very well but have too many side effects. The most feared complication in patients with RA have been the effects of steroids on the bone and gastrointestinal tract.[10,12,13]

It should be mentioned that the presently available NSAIDs, DMARDs and glucocorticoids are rather unsatisfactory, being poorly effective and having dangerous side effects. Therefore, the search for less expensive, more

effective and safer therapies for inflammatory diseases remains a major medical challenge.

1.3 THE INVOLVEMENT OF COPPER

Metal ions play a vital role in a vast number of widely differing biological processes. These processes are quite specific in their metal ion requirements such that certain metal ions in specific oxidation states fulfil the necessary catalytic or structural requirements.[14] The interrelationships between metal ions and binding substances in the body are so complex that disorders or disease involving the metal binding substances may result in the presence of high or low concentrations of metal ions compared with that normally present. A number of major diseases are associated with changes in concentration of the trace metal ions in certain tissues and body fluids. The role of metal ions in medicine can be considered for the following; a). metal poisoning, where excess metal is ingested, b). abnormalities resulting from breakdown of the body's own control system or failure of the metal ion control system and c). the diagnostic or therapeutic use of metal ions in the body.

Of the metals that have been examined, copper appears to be most valuable pointer to disease conditions. For infectious hepatitis, serum copper levels rise up to three times normal value due to an accumulation of ceruloplasmin. Other diseases associated with high copper concentrations in the blood are leukaemia, lymphomas, rheumatoid arthritis, psoriasis, cirrhosis, rephritis and Hodgkins's disease.[14-18]

Biologically active oxidation states of copper are I, II and III, and these oxidation states are found in copper complexes that act to transport copper to body sites where it is required. The richest dietary sources of copper are animal liver, crustacean, shell fish, dried fruits, nuts and chocolate.[19] Dietary copper is readily absorbed in the stomach and small intestine, from where it is

transported to the liver by the blood as a serum albumin complex. It is in the liver that copper is processed and stored as metallothionin complex or converted into ceruloplasmin which is released into the blood to meet normal metabolic needs.[20-22]

Tissue requirements for copper are believed to be met and controlled in a homeostatic fashion based on the absorption, storage, utilization and excretion.[23] However, all tissues contain copper in the form of copper dependent components which include metallo-proteins, metallo-enzymes and low molecular weight (l.m.w) complexes of biological importance.

Copper complexes were observed to be effective in the treatment of RA and other degenerative connective tissue diseases.[23] The traditional approach for RA treatment was by wearing copper bracelets. It was observed that through sweat, bracelets were solubilised and promoted dermal absorption of copper into the blood stream. However, the elevated serum copper levels during RA, and anti-arthritic properties of copper complexes led to the hypothesis that endogenous copper might have a protective function in chronic inflammatory conditions.[22-25] The discovery brought about many articles in the literature indicating that copper complexes can be effective in the alleviation of inflammation associated with RA.

1.3.1 Possible modes of action of copper(II) complexes

Important gains have been made concerning possible biochemical mechanisms of action of copper complexes in relieving inflammation. Although several possibilities exist, the mechanism of action by which copper exhibits anti-inflammatory activity is not yet fully understood. However, Sorenson discussed several modes whereby copper may exhibit its anti-inflammatory activity.[25] These include induction of lysyl oxidase, modulation of prostaglandin synthesis, induction of superoxide dismutase or superoxide dismutase mimetic activity, stabilization of lysosomal membranes and modulation of the activity of histamine.

1) Induction of lysyl oxidase

Lysyl oxidase is a copper dependent enzyme responsible for repair of damaged tissues due to inflammation. The process requires cross-linking and extracellular maturation of the connective tissue components, collagen and elastin. It has been observed that lysyl oxidase activity is induced in copper deficient chicks by copper(II) sulphate administration.[26,27]

2) Modulation of prostaglandin synthesis

Copper complexes have been shown to decrease the synthesis of the pro-inflammatory prostaglandin, PGE_2 and a concomitant increase in the synthesis of the anti-inflammatory prostaglandin, $PGF_{2\alpha}$.

3) Modulation of the activity of Histamine

Modulation of the physiological effects of histamine may also be an important biochemical role for copper complexes. It is found that copper-histamine complexes are an active form of histamine.

4) Stabilization of lysosomal membranes

Copper is also found to be important for redox control of human synovial lysosomes. The synovial fluid contains lysosomal enzymes which are destructive towards cartilage. The permeability of lysosomes is found to be decreased by copper and in addition decreased the ratio of free versus bound lysosomal enzymes.[25]

5) Induction of superoxide dismutase and superoxide mimetic activity

RA has been associated with deficiency or lack of superoxide dismutase enzyme activity. The human superoxide dismutase contains copper at the active site and is required for its dismutase activity. The superoxide anion which initiates inflammation is disproportionated by this enzyme.

1.4 DESIGNING Cu(II) COMPLEXES AS ANTI-INFLAMMATORY AGENTS

The *ab initio* design of therapeutic agents usually depends on a knowledge of the difference between health and disease at a molecular level.[29] The evidence presented in the literature suggests that there is a localized deficiency of copper associated with RA. The fraction of copper concerned with localized deficiency is the labile component comprising the albumin and l.m.w. bound copper and the free metal ions. Most of the serum copper is non-reversibly bound to ceruloplasmin. The l.m.w fraction is involved in the transport of metal ions across cell membranes and between biological binding sites. However, their biological role is not easy to elucidate because they exist well below the limits of analytical means of detection. They are also not amenable to isolation and concentration techniques because these upset the labile equilibria in which they participate.[29]

A computer simulation of the equilibrium reactions between transition metal ions and l.m.w ligands was considered to be the only reliable way to determine which of the thousands of possible complexes would be important under biological or plasma conditions. A blood plasma model developed by May *et al* has been successfully used to account for several processes in drug therapy.[30] This requires the thermodynamic formation constants for all complexes present in the mixture and the overall concentrations of the components. The model provided evidence in support of the hypothesis that administration of l.m.w copper complexes would be beneficial in the treatment of RA.[30-33]

The use of chelating drugs to displace the labile copper equilibrium away from plasma albumin in favour of the tissues is the most straight forward way of utilizing endogenous copper reserves. For this to happen, it requires a drug which is able to compete effectively with the protein for the metal ion and that the predominant metal complex formed should readily diffuse into the

affected synovial tissue. The extent to which administered therapeuticals may be able to fulfil these conditions can be judged by simulating their effects in plasma using ECCLES (Evaluation of Constituent Concentrations in Large Equilibrium Systems) program.[34] In particular a function called plasma mobilization index (p.m.i) is used to ascertain whether the agent is sufficiently powerful and copper specific.

The design of RA agents which reduce inflammation is based upon the assumptions that a). the therapeutic effect of copper administration arises from increase in the total labile copper concentration in the body compartments such as synovial fluid and b). the increase is due to the formation of complexes in plasma that can diffuse into synovial fluid through the separating membrane. The increase in the local concentration of copper at the site of inflammation may be achieved by the two general routes as illustrated in Figure 1.3.[29,35]

The first route is based on the liberation of copper from endogenous reserves while the other on copper administration by oral or topical means. For short term therapy endogenous rather than exogenous sources seem appropriate. The endogenous route can be achieved by a) equilibrium competition for the labile protein-bound copper, b) decreasing the affinity of serum albumin for copper by allosteric effects and c) extracting copper from inert metalloproteins. For oral or topical administration (exogenous route) it is essential to investigate copper chelating agents and their effects in improving the bioavailability of copper, and also explore their possible use in copper chemotherapy. The initial step would be to design and synthesise potential copper mobilizing agents (ligands) containing biofunctional groups or molecules in their structures.

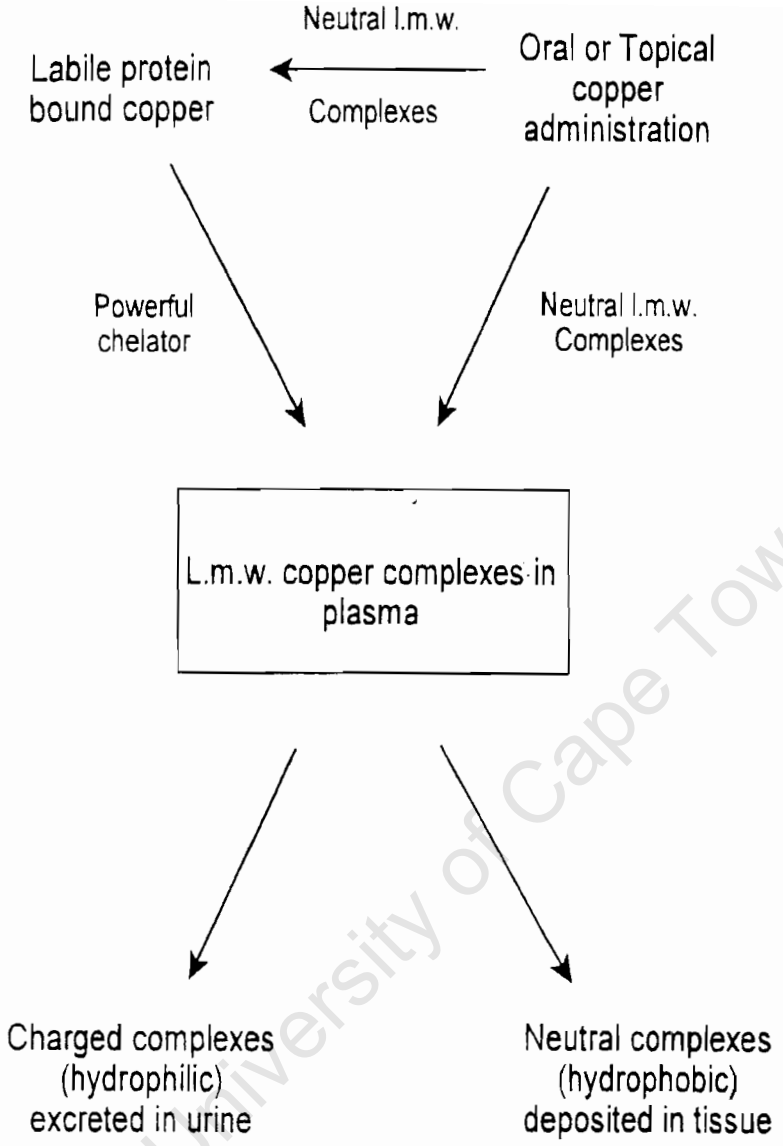

Figure 1.3: Routes for increasing the concentration of l.m.w. copper complexes in blood plasma

1.5 AIM AND OBJECTIVES OF THIS STUDY

The aim of this study was to design ligands that would effectively mobilize copper(II) at the site of inflammation by increasing low molecular weight and membrane penetrable complexes *in vivo*. These ligands would also compete for endogenous reversibly serum bound Cu(II).

In order to achieve this aim, the following objectives were carried out;

- Design and synthesis of PrDH, PrDM, PrDPr and PCUA ligands.
- Determination of formation constants of these ligands with Cu(II), Zn(II), Ca(II) and Ni(II) in aqueous solution using glass electrode potentiometry.
- Elucidation of structures formed between Cu(II) and these ligands in solution using UV-visible, nuclear magnetic resonance and infrared spectroscopy as well as molecular mechanics calculations.
- Use of a computer blood plasma model, together with measured formation constants, to evaluate the plasma mobilizing ability of these ligands.
- Determination of octanol/water partition coefficients as an estimation for dermal absorption for Cu(II) complexes of these ligands.
- Determination of superoxide dismutase activity of Cu(II) complexes with these ligands using a simple *in vitro* assay.
- Finally, performing animal experiments for the determination of tissue distribution, dermal absorption and *in vivo* stability of the Cu(II) complexes.

References:

1. Jackson G.E., Nakani B.S., *J. Chem. Soc. Dalton Trans.*, 1996, 1373-1377.
2. Weyand C.M., *Rheumatology*, 2000, **39**(suppl.1), 3-8.
3. Aeschlinmann A., Simmen B.R., Michel B.A., in; Baumgartner H., Dvorak J., Grob D., Munzinger U., Simmen B.R. (Eds), *Rheumatoid Arthritis*, 1995, Thieme Medical Publishers, Inc., New York.
4. Fischbach M., *Rheumatoid Arthritis*, 1991, Churchill Livingstone, New York.
5. Weder E.J., Dillion T. C., Hambley W.T., Kennedy J.B., Lay A.P., Biffin J.R., Regtop L.H., Davies M.N., *Coord. Chem. Rev.*, 2002, **232**, 95-126.
6. Melvin J.L., *Rheumatic Disease*, 2nd ed, 1982, F.A. Davis Company, Philadelphia.
7. Wilkens R.F., Dahl S.L., *Therapeutic Controversies in the Rheumatic Disease*, 1987, Grune and Stratton, Inc., Orlando.
8. McCarthy D.J., *Arthritis and Allied Conditions, A textbook of Rheumatology*, 11th ed, 1989, pp507-621, Lea and Febiger, Philadelphia.
9. Casono J.J., *Rheumatology in Primary Care*, 1987, pp41-73, W.B. Saunders Company, USA.
10. Weismann M.H., Weinblatt M.E., *Treatment of the Rheumatic Diseases, Companion to the Textbook of Rheumatology,* 1995, pp31-51, W.B. Saunders Company, USA.
11. Hardin J.G., Longenecker L.G, *Handbook of Drug Therapy in Rheumatic Diseases*, 1st ed, 1992, Little, Brown and Company, London.
12. West G.S., *Rheumatology Secrets*, 2nd ed, 2002, Hanley and Belfus, Inc. Philadelphia.
13. Hardin J.G., Longenecker L.G, *Handbook of Drug Therapy in Rheumatic Diseases, Pharmacology and Clinical Aspects*, 1992, Little, Brown and Company, Boston.

14. Hughes M.N., *The Inorganic Chemistry of Biological Processes*, 1974, John Wiley and Sons, London.
15. Bonta I.L., Parnham M.J., Vincent J.E., Bragt P.C., in: Ellis G.P., West G.B., *Prog. Med. Chem.*, 1980, **17**, 186-260.
16. Williams D.R., *The Metals of Life*, 1971, van Norstrand Reinhold Company, London.
17. Osterberg R., in; *Biological role of copper*, 1980, pp283-299, Ciba Foundation Symposium 79, Excerpta Medica, Armsterdam.
18. Blumberg W.E., Aisen P., Peisach J., *The Biochemistry of copper*, 1966, Academic Press, New York and London.
19. Delves H.T., in; *Biological role of copper*, 1980, pp5-22, Ciba Foundation Symposium 79, Excerpta Medica, Armsterdam.
20. Lewis A.J., *Agents Actions*, 1984, **15**, 513.
21. Bremner I., in; *Biological role of copper*, 1980, pp23-48, Ciba Foundation Symposium 79, Excerpta Medica, Armsterdam.
22. Sorenson J.R.J., *Prog. Med. Chem.*, 1989, **26**, 437-547.
23. Sorenson J.R.J., *Prog. Med. Chem.*, 1978, **15**, 211-260.
24. Sorenson J.R.J., *Prog. Med. Chem.*, 1976, **19**, 135-148.
25. Sorenson J.R.J., in; *Metal ions in biological systems, inorganic drugs in deficiency and disease*. (Ed) Sigel H., Marcel Dekker, Inc., 1982, **14**, pp77-113.
26. Bittar-Edward E., Kleinan H.K., (Eds) *Advances in Molecular and Cell Biology*, Jai Press Inc. Connecticut, 1993. **6**, 36.
27. Harris D.E., Rayton K.J., Balthrop E.J., Disilvestro A.R., Garcia-De-Quevedo M., in; *Biological role of copper*, 1980, pp163-182, Ciba Foundation Symposium 79, Excerpta Medica, Armsterdam.
28. Hassan M.H., in; *Biological role of copper*, 1980, pp125-142, Ciba Foundation Symposium 79, Excerpta Medica, Armsterdam.
29. May P.M., Williams D.R., in; *Metal ions in biological systems, inorganic drugs in deficiency and disease*. (Ed) Sigel H., Marcel Dekker, Inc., 1981, **12**, pp283-317.

30. May P.M., Linder P.W., Williams D.R., *J. Chem. Soc. Dalton Trans.*, 1977, 588-595.
31. Jackson G.E., May P.M., Williams D.R., F.E.B.S. Letters, **90**, 1978,
32. Jackson G.E., May P.M., Williams D.R., J. Inorg. Nucl. Chem., 1978, **40**, 1227-1234.
33. Jackson G.E., May P.M., Williams D.R., in; *Metal ions in biological systems, inorganic drugs in deficiency and disease*. (Ed) Sigel H., Marcel Dekker, Inc., 1978, **7**, pp29 - 73.
34. May P.M., in; *Handbook of Metal-Ligand Interactions in Biological Fluids, Bioinorganic Chemistry*, (Ed) Berthon G., 1995, **2**, pp1184-1201, Marcel Dekker, Inc., New York.
35. Kelly M., *PhD Thesis*, University of Cape Town, 1998.
36. http:/www.arc.org.uk/about_arth/booklets/6033/6033/htm.

CHAPTER TWO

LIGAND DESIGN AND SYNTHESIS

2. LIGAND DESIGN AND SYNTHESIS

2.1 INTRODUCTION

The rational approach towards ligand design for selective complexation of metal ions in solution for therapeutic purpose is of great importance. During inflammatory conditions there is an increase demand for copper and this is compensated for by enhanced intestinal absorption and decreased intestinal excretion of copper. However, the exogenous administration of copper(II) for this therapeutic activity requires ligands that can successfully mobilize metal ion at the site of inflammation. For this to happen, the ligands must possess desirable features.

2.2 LIGAND SELECTION

The design for the ligands that can successfully mobilize the metal ion in body fluids depends on the strength of complexes formed. Strong and kinetically labile complexes are mostly desirable. However, very strong or kinetically inert complexes might not release the metal ion at the biological active site. The design strategy in this study is to synthesise the ligands that would enhance absorption of copper(II) from the intestine or dermally, and thereby increasing the concentration of l.m.w complexes. The ligand could also be powerful enough to compete for or exploit copper bonded to serum albumin.

There are several different ways of achieving selective thermodynamic binding in aqueous solution.[1,2] Amongst the criteria is Pearson's hard/soft-acid/base (HSAB) theory in which Cu^{2+} is regarded as a borderline ion. According to this theory, a hard donor atom will prefer to bond to a hard accepter atom and likewise a soft pair of atoms. Moreover, if a range of complexes formed by one metal ion is known, the Irving-Williams series ($Mg^{2+}<Mn^{2+}<Fe^{2+}<Co^{2+}<Ni^{2+}<Cu^{2+}>Zn^{2+}$) may be used to predict the strength of complexes formed by another metal ion in the same series.[2] It has

been observed that the mobilizing efficiency on a ligand increases as the donor atoms change from O to S to N.[7] Of interest is that copper(II) shows a remarkable ability to form bonds at pH ≈ 7 to peptide and amide nitrogens in their ionized state.[3]

The increase in the stability of copper(II) complexes has been associated with increase in the number of donor atoms.[8] In general, the stability of inorganic chelate complexes is affected by the size of the chelate rings formed upon coordination. For example, copper(II) complexes of 5,6,5 membered chelate system are generally more stable than 5,5,5 chelate analoques.[5] The low stability in the formation of the 5,5,5 membered chelate system is due to steric constraints. In the design of the copper(II) mobilizing ligands, nitrogen donor groups are preferred because of their high selectivity towards copper(II) over zinc(II) and calcium(II). The *in vivo* concentration of zinc(II) and calcium(II) are reported to be relatively high and thus can interfere with ligands designed to bind copper(II).[8]

In summary, the following features would be desirable in designing the ligand that would successfully mobilize copper(II) in the body fluids at the biological active sites;

- strong complexation with copper(II) to form stable species under physiological conditions such as temperature and pH.
- high selectivity to copper(II) so that other metal ion equilibria such as calcium(II) and zinc(II) are not disturbed in their essential body functions.
- formation of kinetically labile complexes to be able to transport and release copper(II) at the biological active sites.
- formation of neutral or rather formally uncharged complexes which are also lipophilic to enable transport across cell membranes.

In this study related investigations performed by other authors have been reviewed. Jackson and Kelly[4,7] through computer simulations observed that

copper mobilizing efficiency of a ligand increases as the donor atoms changes from O to S to N. Their investigations also show that as the number of donor atoms in the ligand increases, the stability of the copper complexes increased.[8] However, no significant increase in mobilizing ability was observed above coordination number 4. The results led to the investigation of 3,6,9,12-tetra-azatetradecanedioic acid (TTDA) and 3,6,9-triazaundecanedioic acid (DTDA) (Figure 2.2). Neutrality of the copper complex was achieved by incorporation of two acetate groups on the ligand. These ligands formed more stable complexes with copper(II) than zinc(II) and calcium(II) but were found to be highly hydrophilic and rapidly excreted in urine.[4,8,9]

Further investigations were carried out by Voye and co-workers for N,N'-*bis* [2(dimethylamino)ethyl]ethanediamide (5UM) and N,N'-*bis* [2(dimethylamino) ethyl]propanediamide (6UM) (Figure 2.2).[36,41] This was done in order to increase the lipophilicity of the complex. The incorporation of the amide groups on the ligand was meant to bury the charge within the ligand. Upon metal coordination the amides are expected to lose their protons.[49] It was observed that the copper complexes of these ligands were not neutral at physiological pH. The plasma model simulation studies showed that they were unable to effectively compete with endogenous ligands hence were poor at mobilizing copper *in vivo*.[11]

Gama-Mkhonta and co-workers investigated a series of penta-nitrogen donor ligands in order to improve both stability and lipophilicity of the complexes.[11,12] They investigated 1,13-*bis* (N,N-dimethyl)-5,9-dioxo-7-N-benzyl-1,4,7,10,13-pentaazatridecane (BID), 1,13-*bis* (N,N-dimethyl)-5,9-dioxo-7-phenethyl-1,4,7,10,13-pentaazatridecane (DME), 1,4,7,10,13-pentaaza-5,9-dioxo-7-N-phenethyltridecane (EDA) and 1,13-*bis* (N,N-dimethyl)-5,9-dioxo-1,4,7,10,13-pentaazatridecane (ZDA) (Figure 2.2). It was found from the results that these ligands indeed formed more stable complexes than their tetra-nitrogen analogues. Simulation studies showed that they were better at mobilizing copper as compared to 5UM and 6UM.[11] It

must be noted that computer simulation does not take into account other factors such as hydrophilicity. Unfortunately biodistribution studies were not done for comparison with their analogues.

Nomkoko and co-workers investigated dione dioximes ligands in which the secondary amines and dicarboxylates of TTDA were replaced.[13] 3,3,9,9-tetramethyl-4,8-diazatridecane-2,10-dione dioxime (PrAO) and N,N'-*bis* (2-hydroxyiminopropionyl)propane-1,3-diamine (H_2PAP) (Figure 2.2) were synthesized and investigated. On the basis of simulation studies it was found that these could successfully mobilize copper *in vivo* without altering the equilibria of other endogenous metals. Biodistribution studies on mice gave relatively good results and hence prompting further evaluation and development of anti-arthritic agents.[13-15] The authors also investigated (1,15)-*bis* (N,N-dimethyl)-5,11-dioxo-8-(N-benzyl)-1,4,8,12,15-pentaazapentadecane (BIDPAP) and the results showed that the ligand is not capable of mobilizing copper as compared to PrAO and H_2PAP.[16]

The present study is an advancement of the investigation of polyamido ligands which possess some common properties as those of nitrogen-containing biofunctional molecules such as oligopeptides.[17] They are tetra/penta-nitrogen donors and have diamide groups which upon metal coordination should lose their protons.[18] The dissociation of the amide protons would enable the formation of neutral species. The structures of these ligands are shown in Figure 2.1. Incorporated in these ligands are pyridyl groups. The benzyl and pyridyl groups are mainly found in most of the NSAIDs. However, Cu(II)-NSAIDs complexes are reported to be more effective than their parent NSAIDs.[19] The pyridyl group would be able to impose rigidity to the ligand system due to the aromatic ring system. The nitrogen on the pyridyl group should increase the stability of the complex by the chelate effect. It is expected that the nitrogen in the pyridyl group between amide groups on the ligand would act as an anchor for coordination. Of interest also is the pre-organisation of the ligand structures for

coordination. Moreover, the aromatic groups on these ligands should increase both complex stability and lipophilicity.

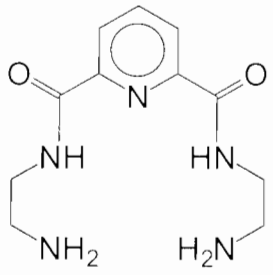

PrDH

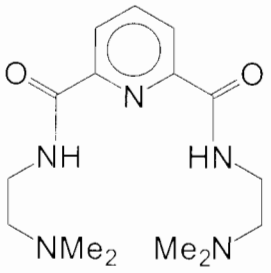

PrDM

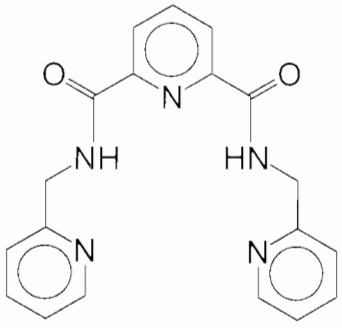

PrDPr

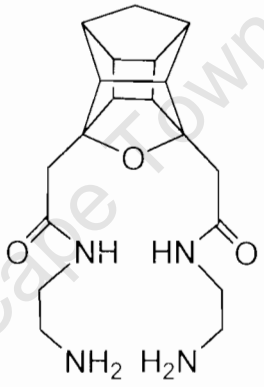

PCUA

Figure 2.1: Schematic representation of ligands in this study

2.3 SYNTHESIS

Solvents such as ethanol, chloroform, dichloromethane, acetone and triethylamine were purified using normal procedures[20] and stored in bottles containing molecular sieve (beads) prior to use. These solvents as well as other reagents used were of analytical grade. All other reagents (starting materials) except those of purity less than 97% were used without further purification.

Various chemicals used in the synthesis of the ligands are listed in Table 2.1.

Table 2.1: Starting materials used for synthesis

Chemical	Purity	Source
Dimethyl-2,6-pyridinedicarboxylate	99 %	Aldrich
Ethylenediamine	99 %	Aldrich
2,6-pyridinedicarbonyl dichloride	97 %	Aldrich
N,N-dimethylenediamine	95 %	Aldrich
2(2-aminomethyl)-pyridine	95 %	Aldrich

Proton(^{1}H) and carbon-13(^{13}C) spectra were obtained from Mercury 300 MHz or Varian Unity Plus 400 MHz instruments. Chemical shifts were recorded in ppm with tetramethylsilane(TMS) (δ scale) as internal reference. Melting points(m.p.) were measured using Reichert Thermovar melting point apparatus while elemental microanalysis was carried out on a Fisons Elemental Analyser C H N O S.

2.3.1 Preparation of N,N'-di(aminoethylene)-2,6-pyridine-dicarbonylamine (PrDH)

N,N'-di(aminoethylene)-2,6-pyridine-dicarbonylamine was synthesised according the method of Zeng and co-workers[21] and Martell and co-workers.[22] Under nitrogen atmosphere dimethyl-2,6-pyridinedicarboxylate (4 g, 0.0204 mol) dissolved in 50 cm^3 methanol was added to a stirred methanol solution (120 cm^3) of ethylenediamine (9 g, 0.1498 mol). The reaction mixture was stirred at room temperature for 2.5 hours after which it was filtered. The solvent and excess ethylenediamine were entirely removed from the filtrate under reduced pressure using a rotary evaporator. The white product obtained was further dried under vacuum. The structure of the compound

was confirmed by NMR spectroscopy, melting point and elemental micro analysis (C H N).

Yield 4.2 g (82%), slightly hygroscopic, m.p. 169 – 173 °C (lit. 170 – 172 °C)[21], ^{1}H NMR(400 MHz) δ_H ($CDCl_3$) 2.89 (t, 4H, NCH_2), 3.48 (t, 1H, $C(O)NCH_2$), 7.91 (t, 1H, Py-H_P), 8.22 (d, 1H, Py-H_M), 8.94 (br t, 2H, C(O)NH), ^{13}C NMR(100.6 MHz) δ_C ($CDCl_3$) 41.41 (CH_2NH_2), 42.14 ($NHCH_2$), 124.81 (Py-C_M), 138.92 (Py-C_P), 148.88 (Py-C_o), 163.81 (C(O)NH), Elemental analysis Anal. found (calc. for $C_{11}H_{17}N_5O_2$) C 51.71 (52.56), H 8.04 (6.83), N 27.05 (27.87). The discrepancy between the observed and calculated values is probably due to the hygroscopic nature of the ligand

2.3.2 Preparation of Bis-(N,N-dimethylethyl)-2,6-pyridine-dicarboxamide (PrDM)

Bis-(N,N-dimethylethyl)-2,6-pyridinedicarboxamide was synthesised according to the method of Danies and co-workers[23], and Mitchell and co-workers.[24] Under nitrogen atmosphere 2,6-pyridinedicarbonyl dichloride (4.82 g, 0.02755 mol) in 35 cm^3 dichloromethane was added dropwise to a stirred solution of N,N-dimethylenediamine (4.14 g, 0.04698 mol) and triethylamine (32.9 cm^3, 0.236 mol) in 160 cm^3 dichloromethane. The reaction was stirred for 1.5 hours after which a slight precipitate formed. The dichloromethane was removed under reduced pressure to afford a red viscous liquid. This liquid was extracted into toluene (3x15 cm^3), filtered and then all the volatiles were removed under reduced pressure. This resulting liquid was dissolved in dichloromethane and passed down through three columns of florisil (25 g each), each time eluting about 150 cm^3 of dichloromethane. The three aliquots were combined and the volatiles were removed under reduced pressure to afford a yellow solid. Recrystallisation from toluene gave white crystals. The structure of the compound was confirmed by NMR spectroscopy, melting point and elemental micro analysis (C H N).

Yield 2.2 g (26%), m.p. 118 – 120 °C, ^{1}H NMR(400 MHz) δ_H ($CDCl_3$) 2.31 (s, 12H, NMe_2), 2.58 (t, 4H, CH_2NMe_2), 3.62 (dt, 4H, NCH_2), 7.99 (t, 1H, Py-H_P), 8.31 (d, 2H, Py-H_M), 8.85 (br t, 2H, C(O)NH), ^{13}C NMR(100.6 MHz) δ_C ($CDCl_3$) 36.93 ($NHCH_2$), 45.26 (NMe_2), 58.77 (CH_2N), 124.71 (Py-C_M), 138.65 (Py-C_P), 149.03 (Py-C_o), 163.92 (C(O)NH), Elemental analysis Anal. found (calc. for $C_{15}H_{25}N_5O_2$) C 58.48 (58.61), H 8.24 (8.20), N 22.73 (22.78).

2.3.3 Preparation of N,N'-bis[2(2-pyridyl)-methyl]pyridine -2,6 dicarboxamide (PrDPr)

N,N'-bis[2(2-pyridyl)-methyl]pyridine-2,6-dicarboxamide was synthesised according to the method of Marlin and co-workers[25], and Hirao and co-workers.[26] Under nitrogen atmosphere 2,6-pyridinedicarbonyl dichloride (5 g, 0.0245 mol) in 100 cm^3 chloroform was added dropwise to a stirred solution of 2(2-aminomethyl)-pyridine (7.95 g, 0.0735 mol) in 150 cm^3 chloroform at 0 °C. The mixture was stirred for 1 hour and then heated to reflux at 60 °C for 2 hours. The solvent and excess 2(2-aminomethyl)-pyridine were removed under reduced pressure using a rotary evaporator. Recrystallisation from acetone gave a white solid and was dried under vacuum. The structure of the compound was confirmed by NMR spectroscopy, melting point and elemental micro analysis (C H N).

Yield 5.1 g (60%), m.p. 150 – 154 °C (lit. 151 – 153 °C)[26] ^{1}H NMR(400 MHz) δ_H ($CDCl_3$) 4.81 (d, 4H, NCH_2), 7.23 (m, 2H, Py-H), 7.39 (m, 2H, Py-H), 7.68 (m, 2H, Py-H), 8.01 (t, 2H, Py-H), 8.34 (d, 2H, Py-H), 8.47 (dd, 2H, Py-H), 9.18 (t, 2H, C(O)NH), ^{13}C NMR(100.6 MHz) δ_C ($CDCl_3$) 44.43 ($NHCH_2$), 122.49, 122.66, 124.78, 137.27, 138.73, 148.75 (Py-C), 148.71, 157.08 (Py-C_{tert}), 163.74 (C(O)NH), Elemental analysis Anal. found (calc. for $C_{19}H_{17}N_5O_2$) C 63.30 (64.00), H 4.89 (4.90), N 19.26 (19.70).

2.3.4 3,5-bis[(aminoethyl)ethanediamide]-4-oxahexacyclo-dodecane (PCUA)

The synthesis of 3,5-bis[(aminoethyl)ethanediamide]-4-oxahexacyclo-dodecane was performed by Professor H.G. Kruger and his group at the University of Kwazulu Natal (South Africa) who supplied us with this ligand. Elemental micro analysis and the results are presented as follows; Elemental analysis Anal. found (calc. for $C_{19}H_{28}N_4O_2$) C 63.76 (63.33), H 7.77 (7.76), N 15.96 (15.55).

The purity of these ligands were also confirmed by acid - base glass electrode potentiometric titrations at 25 ^{o}C and ionic strength, I= 0.15 mol/dm^3 and were found to be greater than 95 %. This was shown by an excellent fit between the calculated and experimental protonation function (Z_H-bar).

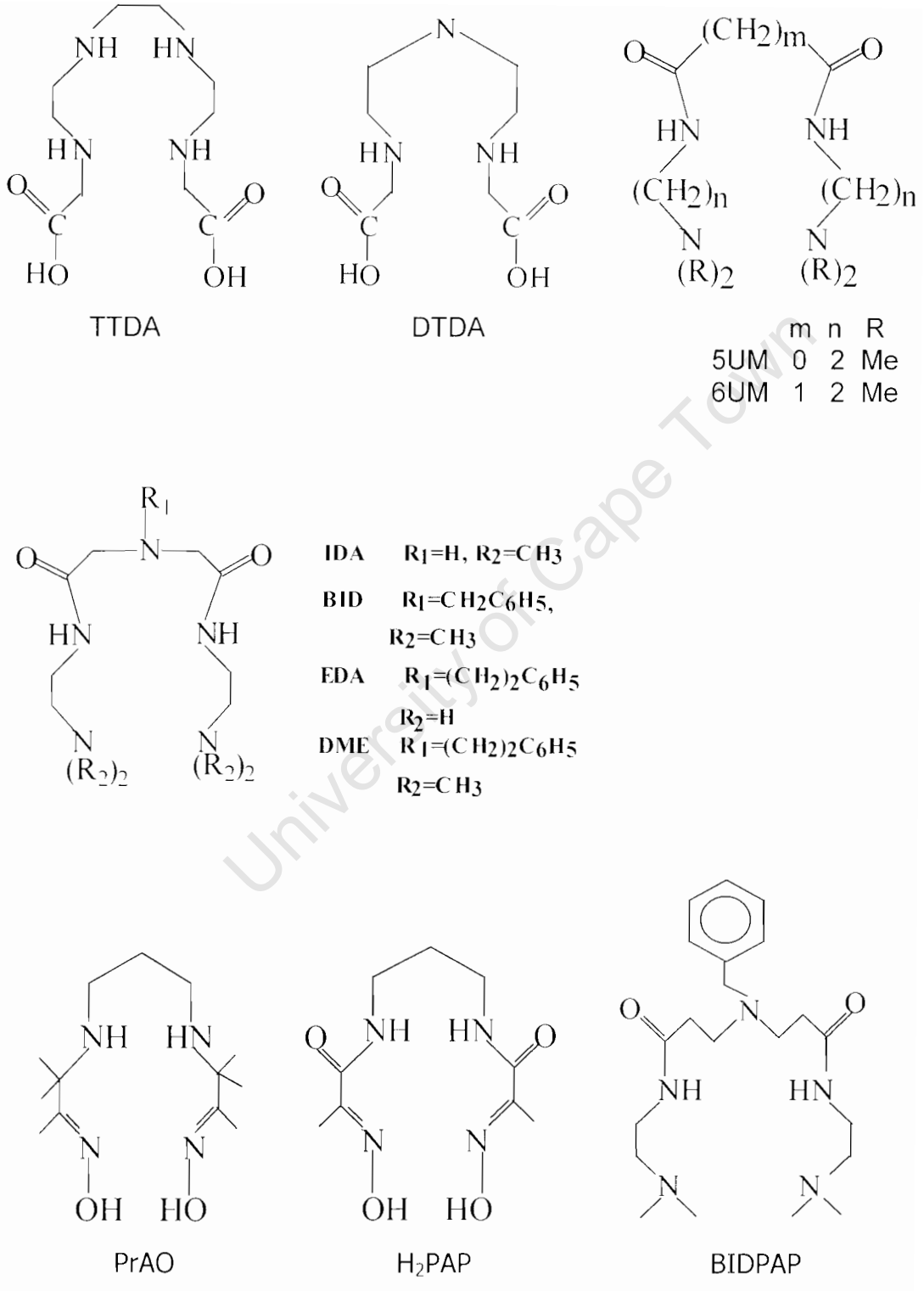

Figure 2.2: Schematic representation of ligands discussed in this chapter.

References:

1. Hancock R.D., Martell A.E., *Chem. Rev.*, 1999, **89**, 1875-1914.
2. Williams D.R., *The Metals of Life*, 1971, van Nostrand Reinhold Company, London.
3. Frausto da Silva J.J.R., Williams R.J.P., *The Biological Chemistry of the Elements: The Inorganic Chemistry of Life,* 1991, Clarendon Press, Oxford.
4. Kelly M., *PhD Thesis*, University of Cape Town, 1998.
5. Voyé A, *PhD Thesis*, University of Cape Town, 1993.
6. Jackson G.E., Jarvis N., in; *Handbook of Metal-Ligand Interactions in Biological Fluids, Bioinorganic Chemistry*, (Ed) Berthon G., 1995, **2**, pp1206-1215, Marcel Dekker, Inc., New York.
7. Jackson G.E., Kelly M.J., *Inorganica Chimica Acta*, 1988, **152**, 152-217.
8. Jackson G.E., Kelly M.J., *J. Chem. Soc. Dalton Trans.*, 1989, 2429-2433.
9. Jackson G.E., in; *Handbook of Metal-Ligand Interactions in Biological Fluids, Bioinorganic Chemistry*, (Ed) Berthon G., 1995, **2**, pp1228-1239, Marcel Dekker, Inc., New York.
10. Jackson G.E., Linder P.W., Voye A., *J. Chem. Soc. Dalton Trans.*, 1996, 4605-4612.
11. Jackson G.E., Gama-Mkhonta L., Voyé A., Kelly M.J., *J. Inorg. Biochem.*, 2000, **79**, 147-152.
12. Gama-Mkhonta L., *PhD Thesis*, University of Cape Town, 1999.
13. Nomkoko T.E., *PhD Thesis*, University of Cape Town, 2002.
14. Nomkoko T.E., Jackson G.E., Nakani B.S., Louw W.K.A., Zeevaart J.R., *J. Chem. Soc. Dalton Trans.*, 2004, 741-749.
15. Nomkoko T.E., Jackson G.E., Nakani B.S., *J. Chem. Soc. Dalton Trans.*, 2004, 1432-1440.

16. Nomkoko T.E., Jackson G.E., Nakani B.S., *Inorg. Chem. Com.*, 2003, **6**, 335-338.
17. Kimura E., *Tetrahedron*, 1992, **48**, no.30, 6175-6217.
18. Bai Sun K., Martell A.E., *J. Chem. Soc.,* 1969, **91**, 4412-4420.
19. Weder E.J., Dillion T. C., Hambley W.T., Kennedy J.B., Lay A.P., Biffin J.R., Regtop L.H., Davies M.N., *Coord. Chem. Rev.*, 2002, **232**, 95-126.
20. Furniss B.S., Hannaford A.J., Smith P.W.G., Tatchell A.R., *Vogel's Textbook of Practical Organic Chemistry*, 5th ed, 1989, Longman Scientific and Technical, England.
21. Zeng Z-Y, He Y-B, Wu J-L, Huang Y-Y, Meng L-Z, *Can. J. Chem.*, 2004, **82**, 454-460.
22. Martell E.A, Motekaitis R.J, *Inorg. Chem.*, 1988, 2718-2724.
23. Davies S.R, Mitchell M.C., Cain C.P., Devitt P.G., Taylor R.J., Kee T.P., *J. Organometallic Chem.,* 1998, **550**, 29-57.
24. Mitchell M.C., Cawley A., Kee T.P., *Tetrahedron letters,* 1995, **36**, no.2, 287-290.
25. Marlin D.S., Olmstead M.M., Mascharak P.K., *Inorg. Chem.*, 1999, **38**, 3258-3260.
26. Hirao T., Moriuchi T., Ishikawa T., Nishimura K., Mikami S., Ohshiro Y., Ikeda I., *J. Mol. Cat. A: Chemical,* **113**, 1996, 117-130.

CHAPTER THREE

GLASS ELECTRODE POTENTIOMETRY

3. GLASS ELECTRODE POTENTIOMETRY

3.1 INTRODUCTION

Potentiometry is one of the oldest, most convenient and successful techniques employed for metal complex equilibrium measurements[1] and has expanded tremendously over the past decades. It has found a significant place in the study of many chemical systems in biological, medical and environmental studies.[2] It is preferred because of its high sensitivity, non-invasiveness and easy accessibility. Glass electrode potentiometry (GEP) has been employed in this study because of the easy availability of the glass electrode, its linear Nernstian response, rapid reversibility and high sensitivity to aqueous hydrogen ions over a wide concentration range. However, the enhancement in the accuracy and predictability of the values arising from GEP require a full mastery of the principles behind electrode calibrations.[2]

Of importance in this study is the determination of stability constants (also known as formation constants) using GEP. The stability constants provide a quantitative measure of the extent to which a metal ion will complex a particular group or ligand.[3] A large number of stability constants have been reported in the literature.[4] Since different workers may report a range of stability constant values under a particular set of conditions, a set of stability constants may be comparable if they have been measured under similar experimental conditions. It is important to note that the position of equilibrium and hence the numerical value of the reported stability constants when expressed in concentration units, is normally dependent upon the temperature and the nature of the medium especially the solvent and ionic strength.[5]

3.2 THEORY

Theory on formation constants and methods used to determine these constants have been widely covered in the literature.[1,2,6-9]

Considering a general metal-ligand formation equilibria involving metal ion (M) and ligand (L), the thermodynamic equilibrium constant is defined as follows;

$$M + L \rightleftharpoons ML \qquad {}^{T}K_1 = \frac{\{ML\}}{\{M\}\{L\}} \tag{3.1}$$

where the symbol { } denotes activity. This equation can be rewritten in terms of concentration;

$$\{ML\} = \gamma_{ML}[ML] \tag{3.2}$$

where γ_{ML} is the activity coefficient of the ML species.

$${}^{T}K_1 = \frac{\gamma_{ML}[ML]}{\gamma_M[M]\,\gamma_L[L]} = \frac{\gamma_{ML}}{\gamma_M\gamma_L}\,{}^{C}K_1 \tag{3.3}$$

The expression $\frac{\gamma_{ML}}{\gamma_M\,\gamma_L}$ becomes a constant at constant ionic strength (I) and

therefore, ${}^{C}K_1$ is a constant (3.4)

Hence, the stepwise formation of the parent complexes can be described by the following set of formation constants at constant ionic strength;

$$M + L \rightleftharpoons ML \qquad K_1 = \frac{[ML]}{[M][L]} \tag{3.5}$$

$$ML + L \rightleftharpoons ML_2 \qquad K_2 = \frac{[ML_2]}{[ML][L]} \tag{3.6}$$

$$ML_{n-1} + HL \rightleftharpoons ML_n + H \qquad K_n = \frac{[ML_n][H]}{[ML_{n-1}][HL]} \tag{3.7}$$

The charges on the species have been omitted for clarity. The product of individual formation constants gives characteristic constants called overall formation constants denoted by the symbol β;

$$M + L \rightleftharpoons ML \qquad \beta_1 = K_1 = \frac{[ML]}{[M][L]} \tag{3.8}$$

$$ML + L \rightleftharpoons ML_2 \qquad \beta_2 = K_1K_2 = \frac{[ML_2]}{[M][L]^2} \tag{3.9}$$

Therefore,
$$\beta_n = K_1K_2...K_n = \frac{[ML_n][H]}{[M][L]^n} \tag{3.10}$$

In general
$$\beta_n = \prod_{i=1}^{n} K_i \tag{3.11}$$

Moreover, the stability constants are affected by temperature as represented by the Van't Hoff equation;

$$\frac{d\ln k}{dT} = \frac{\Delta H^\circ}{RT^2} \tag{3.12}$$

where ΔH° is the standard enthalpy change of reaction and is related to Gibbs free energy ΔG° and entropy ΔS° changes of reaction, T is absolute temperature in Kelvin and R is the universal gas constant in J $K^{-1}mol^{-1}$.

For a complex formation reaction occurring between a metal ion M, ligand L and proton H, the general equilibrium process is given by the following expression; [9-11,18]

$$pM + qL + rH \rightleftharpoons M_pL_qH_r \tag{3.13}$$

where p, q and r are the stoichiometries of the components in the complex. The formation constant for this reaction is described by the mass balance equation as follows;

$$\beta_{pqr} = \frac{[M_pL_qH_r]}{[M]^p[L]^q[H]^r} \tag{3.14}$$

and the concentration of each species $M_pL_qH_r$ in the k^{th} point is given by;

$$[M_pL_qH_r]_k = \beta_{pqr}[M]_k^p[L]_k^q[H]_k^r \tag{3.15}$$

The total concentration of the metal ion (T_M), ligand (T_L) and hydrogen ion (T_H) described by law of mass action at k^{th} point will be;

$$T_{k,M} = [M]_k + \sum_{i=1}^{N} p\,\beta_{pqr}[M]_k^p[L]_k^q[H]_k^r \tag{3.16}$$

$$T_{k,L} = [L]_k + \sum_{i=1}^{N} q\,\beta_{pqr}[M]_k^p[L]_k^q[H]_k^r \tag{3.17}$$

$$T_{k,H} = [H]_k + \sum_{i=1}^{N} r\,\beta_{pqr}[M]_k^p[L]_k^q[H]_k^r \tag{3.18}$$

where $[M]_k$ is the concentration of free aquated metal ions and the summation is over the concentration of all the metal containing species which may be protonated (r>0) or may not (r=0), $[L]_k$ is the concentration of the uncomplexed ligand and the summation is over the concentration of all the protonated and unprotonated ligand containing species and $[H]_k$ is the concentration of hydrogen ion.

It is possible that r may be less that zero (r<0) in which case either a proton has been lost from the complex or a hydroxide ion has been added. In this study the species $M_pL_qH_r$ is denoted by the stoichiometric coefficients p,q,r i.e.

1 1 -1 denotes the complex species MLH_{-1} with r=-1 referring to the removal of a proton from either a coordinated ligand or a bound water molecule, or hydroxide ion addition to the complex.[12,13] $M_pL_qH_r$ can be regarded as a protonated complex if $r \geq 1$.

The electrode cell is the centre of any potentiometric investigation. An electrochemical cell consisting of a test solution surrounding a glass electrode in electrical contact with a reference electrode through a salt bridge can be represented as follows;

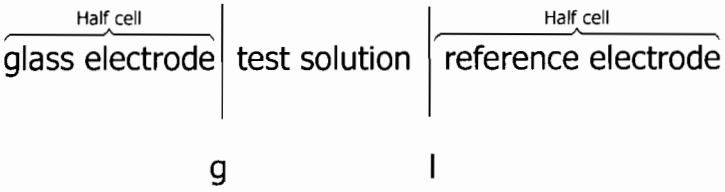

From the reaction cell, the observed potential (E_{cell}) is due to the potential difference between the glass electrode and the reference electrode (E_{ref}), the potential of the liquid junction of the reference electrode (E_{lj}) and the potential at the membrane of the glass electrode (E_g). The reaction cell potential may be represented by the following equation;

$$E_{cell} = E_{ref} + E_{lj} + E_g \qquad (3.19)$$

The glass electrode (half cell) generates a potential that is proportional to the logarithm of the analyte activity (concentration) and is measured relative to an inert reference electrode that is in contact with the sample solution.[14] The Nernstian equation is therefore stated as follows;

$$E_{cell} = E_{ref} + E_{lj} + E_g^{o} + \frac{RT}{F} \ln\{H^+\} \qquad (3.20)$$

where E_{cell} is measured electromotive force (emf), E_g^o is the standard electrode potential, R is the gas constant, T is the temperature of the system, F is Faraday constant and $\{H^+\}$ is the activity coefficient of the hydrogen ion.

The activity (a) of the hydrogen ion (i) is defined with respect to its activity coefficient (γ) and concentration (c) as follows;

$$a_i = c_i \gamma_i \tag{3.21}$$

The ionic strength (I) of a solution is defined by the expression;

$$I = \frac{1}{2}\sum c_i z_i^2 \tag{3.22}$$

where c_i is the concentration of ionic species i and z_i is the charge on that ion.

The activity coefficient of hydrogen ions becomes a constant at constant ionic strength. Since the concentration of the hydrogen ions is a measurable quantity, the cell potential becomes;

$$E_{cell} = E_{const} + \frac{RT}{F}\ln[H^+] \tag{3.23}$$

The temperature dependence of the potential response for hydrogen ion activity (concentration) is demonstrated by the slope factor, $s = \frac{2.303RT}{F}$, in the Nernst equation;

$$E_{cell} = E_{const} + s \log[H^+] \tag{3.24}$$

3.3 EQUILIBRIUM SIMULATION FOR TITRATION ANALYSIS

The Equilibrium Simulation for Titration Analysis (ESTA)[15] is a flexible, important computational tool for the determination of protonation and

formation constants in aqueous chemical equilibria. This program library is used to calculate equilibrium distributions of chemical species, to analyse potentiometric titration data and to manipulate titration data for a variety of purposes. The calculations are performed using a Gauss-Newton method to solve the mass balance equations.

The Gauss-Newton method is used to minimize the objective function, U_{obj}, in the ESTA program. The objective function is optimized by the task OBJE within the ESTA2 module. The optimization is done with respect to the observed emf. In contrast, with the OBJT task, optimization is based on total concentrations. Since the variation in total concentrations is smaller than the variation in emf, OBJT is more robust and faster than OBJE but is less sensitive. Thus in practice OBJT would often be used for initial optimization followed by OBJE for the final optimization. The ESTA program also calculates two important functions which are the formation function, Z-bar, and the deprotonation function, Q-bar. These functions are calculated by the tasks ZBAR and QBAR within ESTA1 module. They are defined differently for the ligand, the binary and the ternary systems. This is because the kinds of equilibria present in the different systems may vary depending on the number of the components that constitute each system.

The program ESTA also incorporates the task SPEC in the ESTA1 module and this calculates the distribution of species present in an equilibrium system as a function of the pH of the solution.

3.3.1 The Objective function

The objective function (U_{obj})[16] may be described as the summation of all the squared residuals of the real parameter values from the calculated values. This function may be represented as:

$$U_{obj} = (N - n_p)^{-1} \sum_{n=1}^{N} n_e^{-1} \sum_{q=1}^{ne} w_{nq} \, (y_{nq}^{obs} - y_{nq}^{calc})^2 \qquad (3.25)$$

where N is the total number of experimental points, n_p is the number of parameters being optimized, n_e is the total number of electrodes, w_{nq} is the weight of the q^{th} residual at the n^{th} point, y_{nq}^{obs} is the observed variable of the q^{th} residual at the n^{th} point and y_{nq}^{calc} is the calculated variable of the q^{th} residual at the n^{th} point.

The optimization of the resulting data can be achieved by minimization of the objective function. In order to minimize U_{obj}, a Gauss-Newton approach is employed and this assumes that the function is quadratic with respect to all the parameters. Therefore U_{obj} can be expressed as;

$$U_{obj} = \mathbf{a} + \mathbf{p}^t\mathbf{b} + \frac{\mathbf{p}^t H \mathbf{p}}{2} \qquad (3.26)$$

where **a** and **b** are Gauss-Newton quadratic parameter vectors, **p** is the optimization parameter vector, $\mathbf{p}^t$ is the transpose of **p** and H, the Hessian, is given by;

$$H_{sr} = \frac{d^2 U_{obj}}{dp_s dp_r} \qquad (3.27)$$

A well defined system with good initial estimates often converges. The calculations are terminated if the resultant shift vectors are large or if the shift vector has an upward gradient. Once the U_{obj} is minimized, the standard deviation, the Hamilton R-factor and its limit and the correlation coefficients are then calculated and reported with the optimized values of the stability constants.

3.3.2 Formation and Deprotonation functions

The ESTA programs calculate two important functions from the titration data. These functions are the formation function (Z-bar) and the deprotonation function (Q-bar). These functions are defined differently depending on the presence or absence of a metal ion.

In the absence of a metal ion the protonation function is expressed as;

$$Z_H\text{-bar} = \frac{T_H^* - [H^+] + [OH^-]}{T_L} \qquad (3.28)$$

where T_L is the total ligand concentration and T_H^* is the total hydrogen ion concentration and is defined by;

$$T_H^* = [H^+] - [OH^-] + \sum r\beta_{0qr}[L]^q[H]^r \qquad (3.29)$$

The Z_H-bar function is plotted against pH. Z_H-bar may be described as the average number of hydrogen ions bound to the ligand at each pH.

The complex formation function, Z_M-bar, measures the average number of ligands bound per metal ion at each concentration of the ligand. This function may be represented as;

$$Z_M\text{-bar} = \frac{T_L - [L]}{T_M} \qquad (3.30)$$

where T_M is the total metal concentration and [L] is the free-ligand concentration. Z_M-bar applies only to mononuclear binary complexes. A plot of this function against pL (-log[L]) gives a pictorial representation of the equilibria.

On the other hand, the deprotonation function, Q_M-bar, is the average number of protons released from the ligand per metal ion as a result of complexation.

$$Q_M\text{-bar} = \frac{T_H^* - T_H}{T_M} \tag{3.31}$$

where T_H is the total proton concentration and T_H^* is the calculated total concentration of protons that would be necessary to give rise to the observed pH in the absence of the metal ions or rather if no complexation took place.

In binary systems, a formation function representing the number of protons that would be on the ligand in the absence of the metal ion, is simultaneously defined as;

$$n\text{-bar} = \frac{T_H^* - [H^+] + [OH^-]}{T_L} \tag{3.32}$$

The difference between n-bar and Q_M-bar gives the number of protons on the complex. This can be represented as;

$$r = (q \times n_{bar}) - (Q_{bar} \times p) \tag{3.33}$$

where p and q are the stoichiometric coefficients of the metal and the ligand respectively. If $p = q = 1$, and $n_{bar} = Q_{bar}$, then $r = 0$ and hence the ML species stability constant is given by β_{110}. For $r < 0$, it is either the deprotonation of the complex formed or the formation of the hydroxo species.

Polynuclear complexes arise whenever there is a ligand capable of bonding to more than one metal ion. Such ligands include hydroxide, carboxylate etc., as well as multidentate ligands that may act in a bridging fashion.

3.3.3 Standard deviation and Hamilton R-factor

Standard deviations[16,17] are errors estimated for the parameters being optimized by the method of least-squares. The standard deviation of the r^{th} optimized parameter may be calculated as follows;

$$\delta_r = \left[\frac{U_{obj} \times G_{rr}}{N - n_p} \right]^{0.5} \tag{3.34}$$

where G is the reciprocal of the Hessian, $G = H^{-1}$

The agreement between the experimental and calculated values of the refined data is indicated by the Hamilton R-factor.[16] It is represented as:

$$R^H = \left[\frac{U_{obj}}{\sum n_e^{-1} \sum w_{nq} (y_{nq}^{obs})^2} \right]^{0.5} \tag{3.35}$$

The R-factor is compared with its limit as follows:

$$R_{lim}^H = \left[\frac{N}{\sum n_e^{-1} \sum w_{nq} (y_{nq}^{obs})^2} \right]^{0.5} \tag{3.36}$$

where symbols have their usual meaning as outlined in section 3.3.1. The R_{lim}^H is the best possible R value based on the random error in the analytical data and the number of variables. Thus the closer R^H gets to the R_{lim}^H the better the agreement between the theoretical model and the experimental data. However, if $R^H < R_{lim}^H$ the model is within the maximum allowed experimental error.[18]

3.4 EXPERIMENTAL

3.4.1 Equipment

Potentiometric titrations were performed using a Metrohm 6.0222.100 Combined LL pH glass electrode. The slope of the electrode system was calibrated in terms of hydrogen ion activity using buffer solutions of known pH and E_{const} determined by strong acid - strong base titrations at 25 ^{o}C. The emf was monitored using a Radiometer PHM 84 Research pH meter. The reaction vessel was kept at a constant temperature of 25 ^{o}C by circulating water from a thermostated water bath. Titrant such as sodium hydroxide (NaOH) was dispensed by the use of Metrohm 665 Dosimat piston burette.

All titrations were performed under an inert atmosphere of nitrogen. This nitrogen was purified by passing it through a series of gas bottles containing 50% potassium hydroxide to remove carbon dioxide (CO_2), Fieser's solution to remove traces of oxygen (O_2), glass wool, distilled water and background electrolyte solution of ionic strength 0.15 mol/dm^3 (Cl^-)Na^+ to humidify the gas. The potentiometric titration system was controlled and monitored through a computer.

3.4.2 Preparation and standardisation of solutions.

All solutions were prepared with recrystallized NaCl as background electrolyte, at ionic strength of 0.15 mol/dm^3 (Cl^-)Na^+ using glass distilled water which had been boiled to remove CO_2 and kept in a container protected by a CO_2 trap. All reagents except ligand samples were commercially available and of analytical grade. These were used without further purification.

Hydrochloric acid (HCl) solutions were prepared to a concentration of 0.02 M from Merck ampoules (1.09973 – Titrisol) in background electrolyte. The solutions were standardised against recrystallized sodium tetraborate

decahydrate (borax) $Na_2B_4O_7 \cdot 10H_2O$. NaOH solutions were prepared under a nitrogen atmosphere to a concentration of 0.1 M from Merck ampoules (1.09959 – Titrisol). Standardisation of these solutions was done against recrystallized potassium hydrogen phthalate (KHP) using the Gran method.[20] The 0.1 M NaOH solutions were further standardised against 0.02 M HCl solutions. The acid – base titrations were also used to check the carbonate content of the NaOH solution by use of the Gran method.[20]

Solutions of ligands were prepared by dissolving accurately weighed samples and standardized by acid – base titrations according to the Gran method.[20,22,23] The dissolution of PrDPr samples was enhanced by preparing samples in 0.01M HCl, stirring overnight and then heating. Standard solutions of divalent cations Cu(II), Ni(II), Ca(II) and Zn(II) were prepared from $CuCl_2 \cdot 2H_2O$, $NiCl_2 \cdot 6H_2O$, $CaCl_2 \cdot 2H_2O$ and $ZnCl_2$ respectively. These solutions were standardised by direct titration against 0.01 M standard solution of the disodium salt of ethylenediamine tetraacetic acid (EDTA) using standard methods.[19,21] The concentrations of the metal ions ranged between 0.01898 mol/dm^3 and 0.02013 mol/dm^3. A small amount of standardised HCl was added to the metal ion solutions to prevent hydrolysis of the metal ions.[24] The formation of the metal hydroxide would give inaccurate concentrations of hydrogen ions present in the metal ion solution.

3.4.3 Titrations and Data analysis

Prior to acid – base titrations the electrode was calibrated and the Nernstian slope was determined using buffer solutions of pH values 4.00, 6.85 and 9.18 prepared according to Vogel's method.[19,21] The calibration of the glass electrode was performed to suit the conditions such as temperature (25 ^oC) and ionic strength (I= 0.15 mol/dm^3). The strong acid-strong base titrations were performed in order to calculate the values of the response intercept (E_{const}), slope (s) and the dissociation constant of water (pKw) by introducing titration data into an ESTA file template. The value of s varied between 58.96

and 59.03 over the pH range of 2 to 11. The values of E_{const} varied between 348.41 mV and 353.20 mV while the average pKw value was 13.73.

The ligand protonation titrations were performed by dispensing aliquots of the ligand solutions into the titration vessel. The standardised HCl solution was dispensed into the vessel to ensure complete protonation of the ligand and diluted to 20 cm^3 using background electrolyte solution. This solution was titrated against the standardised NaOH solution at 25 ^oC. The same procedure was carried out for the metal-ligand complexometric titration but with initial varying concentrations of the metal ions. The concentration of the metal ions in the resultant solution varied between 3.13×10^{-4} mol/dm^3 and 1.02×10^{-3} mol/dm^3. The initial varying concentration ratios of ligand to metal (C_L / C_M) varied from 1.01 to 3.33.

The data obtained from these titrations were input into ESTA file templates for the determination of protonation and stability constants. The task BETA of the ESTA programs was used to evaluate the initially estimated complex species and their formation constants. The output of this task was introduced into the task OBJE within the ESTA2A module to give optimised values of the stability constants and the ligand concentration describing the system.

Complex formation and deprotonation functions were calculated from stability constants obtained using the tasks ZBAR and QBAR within the ESTA1 module to find out if the model fitted the system. The models were assumeed to be plausible when the observed and calculated plots of the Z_H-bar, Z_M-bar and Q_M-bar overlapped and output data gave acceptable values of standard deviation and Hamiltonian R-factors. Finally the task SPEC within the ESTA1 module was used to calculate the species distribution as a function of pH for all species in solution over the pH range of 2 to 11.

3.5 RESULTS AND DISCUSSION

3.5.1 Protonation formation function

The protonation constants for H^+ - L equilibria were evaluated in the pH range 2 – 11 and were determined using the ESTA library of computer speciation programs. The protonation curves and species distribution graphs for the ligand systems obtained from the output data are presented in Figures 3.1 – 3.3. The protonation constants for the ligands PrDH, PrDM and PrDPr are given in Table 3.1. The protonation constants for PCUA are included for comparison.

3.5.1.1 H^+-[PrDH] system

Figure 3.1(a) shows the protonation formation function, Z_H-bar, as a function of pH for the ligand PrDH. The function levels off at 2 and then rises slightly above 2.2 indicating that there are three dissociable protons in the ligand system. The levelling at Z_H-bar = 2 is due to protons added to the terminal primary amino groups in the ligand. The rising of the function at low pH (pH < 2.4) is due to the protonation of the acidic pyridyl nitrogen. However, the function curve did not rise to Z_H-bar = 3 because complete protonation of the pyridyl nitrogen occur below the reliable measurable pH range of our glass electrode is 2 – 11.

An excellent agreement between the theoretical and experimental curves for different total ligand concentrations in Figure 3.1(a) lends confidence to the model. This is also supported by low standard deviations in $\log\beta_{0qr}$ and Hamilton R-factors. Figure 3.2(b) shows calculated species distribution curves for PrDH. The plots indicate that the ligand solution has a mixture of di-protonated and tri-protonated species at pH < 4. The di-protonated species predominates at pH < 8.3 whereas the neutral form of the ligand predominates at pH > 9.3.

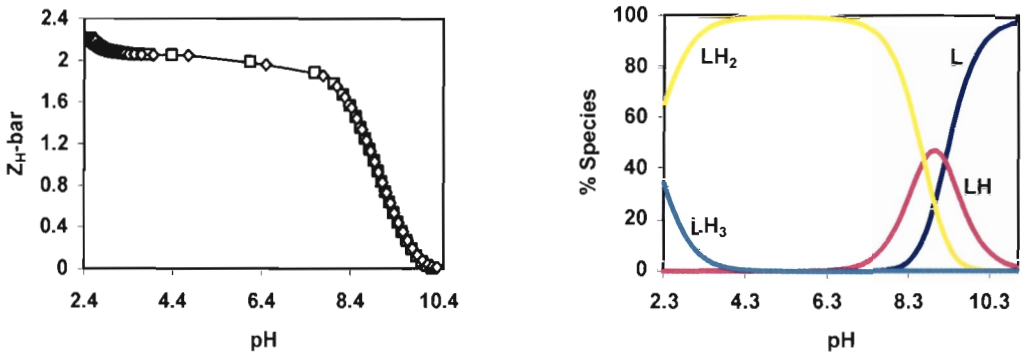

(a) **(b)**

Figure 3.1 (a): Protonation formation curves for PrDH versus pH. The symbols represent titrations performed with different starting ligand concentrations, [(◇) 0.0012 and (□) 0.0031 mol dm^{-3}] and theoretical (solid line) curve. **(b):** calculated protonation species distribution curves against pH for ligand PrDH.

-

3.5.1.2 H^+-[PrDM] system

Figure 3.2(a) shows average number of protons bound to ligand PrDM as a function of pH. As in the PrDH system, the protonation function curve indicates that there are three dissociable protons in the PrDM system. The levelling off at Z_H-bar = 2 reflects two similar protons added to the terminal amino groups and the rising of the curve at pH < 2.4 is indicative of a proton adding to the pyridyl nitrogen group. At high pH (pH > 9.8) the curve levels off at zero indicating that the last proton is lost at this pH.

The theoretical and experimental curves are well superimposible, and this, as well as the low standard deviations and Hamilton R-factors confirm the validity of this model. The calculated and species distribution curves shown in Figure 3.2(b) indicate that the solution has a mixture of di-protonated and tri-protonated species at pH < 3.5. The di-protonated species predominates at pH < 7.9 and the neutral form of the ligand predominates at pH > 8.9.

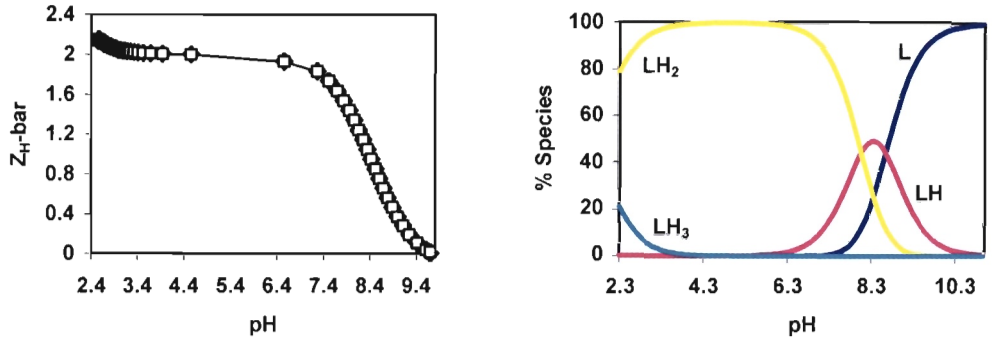

(a) **(b)**

Figure 3.2 (a): Protonation formation curves for PrDM as a function of pH for different starting ligand concentrations, [(◇) 0.0013 and (□) 0.0034 mol dm^{-3}] and theoretical (solid line) curve. **(b):** calculated protonation species distribution curves as a function of pH for ligand PrDM.

3.5.1.3 H^+-[PrDPr] system

The Z_H-bar function in Figure 3.3(a) indicates that there are three dissociable protons in the PrDPr system. Unlike the previous systems, the PrDPr curves do not level off at Z_H-bar of 2 although there is an inflection at this point. The reason for this is the overlap of the three protonation steps. This is clearly seen in the speciation diagrams (Figure 3.3(b)). At pH = 6.2 (Z_H-bar = 0) the ligand is shown to be unprotonated.

The excellent agreement between the experimental and theoretical curves as well as the low standard deviations and Hamilton R-factors lends confidence to this model. The calculated speciation graphs in Figure 3.3(b) show that the solution has a mixture of protonated species at pH range 2.2 – 6.2. This is because of the closeness of pKa values for the protonated sites of the ligand. At pH > 6.2 only the neutral form of the ligand species is present in solution.

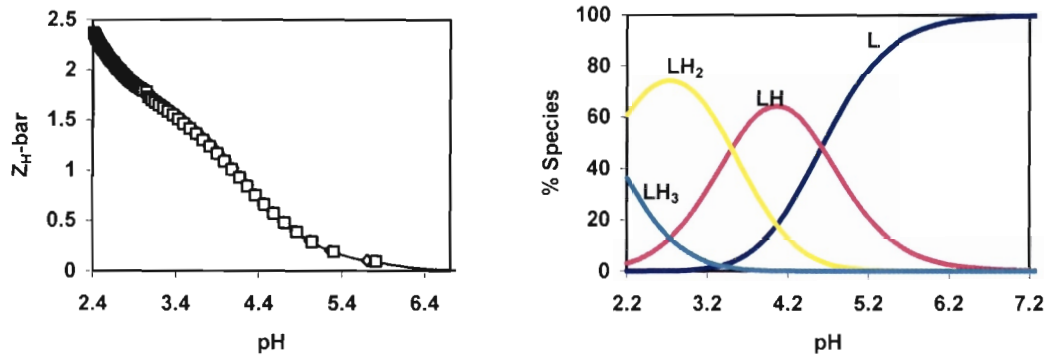

(a) **(b)**

Figure 3.3 (a): Protonation formation curve as a function of pH for different starting ligand concentrations, [(◇) 0.0010 and (□) 0.0031 mol dm^{-3}] and theoretical (solid line) curve. **(b):** calculated protonation species distribution curves as a function of pH for ligand PrDPr.

3.5.1.4 Discussion - Protonation

The protonation constants for the H^+ - L equilibria are presented in Table 3.1. Protonation or deprotonation of the amide nitrogens was not observed because they are too basic ($pK_a \geq 15$)[28] for the measurable pH range 2 – 11 of our glass electrode. Several workers[28-31] have also observed that protonation of the amide nitrogen is not possible in this pH range. However, reports show that the deprotonation of the amide protons is facilitated by the presence of metal ions such as copper(II).[27,28] The results show low standard deviation and R-factors for all protonation models and the R-factors are close or less than their corresponding limits thus giving confidence in the chosen models.

PrDH has three measurable acid dissociation constants with pK_{a1} = 2.032 for the pyridyl nitrogen, pK_{a2} = 8.684 and pK_{a3} = 9.197 for the two terminal amines. The low pK_a or rather acidity of the pyridyl nitrogen is due to the electronic repulsion effect and also the base weakening effect of the CONH

group.[32] The pK_a values of the pyridyl nitrogen in pyridine and 2-methylpyridine are reported as 5.34 and 6.14 respectively.[33] The introduction of a carbonyl group in 2-methylpyridine to afford 2-acetylpyridine gives a pK_{apy} value of 2.66.[4] Therefore, it would be expected that the pyridyl protonation constant in PrDH to decrease further when two amide groups are present. The difference in pK_a's of the two terminal amines by 0.513 log units indicates repulsion when a proton is added to a molecule already containing a proton. The pK_a values of this ligand agree with those determined by Motekaitis and Martell.[25] The variation is due to the fact that experiments were performed in different solvents. Motekaitis and Martell carried out titrations using 70% dioxane – 30% water solution.

Table 3.1: $\log\beta_{pqr}$'s of PrDH, PrDM, PrDPr and PCUA determined at 25 °C and I = 0.15 mol dm^{-3} $(Cl^-)Na^+$. δ_{pqr} denotes the standard deviation in $\log\beta_{01r}$, R^H is the Hamilton R-factor and $R_{lim}{}^H$ its limit, n_T and n_P are the number of titrations and points respectively. The general formula of a complex is $M_pL_qH_r$ denoted by the stoichiometric coefficients pqr where p = 0.

Ligand	p q r	$\log\beta_{pqr}$	δ_{pqr}	logK	R^H	$R_{lim}{}^H$	$n_T(n_P)$	Lit.
PrDH	0 1 1	9.197	0.011	9.197	0.009	0.010	2(162)	9.42[25]
	0 1 2	17.881	0.008	8.684				17.95
	0 1 3	19.914	0.039	2.032				19.77
PrDM	0 1 1	8.647	0.011	8.647	0.010	0.012	2(144)	
	0 1 2	16.718	0.009	8.071				
	0 1 3	18.456	0.066	1.738				
PrDPr	0 1 1	4.624	0.011	4.624	0.010	0.012	2(154)	
	0 1 2	8.132	0.012	3.508				
	0 1 3	10.111	0.047	1.979				
PCUA	0 1 1	9.517	0.014	9.517	0.013	0.019	2(168)	9.52[26]
	0 1 2	17.809	0.016	8.292				17.81

A similar protonation scheme is observed for PrDM with pK_{a1} = 1.738, pK_{a2} = 8.071 and pK_{a3} = 8.647 for the pyridyl nitrogen and two terminal tertiary amino groups respectively. The observable reduction in pK_a's for the terminal amino groups is due to steric hindrance and solvation effects as one moves

from primary to tertiary amines. The difference of 0.576 log units between pK_{a2} and pK_{a3} is almost equal to that of PrDH. The decrease in basicity for the terminal amino groups is observed in related ligands, N,N'-bis[aminoethyl] ethanediamne, i.e. H_2N-CH_2-CH_2-NH-C(O)-C(O)-NH-CH_2-CH_2-NH_2, 5UH, ($logK_{H1}$ = 9.31 and $logK_{H2}$ = 8.43)[34,35] and N,N'-bis[2-(dimethylamino)-ethyl] ethanediamide, i.e. Me_2N-CH_2-CH_2-NH-C(O)-C(O)-NH-CH_2-CH_2-NMe_2, 5UM, ($logK_{H1}$ = 8.72 and $logK_{H2}$ = 7.92).[29,36] PCUA exhibits more basic terminal primary amines due to the positive inductive effect of the large number of carbon atoms in the cage moiety.[26]

PrDPr shows three pK_a values arising from three pyridyl nitrogens. The pK_{a1} = 1.979 is assigned to the protonation of the central pyridyl nitrogen whereas pK_{a2} = 3.508 and pK_{a3} = 4.624 are for the protonation of the terminal pyridyl nitrogens. The chemical environment associated with the central pyridyl nitrogen is the same as that found in PrDH and PrDM thus giving the same or very close pK_{a1} values. However, pK_{a2} and pK_{a3} values are greater than the pK_{a1} value because terminal pyridyl groups have methyl groups adjacent to pyridyl nitrogens. Unlike the CONH group which lowers the basicity of the pyridyl nitrogen, the methyl group increases the basicity by a positive inductive effect. The difference of 1.116 log units between pKa_2 and pKa_3 indicates electronic repulsion on addition of a proton to a charged species or rather to an already doubly protonated molecule.

3.5.2 Complex formation and deprotonation functions

The stability constants ($log\beta_{pqr}$) were evaluated and confirmed by the Z_M-bar and Q_M-bar functions derived from experimental data. The complex formation function, Z_M-bar, measures the average number of ligands bound per metal ion due to complexation. This function is plotted against the negative logarithm of the free ligand concentration (pL). The deprotonation function, Q_M-bar, which indicates the average number of protons released due to complexation is plotted against pH. This function is compared with n-bar

which measures the average number of protons that would be bound to the ligand in the absence of complexation.

3.5.2.1 M^{2+}-[PrDH] systems

Figure 3.4 shows the complex formation curves as a function of pL and, deprotonation function curves and species distribution graphs against pH for the ligand PrDH with Cu(II). The Z_M-bar function in Figure 3.4(a) levels off at 1.5 indicating that ML is not the predominant species in solution. In fact MLH_{-1} is the predominant species as shown by speciation graphs in Figure 3.4(c). At pH 8.1 this species reaches 98% formation whereas ML reaches 36% formation at pH 6.3. Moreover, the fanning back for higher metal to ligand ratios indicates loss of an amide proton upon metal coordination.[37,38]

The deprotonation function in Figure 3.4(b) rises to maximum value of about 2.7 at pH 7.8 indicating that approximately three protons have been released from the ligand due to complexation. At this pH the ligand has only two protons or rather Q_M-bar(=2.7) > n-bar(=2) suggesting the formation of MLH_{-1} species as a result of the release of an amide proton. The falling of Q_M-bar curves parallel to the n-bar curve indicates no further complexation. However, at pH > 9.5 these curves rise due to the presence of hydroxo and/or mixed hydroxo species or rather formation of the MLH_{-2} species. From the speciation graphs MLH_{-1} predominates over a wide pH range of 6.4 – 10 and, MLH and ML species do not exceed 30% formation. It is also observed that complexation commences at about pH 4 when the protonated MLH species is formed.

An excellent agreement between the theoretical and experimental complex formation and deprotonation functions at different metal to ligand ratios supports the potentiometric model chosen in data analysis. Titrations were replicated under identical conditions and this showed good reproducibility. The ESTA[15] suite of programs yielded results given in Table 2 after the

optimization process. The low standard deviation and Hamilton R-factors also lend confidence to the selected model. It is worth noting that several possible species were tried but were rejected by the optimization process.

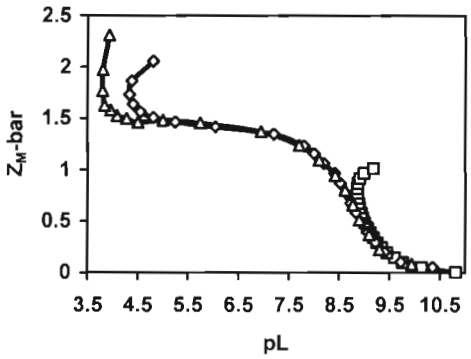

(a)

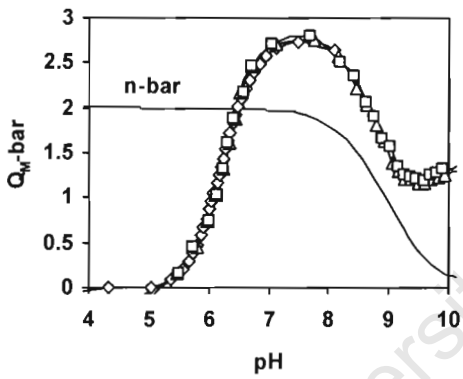

(b)

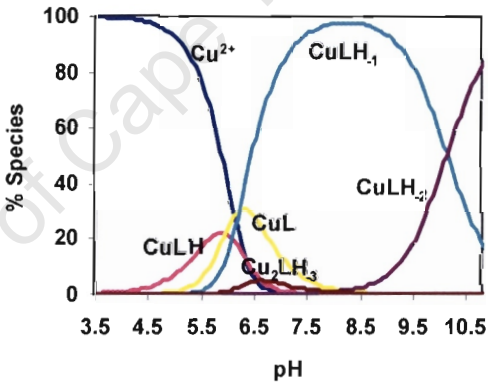

(c)

Figure 3.4 (a): Formation function and **(b):** deprotonation function curves [with M:L ratios 1:1(□), 1:2(◇) and 1:3(Δ), and theoretical (solid line) curve.] against pL and pH respectively and **(c):** calculated species distribution graphs [with M(0.00051 mol dm^{-3}) - L(0.00109 mol dm^{-3})] as a function of pH for ligand PrDH with Cu(II).

Table 3.2: $\log\beta_{pqr}$'s of PrDH with Cu(II), Ni(II), Zn(II) and Ca(II) determined at 25 °C and I = 0.15 mol dm^{-3} $(Cl^-)Na^+$. Other symbols have their usual meaning as defined in Table 3.1.

Ligand	Metal ion	p q r	$Log\beta_{pqr}$	δ_{pqr}	R^H	$R_{lim}{}^H$	$n_T(n_P)$
PrDH	Cu(II)	1 1 1	14.810	0.058	0.021	0.012	6(481)
		1 1 0	8.686	0.043			
		1 1 -1	2.518	0.021			
		1 1 -2	-7.639	0.028			
		2 1 -3	-7.322	0.142			
	Ni(II)	Model 1					
		1 1 1	13.878	0.012	0.021	0.011	6(496)
		1 1 -1	-1.818	0.016			
		1 1 -2	-10.919	0.019			
		Model 2					
		1 1 0	6.079	0.036	0.041	0.022	
		1 1 -1	-2.004	0.036			
		1 1 -2	-10.938	0.037			
	Zn(II)	1 1 1	13.157	0.041	0.020	0.011	6(472)
		1 1 0	4.293	0.131			
		1 1 -1	-3.418	0.027			
		1 1 -2	-13.612	0.241			
	Ca(II)	1 1 1	12.321	0.036	0.014	0.011	6(428)
		1 1 0	3.007	0.038			
		1 1 -1	-8.866	0.232			

For the complexation of PrDH with Ni(II), the Z_M-bar function shown in figure 3.5(a) rises steadily to a value of approximately 0.5 before steeply rising to Z_M-bar > 1.5. This indicates the presence of MLH species[39] and it is clearly shown by the species distribution graphs in Figure 3.5(c) where this species reaches up to 48% formation at pH 7.2. The fanning back of the Z_M-bar curves indicates the presence of hydroxo species.

On the other hand the Q_M-bar curves in Figure 3.5(b) rise to the value 2.7 at pH 8.3 thus indicating the release of approximately three protons due complexation of PrDH with Ni(II). At this pH, Q_M-bar(=2.7) > n-bar(=2) indicating the formation of MLH_{-1} species which reaches up to 62% formation as shown by speciation graphs. At pH range 8.3 – 9.3, Q_M-bar curves run

parallel to the n-bar curve indicating no further complexation before rising at pH > 9.3 due to the formation of hydroxo and/or mixed hydroxo species.

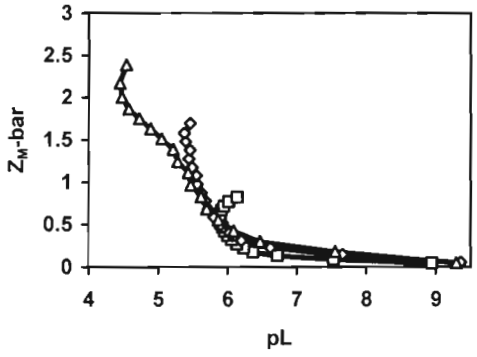

(a)

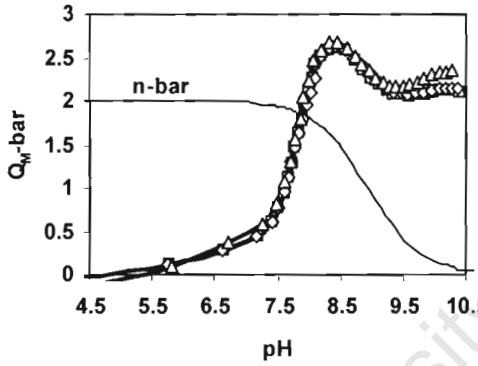

(b)

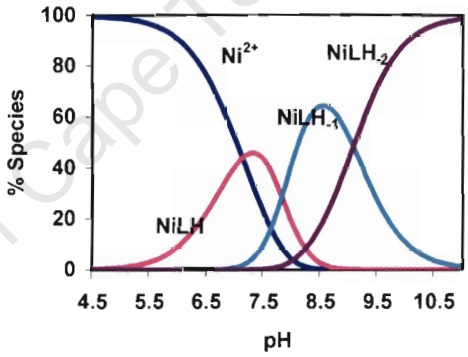

(c)

Figure 3.5 (a): Formation function and **(b):** deprotonation function curves [with M:L ratios 1:1(□), 1:2(◇) and 1:3(Δ), and theoretical (solid line) curve.] against pL and pH respectively and **(c):** calculated species distribution graphs [with M(0.00050 mol dm^{-3}) - L(0.00104 mol dm^{-3})] as a function of pH for ligand PrDH with Ni(II).

The potentiometric data analysis by the ESTA suite of programs gave two models for the Ni(II)-PrDH system. These models are presented in Table 2 and consist of MLH_{-2}, MLH_{-1} and either ML or MLH. This posed a difficulty in deciding on the model which best describes the system because they both generated the same theoretical and experimental formation and deprotonation functions with excellent agreement and reproducible replicates of titrations for different metal to ligand ratios. The low standard deviation

and Hamilton R-factors also lend confidence to these two models. The two models describe the experimental data equally well as far as statistical criteria are concerned and also on chemical grounds. However, the model with the MLH species is most likely to be formed based on the splitting of the Q_M-bar curves at low pH values.

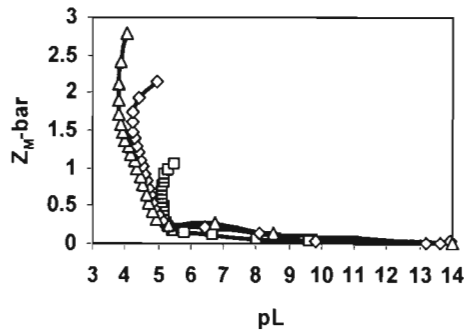

(a)

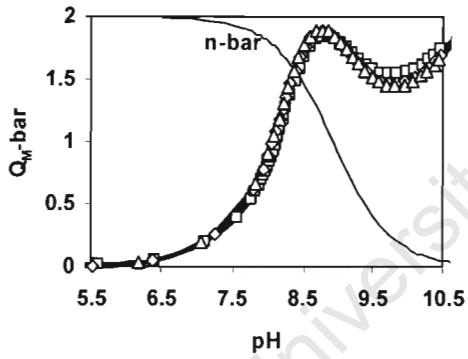

(b)

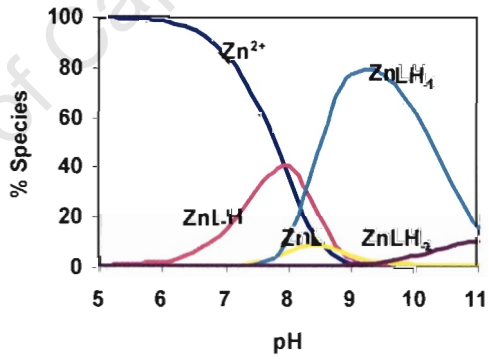

(c)

Figure 3.6 (a): Formation function and **(b):** deprotonation function curves [with M:L ratios 1:1(□), 1:2(◇) and 1:3(Δ), and theoretical (solid line) curve.] against pL and pH respectively and **(c):** calculated species distribution graphs [with M(0.00047 mol dm^{-3}) - L(0.00104 mol dm^{-3})] as a function of pH for ligand PrDH with Zn(II).

Like Ni(II)-PrDH system, the Z_M-bar function for the Zn(II)-PrDH system shown in Figure 3.6(a) does not level at 1 indicating that ML is not the predominant species. The metal assisted amide deprotonated MLH_{-1} species is in fact the predominant species as shown in Figure 3.6(c). The fanning back

of Z_M-bar is characteristic of the presence of hydroxo and/or mixed hydroxo species. ML species coexist with significant levels of MLH and MLH_{-1} over the pH range 7.5 – 9.5.

The deprotonation function curves in Figure 3.6(b) show that complexation commences at pH 5.5. The rising of Q_M-bar at pH > 9.5 is indicative of the presence of hydroxo species. The potentiometric data analysis gave results for the model presented in Table 2 with low standard deviation and Hamilton R-factors. The model is also confirmed by the excellent agreement between the theoretical and experimental formation and deprotonation function curves for different metal to ligand ratios.

Unlike the metal ions discussed above, Ca(II) seems to have low but measurable affinity for the donor atoms of ligand PrDH. This is confirmed by the complex formation function in Figure 3.7(a) which does increase to significant levels in the pH range investigated.

Furthermore, the Q_M-bar function remains almost constant at a value close to zero as shown in Figure 3.7(b). The splitting of the Q_M-bar and Z_M-bar function curves at pH < 9 is due to the presence of the MLH species. Moreover, this species dominates at a wide pH range 6.5 – 10.5 as illustrated by the speciation graphs in Figure 3.7(c). Despite this limited complexation, there is, however, a good agreement between the theoretical and experimental Z_M-bar and Q_M-bar functions to validate the selected model. The low standard deviation and Hamilton R-factors given in Table 2 also lend confidence this model.

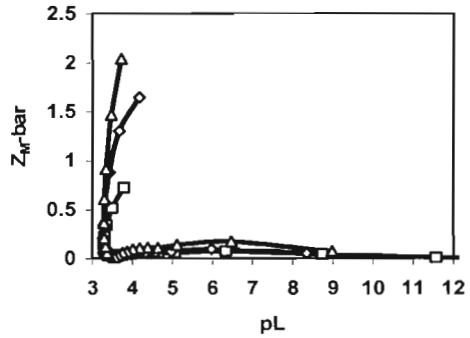

(a)

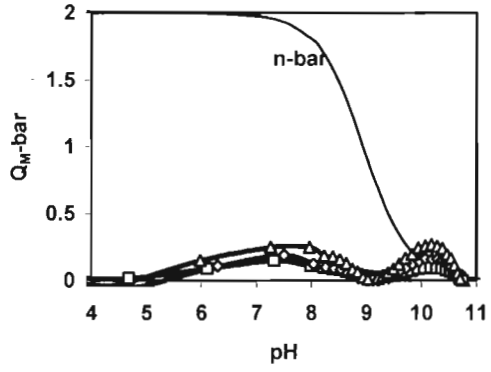

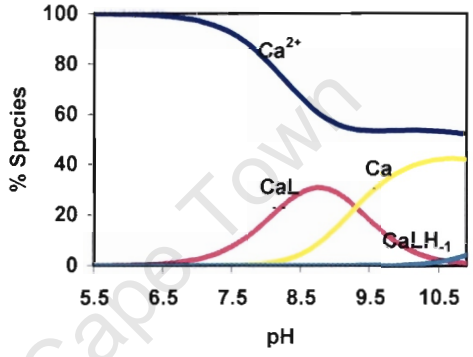

(b) **(c)**

Figure 3.7 (a): Formation function and **(b):** deprotonation function curves [with M:L ratios 1:1(□), 1:2(◇) and 1:3(Δ), and theoretical (solid line) curve.] against pL and pH respectively and **(c):** calculated species distribution graphs [with M(0.00047 mol dm^{-3}) - L(0.00104 mol dm^{-3})] as a function of pH for ligand PrDH with Ca(II).

3.5.2.2 M^{2+}-[PrDM] systems

The complex formation behaviour of the Cu(II)-PrDM system is shown in Figure 3.8(a). The Z_M-bar shows that ML is not the predominant species by levelling off at approximately 1.5. The speciation graphs in Figure 3.8(c) show that ML, MLH_{-1} and MLH_{-2} are present in significant levels i.e. 68% (pH 6.5), 84% (pH 8.1) and 100% (pH 10.8) formation respectively. The fanning back of the curves at high pH for high metal to ligand ratios is presumably due to the formation of MLH_{-1} and MLH_{-2} species.

The rising of Q_M-bar to 2.6 in Figure 3.8(b) indicates that metal assisted deprotonated MLH_{-1} is being formed. The function also rises at pH > 9 due to the presence or dominance of the MLH_{-2} species. The optimization process by the ESTA programs gave three models for the Cu(II)-PrDM system presented in Table 3.3. For model 2 and 3 the species calculated are ML, MLH_{-1}, MLH_{-2} and either M_2LH_{-2} or M_2LH_{-3} whereas model 1 consists of MLH, ML, MLH_{-1} and MLH_{-2} species. These posed difficulties in deciding on the model which best describes the system. The three models gave the same theoretical and experimental Z_M-bar and Q_M-bar functions. However, the calculated speciation graphs for model 1 and 2 showed insignificant levels of formation for MLH and M_2LH_{-2} species respectively. In fact both species are present at formation levels of less than 1%. For model 3, M_2LH_{-3} species reaches up to 2.8% formation as shown in Figure 3.8(c). Possibilities exist in forming these relatively insignificant species as will be presented under discussion – complexation section. The model 3 has been chosen to represent the Cu(II)-PrDM system based on the statistical data given in Table 3.3 and also function curves and speciation graphs. The results for all these models show low standard deviations and Hamilton R-factors as well as excellent agreement and reproducibility of repeat titrations at different metal to ligand ratios thus giving confidence to the models.

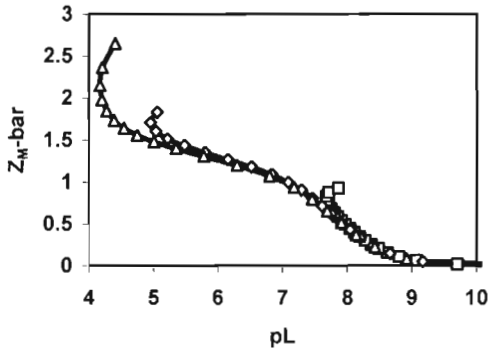

(a)

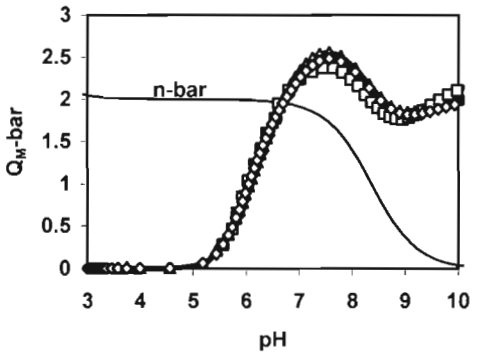

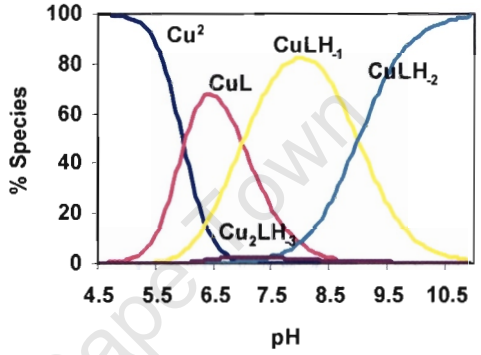

(b) **(c)**

Figure 3.8 (a): Formation function and **(b):** deprotonation function curves [with M:L ratios 1:1(□), 1:2(◇) and 1:3(Δ), and theoretical (solid line) curve.] against pL and pH respectively and **(c):** calculated species distribution graphs [with M(0.00051 mol dm^{-3}) - L(0.00109 mol dm^{-3})] as a function of pH for ligand PrDM with Cu(II).

For the Ni(II)-PrDM system, the metal ion appears to coordinate weakly to PrDM. This is revealed by the Z_M-bar in Figure 3.9(a) which remains close to zero before fanning back at pL $\leq$ 4. This is indicative of the formation of hydroxo and/or mixed hydroxo species. The MLH is the minority species (≈ 15% formation) in solution as shown in Figure 3.9(c). The Q_M-bar in Figure 3.9(b) rises at pH > 9.5 due to the formation of MLH_{-1} and MLH_{-2} species. The splitting of the curves at low pH for different metal to ligand ratios is due to the presence of MLH species.

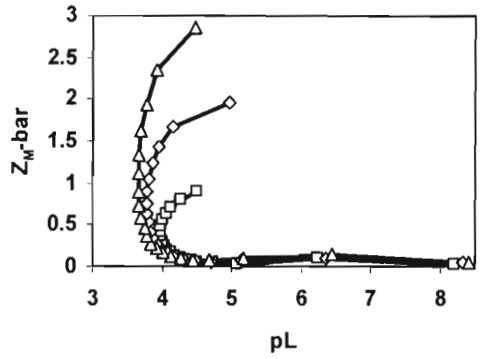

(a)

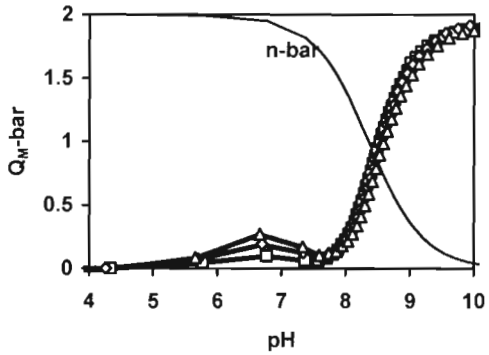

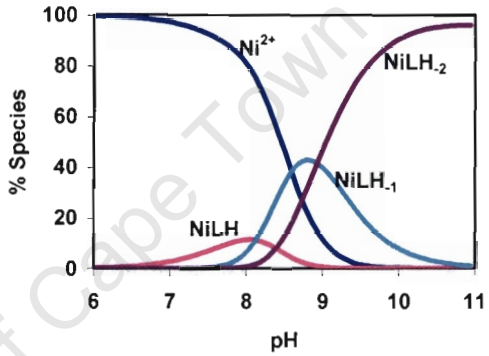

(b) **(c)**

Figure 3.9 (a): Formation function and **(b):** deprotonation function curves [with M:L ratios 1:1(□), 1:2(◇) and 1:3(Δ), and theoretical (solid line) curve.] against pL and pH respectively and **(c):** calculated species distribution graphs [with M(0.00050 mol dm^{-3}) - L(0.00109 mol dm^{-3})] as a function of pH for ligand PrDM with Ni(II).

Moreover, the potentiometric data analysis generated two models similar to that of Ni(II)-PrDH system and these models are presented in Table 3.3. Both models gave well superimposible theoretical and experimental formation and deprotonation functions as well as low standard deviation and Hamilton R-factors. The model with the MLH species is chosen based on the splitting feature observed on the Q_M-bar curves.

Table 3.3: $\log\beta_{pqr}$'s of PrDM with Cu(II), Ni(II), Zn(II) and Ca(II) determined at 25 °C and I = 0.15 mol dm^{-3} $(Cl^-)Na^+$. Other symbols have their usual meaning as defined in Table 3.1.

Ligand	Metal ion	p q r	$\log\beta_{pqr}$	δ_{pqr}	R^H	$R_{lim}{}^H$	$n_T(n_P)$
PrDM	Cu(II)	Model 1					
		1 1 1	12.252	0.756	0.018	0.012	6(486)
		1 1 0	7.839	0.013			
		1 1 -1	0.829	0.017			
		1 1 -2	-8.185	0.020			
		Model 2					
		1 1 0	7.833	0.015	0.018	0.012	
		1 1 -1	0.806	0.016			
		1 1 -2	-8.193	0.019			
		2 1 -2	-2.948	0.308			
		Model 3					
		1 1 0	7.850	0.013	0.017	0.012	
		1 1 -1	0.717	0.019			
		1 1 -2	-8.255	0.019			
		2 1 -3	-9.322	0.099			
	Ni(II)	Model 1					
		1 1 1	11.219	0.070	0.015	0.011	6(222)
		1 1 -1	-4.986	0.018			
		1 1 -2	-13.942	0.014			
		Model 2					
		1 1 0	2.168	0.382	0.015	0.012	
		1 1 -1	-5.050	0.018			
		1 1 -2	-13.986	0.013			
	Zn(II)	1 1 1	12.270	0.034	0.019	0.012	6(491)
		1 1 0	3.657	0.027			
		1 1 -1	-4.448	0.041			
		1 1 -2	-13.082	0.042			
	Ca(II)	1 1 1	11.424	0.054	0.015	0.010	6(463)
		1 1 0	2.837	0.045			

The formation function for the Zn(II)-PrDM system in Figure 3.10(a) levels at pL $\leq$ 4.5 (high pH). As also seen from the speciation graphs in Figure 3.10(c), ML is not the predominant species in solution. The Q_M-bar in Figure 3.10(b)

shows that complexation commences at pH 4.5 when MLH species is being formed. The data analysis by ESTA programs gave results for the model presented in Table 3.3.

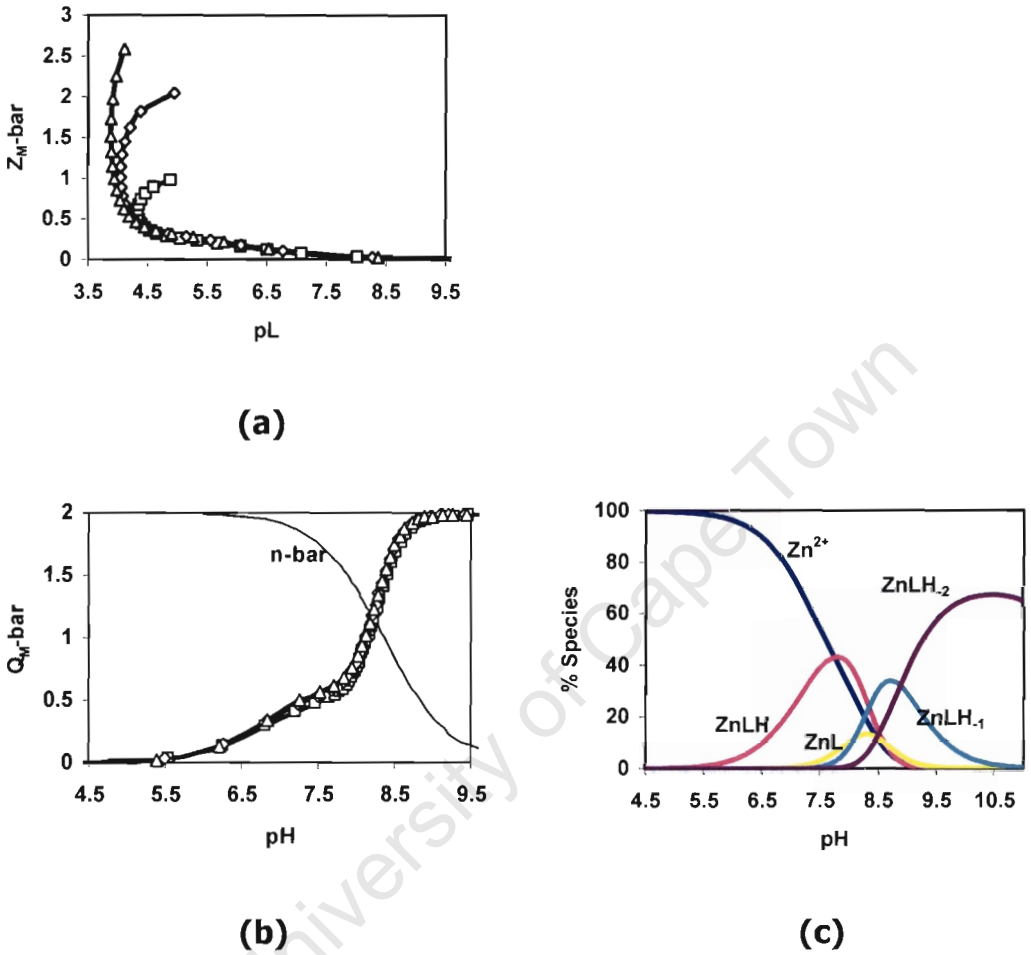

Figure 3.10 (a): Formation function and **(b):** deprotonation function curves [with M:L ratios 1:1(□), 1:2(◇) and 1:3(Δ), and theoretical (solid line) curve.] against pL and pH respectively and **(c):** calculated species distribution graphs [with M(0.00047 mol dm^{-3}) - L(0.00100 mol dm^{-3})] as a function of pH for ligand PrDM with Zn(II).

Like in Ca(II)-PrDM, the Ca^{2+} has low but measurable affinity for the donor atoms of PrDM. This is observed from Z_M-bar and Q_M-bar functions shown in Figure 3.11(a) and 3.11(b) respectively. The speciation graphs in Figure 3.11(c) show species formed by the complexation of PrDM with Ca(II). The good agreement between theoretical and experimental formation and

deprotonation functions as well as low standard deviations and Hamilton R-factors confirm the validity of this model.

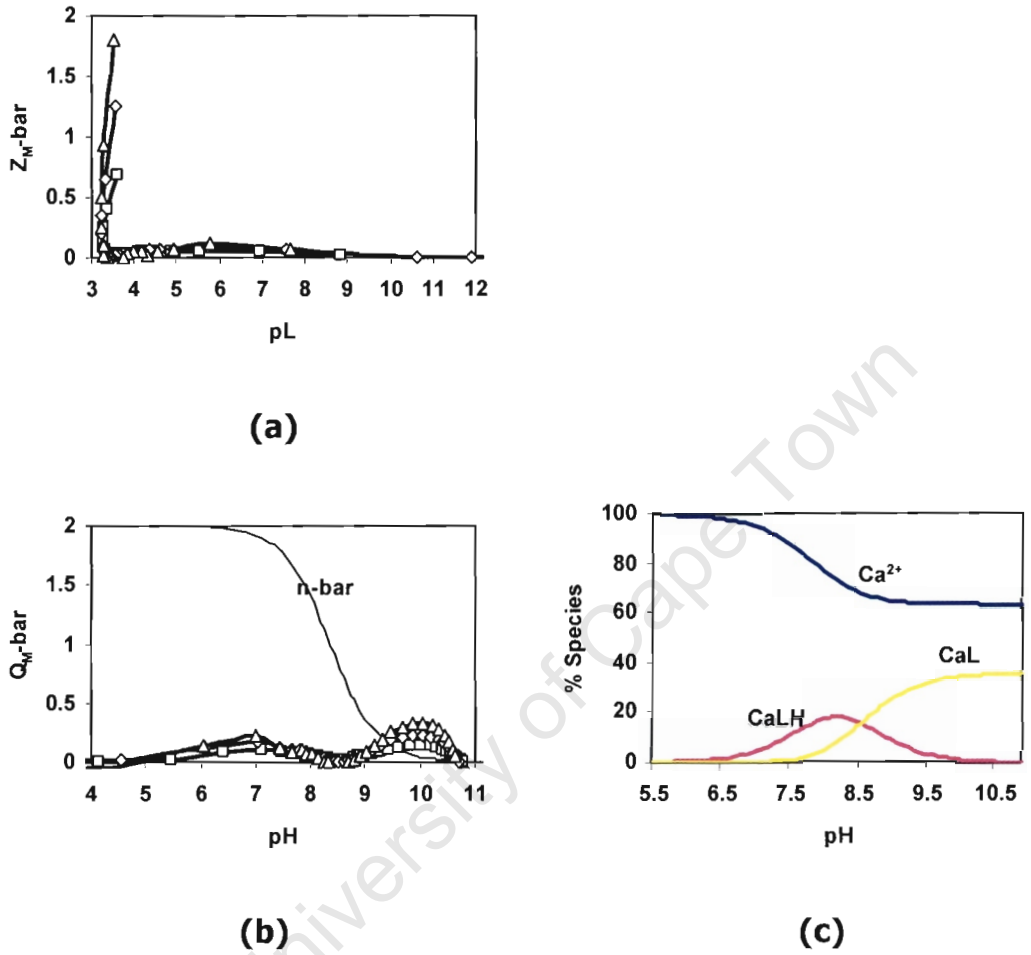

Figure 3.11 (a): Formation function and **(b):** deprotonation function curves [with M:L ratios 1:1(□), 1:2(◇) and 1:3(Δ), and theoretical (solid line) curve.] against pL and pH respectively and **(c):** calculated species distribution graphs [with M(0.00050 mol dm^{-3}) - L(0.00100 mol dm^{-3})] as a function of pH for ligand PrDM with Ca(II).

3.5.2.3 M^{2+}-PrDPr

The complexation of PrDPr with Cu(II) seems to be different from that of the PrDH and PrDM systems as observed from the formation and deprotonation functions in Figure 3.12(a) and 3.12(b) respectively. The Z_M-bar curves level off at ≈ 0.5 indicating that ML is not the predominant species in solution. The

splitting of the curves for different metal to ligand ratios is due to the presence of MLH. The fanning of Z_M-bar is indicative of hydroxo and/or mixed hydroxo species. Since a complete deprotonation (n-bar = 0) of PrDPr occurs at pH 6.2, the metal assisted deprotonation of the amide is likely to occur thus forming MLH_{-1} species.

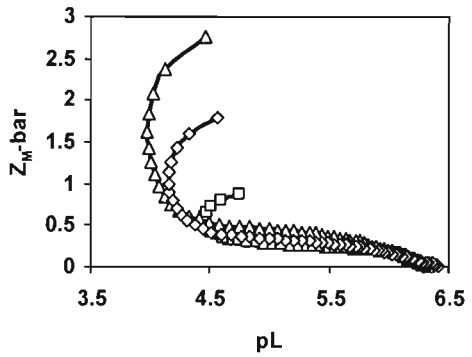

(a)

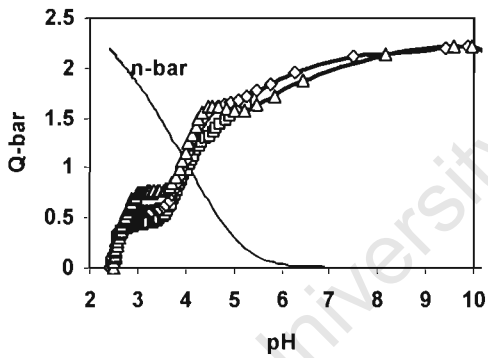

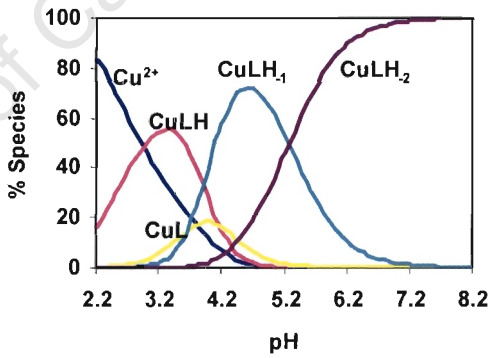

(b) **(c)**

Figure 3.12 (a): Formation function and **(b):** deprotonation function curves [with M:L ratios 1:1(□), 1:2(◇) and 1:3(Δ), and theoretical (solid line) curve.] against pL and pH respectively and **(c):** calculated species distribution graphs [with M(0.00051 mol dm^{-3}) - L(0.00101 mol dm^{-3})] as a function of pH for ligand PrDPr with Cu(II).

On the other hand Q_M-bar rises vertically at pH 2.5 revealing that complexation occurs at the very beginning of the titrations. In fact the speciation graphs in Figure 3.12(c) show that MLH is already formed (18% formation) at the start of the titration. The Q_M-bar levels off in the pH range

2.8 – 3.8 indicating no further complexation in this pH span. Another rise is observed at pH range 3.8 – 4.8 due to the formation of MLH_{-1} species and hydroxo species formed at pH > 4.8. Despite the split of the curves at different metal to ligand ratios due to the formation of MLH species, the theoretical and experimental formation and deprotonation functions have excellent agreement. This lends confidence to the selected model. The low standard deviations and Hamilton R-factors presented in Table 3.4 with corresponding formation constants confirm this model.

Table 3.4: $\log\beta_{pqr}$'s of PrDPr with Cu(II), Ni(II), Zn(II) and Ca(II) determined at 25 °C and I = 0.15 mol dm^{-3} $(Cl^-)Na^+$. Other symbols have their usual meaning as defined in Table 3.1.

Ligand	Metal ion	p q r	$Log\beta_{pqr}$	δ_{pqr}	R^H	$R_{lim}{}^H$	$n_T(n_P)$
PrDPr	Cu(II)	1 1 1	8.421	0.032	0.012	0.012	6(518)
		1 1 0	4.344	0.032			
		1 1 -1	0.575	0.021			
		1 1 -2	-4.679	0.028			
	Ni(II)	1 1 1	7.701	0.077	0.027	0.021	6(546)
		1 1 0	3.688	0.041			
		1 1 -1	-2.653	0.035			
		1 1 -2	-9.839	0.032			
	Zn(II)	1 1 1	6.903	0.038	0.011	0.012	6(518)
		1 1 0	2.764	0.036			
		1 1 -1	-3.903	0.026			
		1 1 -2	-10.983	0.014			
	Ca(II)	1 1 1	6.612	0.041	0.024	0.011	6(456)
		1 1 0	2.460	0.131			

The complexation behaviour of PrDPr with Ni(II) and Zn(II) are the same as revealed by the formation and deprotonation functions in Figure 3.13 and 3.14 respectively. At pL 6, Z_M-bars rise to ≈ 0.1 before falling to zero after which they rise again to Z_M-bar ≈ 0.5. This manoeuvre is also observed in the Q_M-bar curves. However, the percentage formation of species for the Ni(II)-PrDPr system is more than of Zn(II)-PrDPr for all species except MLH_{-2} as

shown in Figure 3.12(c) and 3.13(c) respectively. The formation constants for all the selected models are presented in Table 3.4.

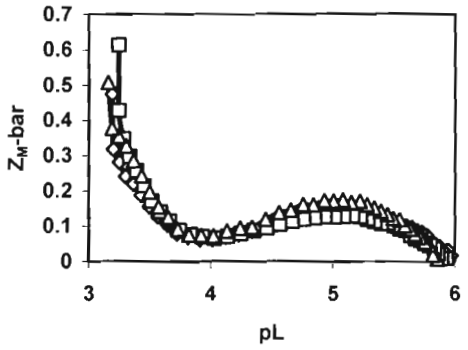

(a)

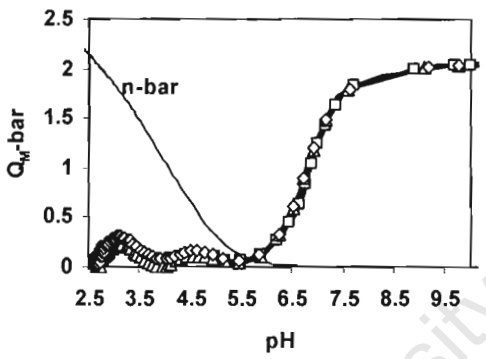

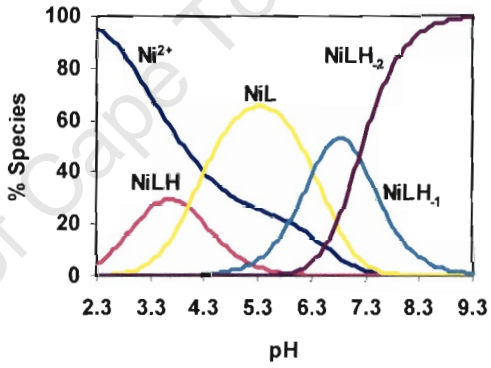

(b) **(c)**

Figure 3.13 (a): Formation function and **(b):** deprotonation function curves [with M:L ratios 1:1(□), 1:2(◇) and 1:3(Δ), and theoretical (solid line) curve.] against pL and pH respectively and **(c):** calculated species distribution graphs [with M(0.00050 mol dm^{-3}) - L(0.00101 mol dm^{-3})] as a function of pH for ligand PrDPr with Ni(II).

There is little or no interaction between Ca(II) and PrDPr in solution as observed from Z_M-bar and Q_M-bar functions in Figure 3.15(a) and 3.15(b) respectively. The species formed do not exceed 20% formation as seen in Figure 3.15(c) and the solution is mainly dominated by free Ca^{2+} ions in the pH investigated. However, the stability constants for all the species are presented in Table 3.4 with their corresponding low standard deviations and Hamilton R-factors.

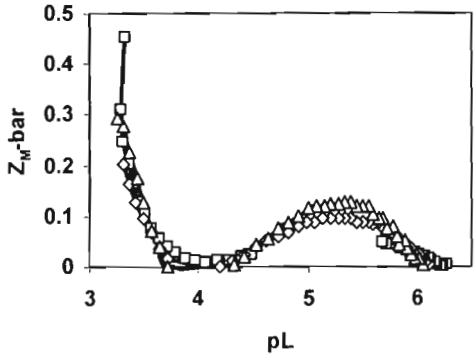

(a)

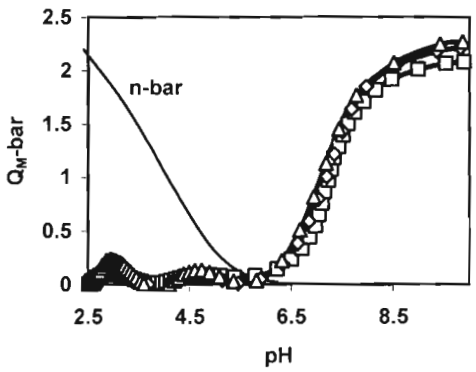

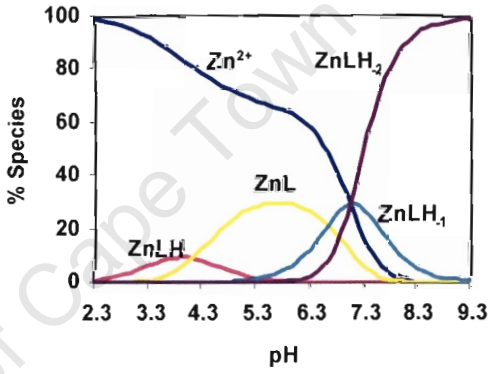

(b) **(c)**

Figure 3.14 (a): Formation function and **(b):** deprotonation function curves [with M:L ratios 1:1(□), 1:2(◇) and 1:3(Δ), and theoretical (solid line) curve.] against pL and pH respectively and **(c):** calculated species distribution graphs [with M(0.00047 mol dm^{-3}) - L(0.00100 mol dm^{-3})] as a function of pH for ligand PrDPr with Zn(II).

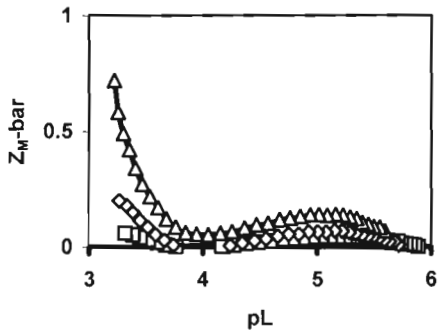

(a)

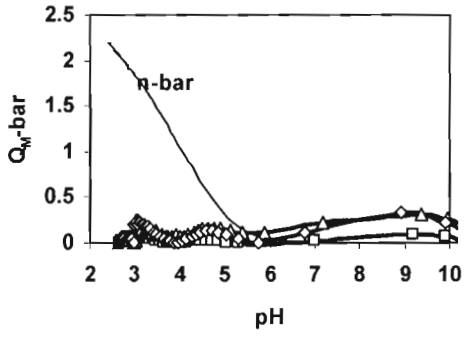

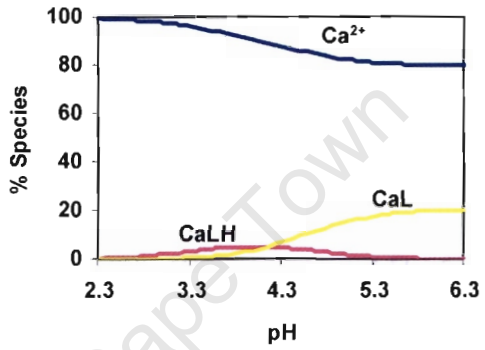

(b) **(c)**

Figure 3.15 (a): Formation function and **(b):** deprotonation function curves [with M:L ratios 1:1(□), 1:2(◇) and 1:3(△), and theoretical (solid line) curve.] against pL and pH respectively and **(c):** calculated species distribution graphs [with M(0.00050 mol dm^{-3}) - L(0.00100 mol dm^{-3})] as a function of pH for ligand PrDPr with Ca(II).

3.5.2.4 Discussion – Complexation

The ligands in this study are based on the pyridine-2,6-dicarboxamide moiety (Figure 3.16) and this contains two ethylene linkages. Once deprotonated the pyridine-2,6-dicarboxamido unit should be strictly planar and maintains planarity in various metal complexes.[40-42] The basal plane is defined by the N_{amido}-N_{py}-N_{amido} coordination by the planar pyridine-2,6-dicarboxamido portion of the ligand. The central pyridine nitrogen acts as an anchor for amide coordination. It is also the first one to be coordinated to the metal ion thus allowing the metal to be in close proximity for the amide ionization.

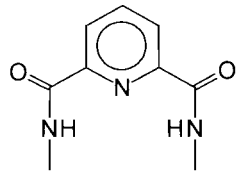

Figure 3.16: Pyridine-2,6-carboxamide unit

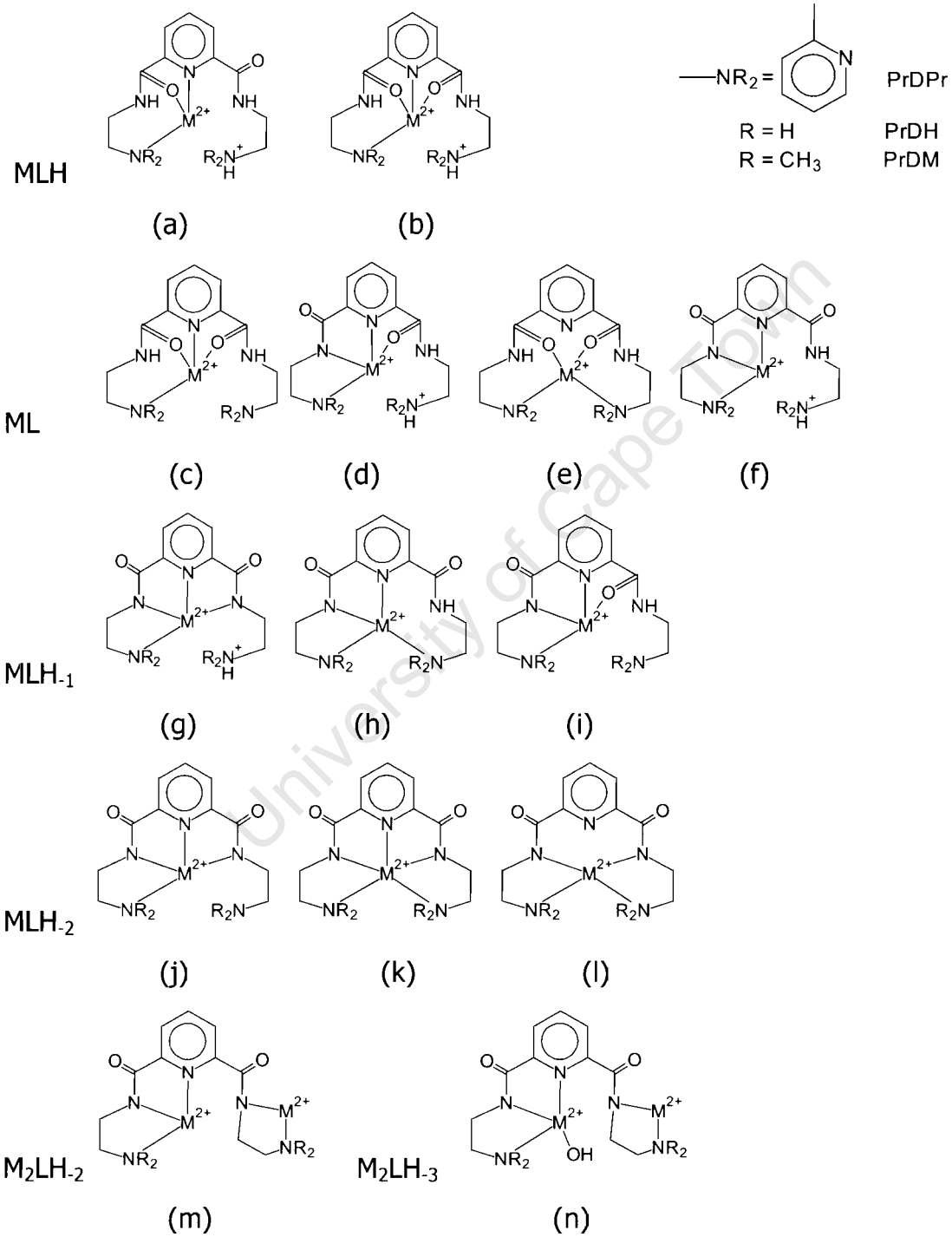

Figure 3.17: Schematic representation of proposed structures of the various Metal-Ligand species.

On the basis of the selected equilibria presented in Table 3.2-3.4 and Figure 3.4-3.15, the proposed structures for various species have been postulated and presented in Figure 3.17. The comparison of the formation constants for the mononuclear ML species of PrDH, PrDM and PrDPr with Cu(II) reveals that the ML species of Cu(II)-PrDH system has the greatest stability. This is probably due to less steric hindrance as different (-bulky) groups are introduced at the terminal sites. The value of $\log\beta_{110}$ for the Cu(II) complex of PrDH (=8.686) is 0.847 log units higher than that of PrDM (=7.839) and 4.342 log units higher than that corresponding constant of PrDPr (=4.344). Jackson and co-workers[43] have reported $\log\beta_{110}$ values in the range 9.22 – 10.77 for four related dioxo-penta nitrogen donor ligands, L^{3c} - L^{3f}, (Figure 3.18). The decrease in stability in the present study is due to the incorporation of the less basic or rather acidic pyridyl groups in the ligands.

The proposed structures of the MLH species for ligands in the present study are given in Figure 3.17(a,b). The MLH species is formed by the deprotonation and coordination of the central pyridyl nitrogen and one of the terminal amino/pyridyl nitrogens as well as coordination of one or both carbonyl oxygen(s) to the metal ion. Between the two structures, (a) seems a more likely coordination geometry. The coordination geometry of structure (b) may be destabilized by the rigidity of the pryridine moiety of the ligand in allowing both carbonyl oxygens coordination. It is expected that as the pH increases, Cu(II) would induce ionization of the amide protons[27,28] and there would also be a transition from Cu-O to Cu-N in the coordination arrangement.[44] The ML species is formed by the deprotonation of the MLH species and the possible structures of this species are given in Figure 3.17(c-f). The infrared study by Steenland and co-workers[32] on the coordination of Cu(II) by dioxo-pentaaza macrocycles, L^{3a} - L^{3b}, (Figure 3.18) in aqueous solution showed absorptions attributed to amide coordination to Cu(II) through the carbonyl oxygen in the MLH and ML species. From the four structures, (d) is highly strained due to the three contiguous five-membered chelate rings whereas (a) and (e) have less stable 7,5,5 and 7,8,7 membered

rings respectively. The rigidity of the pyridine moiety would also destabilize structures (c) and (e) upon coordination of Cu(II) through the carbonyl oxygens. Structure (f) is favoured due to the stable 5,5 membered rings.

The pK_a ($log\beta_{110}$ - $log\beta_{11-1}$) values for the conversion of ML to MLH_{-1} species for the Cu(II) complexes of PrDH, PrDM and PrDPr are 6.168, 7.01 and 3.769 respectively. Steenland and co-workers[32] measured pK_a ($log\beta_{110}$ - $log\beta_{11-1}$) values of 3.9 and 6.8 for the dioxo-pentaaza macrocycles while Jackson and co-workers[43] measured values in the range 7.03 – 8.13 for the linear dioxo-penta nitrogen donor ligands. The possible structures for the MLH_{-1} species are given in Figure 3.17(g-i). The structure (g) indicates that both amides are coordinated while one terminal amino/pyridyl group remains protonated. Brooker and co-workers[45] reported similar structures for Cu(II) with dioxo-penta nitrogen donor ligands. However, this structure is highly strained due to the three contiguous five-membered rings. Structure (h) has a less strained 8 membered ring and this makes (h) to be preferred over (g). Structure (i), where the amide and the carbonyl oxygen are coordinated to the metal ion while the terminal amino/pyridyl group is not, is unlikely.

The MLH_{-2} species forms from the deprotonation of MLH_{-1} species with pK_a ($log\beta_{11-1}$ - $log\beta_{11-2}$) values 10.157, 8.972 and 5.254 for Cu(II) with PrDH, PrDM and PrDPr respectively. These pK_a's are slightly higher than the corresponding first protonation constants of the free ligands. This proton could come from the coordinated water molecule or the coordinated amide nitrogen. The postulated structures of the MLH_{-2} species are given in Figure 3.17(j-l). The structure (j) has the uncoordinated terminal amino/pyridyl group while (l) has uncoordinated pyridine nitrogen. The structure (l) is less favoured over (j) due to the large 8 membered chelate ring. Structure (k) has all nitrogen atoms coordinated to the metal ion making this species to be more strained. The possible geometry of the MLH_{-2} species of the Cu(II) complexes are of distorted square pyramidal and distorted octahedral arrangement for N_5 and N_4 coordinate complexes respectively. The M_2LH_{-2}

and M_2LH_{-3} species are given in Figure 3.17(m) and 3.17(n) respectively. These polynuclear species are only found in the complexation of Cu(II) especially with PrDH and PrDM. These species are likely to be formed at low or rather 1:1 metal to ligand ratios.

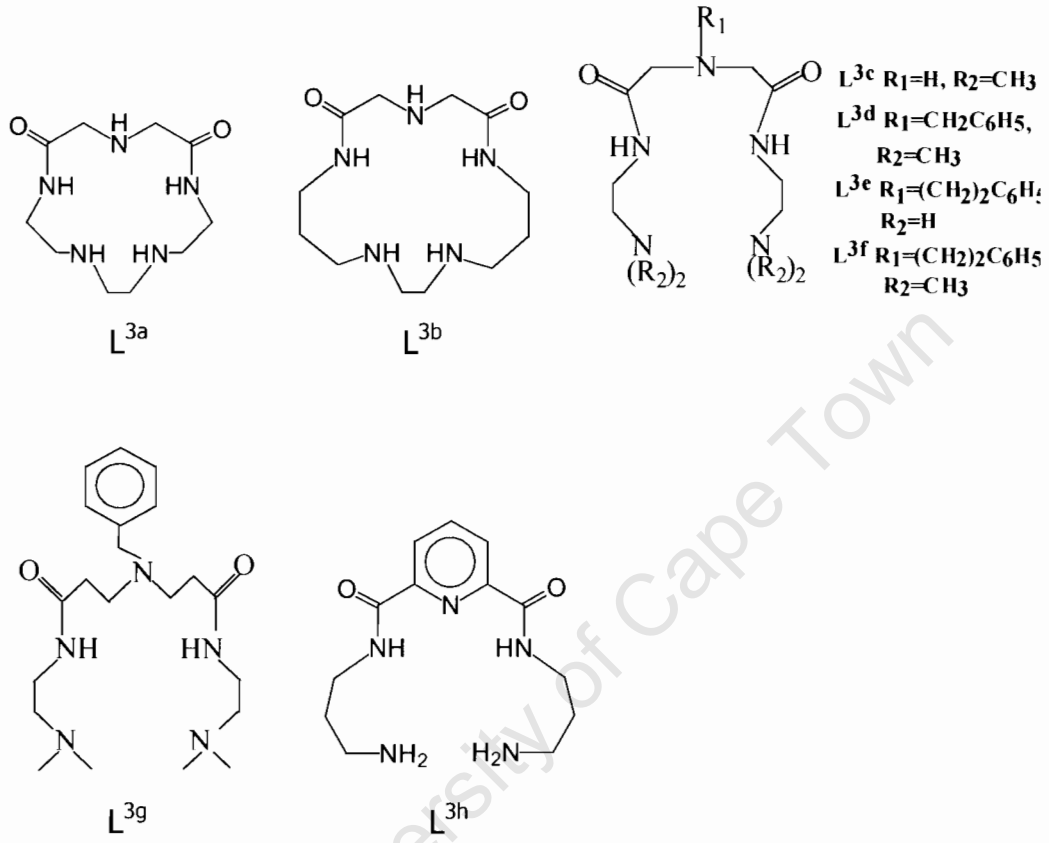

Figure 3.18: Schematic representation of ligands discussed in this chapter.

The formation equilibria for Ni(II), Zn(II) and Ca(II) show that these metal ions also form relatively stable complexes with PrDH, PrDM and PrDPr. However, it is observed that Cu(II) forms more stable complexes than these metal ions. For example, the stability constants (logβ's) of the ML species of PrDH with Cu(II), Ni(II), Zn(II) and Ca(II) are 8.686, 6.079, 4.293 and 3.007 respectively. The difference in stability of some 4-5 log units is observed between Cu(II) and the *in vivo* competitors Zn(II) and Ca(II). Unlike PrDH and PrDPr, the stability constant of the ML species of Zn(II)-PrDM ($\log\beta_{110}$=3.657) is greater than that of Ni(II)-PrDM ($\log\beta_{110}$=2.168) which is

contrary to the Irving-Williams series.[46] This is also evidenced by the corresponding formation and deprotonation function curves as shown in Figure 3.10(a,b) and 3.9(a,b). Amongst the four metal ions, Ca(II) forms weak complexes with all the ligands. Furthermore, Ca(II) does not induce amide deprotonation except for the PrDH system. It is observed that the stability of the M-L complexes is in the order M(II)-PrDH > M(II)-PrDM > M(II)-PrDPr. This is due to the different basicities of the terminal N-donor groups which is in the order $-NH_2$ > $-N(CH_3)_2$ > -Py.

For the complexation of PrDH with Ni(II) and Zn(II) for the formation of the MLH_{-1} species by the deprotonation of ML, the calculated pK_a ($log\beta_{110}$ - $log\beta_{11-1}$) values are 8.083 and 7.711 respectively. Like the Cu(II)-PrDH system the MLH_{-1} species predominates over a wide range of pH 7-11. Similarly the metal assisted deprotonated MLH_{-1} species of PrDM with Ni(II) and Zn(II) has pK_a values of 7.218 and 8.105 respectively. For Ni(II), the calculated pK_a values for the formation of the MLH_{-1} species of both PrDH and PrDM are 1.8-2.6 log units lower than the first and second hydrolysis constants of Ni(II) ($pK_{M\text{-}OH}$ = 9.86 and 9.14). On the other hand the pK_a values of the formation of MLH_{-1} species for Zn(II) with PrDH and PrDM are 1-1.5 log units lower than the first hydrolysis constant of Zn(II) ($pK_{M\text{-}OH}$ = 9.17). For the formation of the neutral MLH_{-2} species the calculated pK_a ($log\beta_{11-1}$ - $log\beta_{11-2}$) values are lower than the first hydrolysis constants of the metal ions for both ligands. However, direct evidence for the amide proton dissociation on complexation has been obtained from aqueous (D_2O) infrared studies for Cu(II) and Ni(II) complexes in solution.[32,47]

The low formation constants of the MLH_{-1} and MLH_{-2} species of the Zn(II) complexes as compared to those of Cu(II) and Ni(II) are due to the lesser ability of Zn(II) to deprotonate the amide moieties.[48] It is known that Zn(II) prefers a tetrahedral geometry as observed with the majority of its simple systems.[49,50] It has been reported that the linear and macrocyclic dioxo-tetra N-donor ligands form square planar coordinate geometry with both Cu(II) and

Ni(II) in solution while macrocyclic dioxo-penta N-donor ligands form square pyramidal or distorted octahedral coordinate geometry.[51-53] For the distorted octahedron, four nitrogen atoms are bound in the plane whereas the fifth nitrogen and water molecule occupy the axial positions. However, it was also observed that Cu(II) forms more stable complexes with tetra N-donor ligands than penta N-donor ligands.[52]

Brooker and co-workers[45,54] have designed and studied 2,6-bis(1-propanecarboxamido-3-amino)pyridine, L^{3h}, (Figure 3.18) in solid state and solution for Cu(II) and Ni(II) complexation. This ligand is analogous to PrDH and PrDM. Cu(II) formed a square pyramidal complex with four basal plane nitrogen donor atoms and an apical site occupied by an oxygen donor from acetate ion. On other hand, Ni(II) formed square planar geometry with four coordinated nitrogen donor atoms. Of interest is to observe that the uncoordinated terminal amino group is protonated while both amides are coordinated. This is also observed for both PrDH and PrDM with Cu(II) whereby the MLH_{-1} species forms at low pH (pH 5.5). This is indicative of the ability of Cu(II) to deprotonate the amide groups and also that the central pyridine nitrogen plays a major role as an anchor for the metal coordination. At high pH the terminal amino groups would be deprotonated thus forming MLH_{-2} species.

The coordination chemistry of PrDPr with Cu(II) Ni(II) and Zn(II) has been studied in solid state.[42,55] This ligand is found to form a binuclear structure of $[Cu_2(PrDPr)_2]$ as a major complex and monomeric CuPrDPr as a minor complex. Ni(II) and Zn(II) form trinuclear complexes as major species. However, the minor monomeric species of the metal ions suggested four N-donor coordination arrangements with uncoordinated terminal pyridine groups. The present study of PrDPr with Cu(II), Ni(II) and Zn(II) indicates that four different mononuclear species are formed in solution. The MLH_{-1} and MLH_{-2} species form at low pH and the speciation graphs show that there is already complexation at the start of the titration. This is due to the

incorporation of the pyridyl groups which tend to coordinate to metal ions at low pH. The calculated pK_a ($log\beta_{111}$ - $log\beta_{110}$) values (≈4) of the formation of the ML species are close to the first and second protonation constants of the ligand (pK_{a1} = 4.624 and pK_{a2} = 3.508) for all the four metal ions investigated. The deprotonation of the amide groups results in the formation of the MLH_{-1} and MLH_{-2} species for all metal ions except Ca(II). These species are formed below and/or at physiological pH. The calculated pK_a ($log\beta_{110}$ - $log\beta_{11-1}$, $log\beta_{11-1}$ - $log\beta_{11-2}$,) values of the formation of these species are lower than the first and second hydrolysis constants respectively of the corresponding metal ions.

Table 3.5: Selectivity factors of the studied ligands towards Cu(II) compared with the other investigated metal ions.

Ligand	Cu(II)/Ni(II)	Cu(II)/Zn(II)	Cu(II)/Ca(II)
PrDH	4.336	5.936	11.384
PrDM	6.703	5.165	
PrDPr	3.228	4.478	

The metal ion selectivity of a ligand is generally defined as the difference in the formation constants of the complexes formed with all metal ions likely to be present under the same conditions of pH.[56,57] In this study the selectivity of Cu(II) is defined as the difference in formation constants of $[CuLH_{-1}]$ with that of the corresponding species for a particular M-L system. The MLH_{-1} species has been chosen because it forms at the physiological pH for Cu(II) with PrDH, PrDM and PrDPr. The calculated selectivity factors given in Table 3.5 indicate that the studied ligands are more selective for Cu(II) as compared to Ni(II), Zn(II) and Ca(II). The calculated selectivity factors are in the range of 3-11 orders of magnitude in favour of Cu(II). The higher formation constants of Cu(II) with these ligands are due to the ease with which this metal ion deprotonates the amide groups. The selectivity factors are in the order Cu(II)/Ca(II) > Cu(II)/Zn(II) > Cu(II)/Ni(II) except for PrDM

that has the order Cu(II)/Ni(II) > Cu(II)/Zn(II) which contradicts the Irving-Williams series.[46] However, the selectivity demonstrates favourable complexation for Cu(II) by these ligands relative to the *in vivo* competitors, Zn(II) and Ca(II). The *in vivo* Zn(II) and Ca(II) ions are present in high concentrations and therefore, could upset the favourable selectivity for Cu(II). Moreover, the favourable selectivity for Cu(II) over these metal ions is brought about by the preferred tetragonally distorted geometry due to the ligand field Jahn-Teller distortion. This is observed in the copper-carrying plasma protein, albumin, whereby peptide nitrogens are ionized and Cu(II) bonds in roughly square planar fashion to four nitrogens.[58] A further study on selectivity will be discussed later under the blood plasma modelling section in Chapter 5.

References

1. Martell A.E., Motekaitis R.J., *Determination and Use of Stability Constants*, 1988, VCH, New York.
2. Linder P.W., Torrington R.G., Williams D.R., *Analysis Using Glass Electrodes*, 1984, Open University Press, Milton Keynes.
3. Hughes M.N., *The Inorganic Chemistry of Biological Processes*, 1972, John Wiley and Sons, London.
4. Martell A.E., Smith R.M., Motekaitis R.J., *NIST Critical Stability Constants of Metal Complexes Database,* 1993, Texas A & M University College Station, TX.
5. Williams D.R. (ed), *An Introduction to Bioinorganic Chemistry*, 1976, Charles C. Thomas, USA.
6. Hartley F.R., Burgess C., Alcock R., *Solution Equilibria*, 1980, 33-144.
7. Rossotti F.J.C., Rossotti H., *The Determination of Stability Constants, and other Equilibrium Constants in Solution,* 1961, McGraw-Hill Book Company, Inc., New York.
8. Eisenman G., *Glass Electrodes for Hydrogen and other Cations, Principles and Practice*, 1967, Marcel Dekker, Inc., New York.
9. Beck M.T., Nagypal I., *Chemistry of Complex Equilibria*, 1990, Ellis Horwood Ltd, Chichester.
10. May P.M., Murray K., Williams D.R., *Talanta*, 1985, **32**, no6, 483-489.
11. Katz A.K., Glusker J.P., Beebe S.A., Bock C.W., *J. Am. Chem. Soc.*, 1996, **118**, 5752-5763.
12. Jackson G.E., Kelly M. J., *J. Chem. Soc. Daltan Trans.*, 1989, 2429-2433.
13. Jackson G.E., Nakani B.S., *J. Chem. Soc. Daltan Trans.*, 1996, 1373-1377.
14. Willard H.H., Merritt L.L., Dean J.A., Settle F.A., *Instrumental Methods of Analysis*, 7th ed, 1988, Wadsworth Publishing Company, Calfornia.
15. Murray K., May P.M., *ESTA (Equilibrium Simulation for Titration Analysis) manual*, Version.3, 1989, UWIST, Cardiff, Wales.

16. May P.M., Murray K., Williams D.R., *Talanta*, 1988, **35**, no11, 825-830.
17. May P.M., Murray K., Williams D.R., *Talanta*, 1988, **35**, no12, 927-932.
18. Vacca A., Sabatini A., Gristina M.A., *Coord. Chem. Rev.* 1972, **8**, 45-53.
19. Bassett J., Denny R.C., Jeffrey G.H., Mendham J. (Eds), Vogel's Textbook of *Quantitave Inorganic Analysis including Elementary Instrumental Analysis*, 1978, Longman, London.
20. Rossotti J.C., Rossotti H., *J. Chem. Education*, 1965, **42**, 375-378.
21. Furniss B.S., Hannaford A.J., Smith P.W.G., Tatchell A.R., *Vogel's Textbook of Practical Organic Chemistry*, 5th ed, 1989, Longman Scientific and Technical, England.
22. Gran G., *Analyst*, 1952, **77**, 661-671.
23. Gran G., *Acta Chem. Scand.*, 1950, **4**, 559-577.
24. Baes C.F., Mesmer R.E., *Hydrolysis of Cations*, 1976, John Wiley and Sons, New York.
25. Motekaitis R.J., Martell A.E., *Inorg. Chem.*, 1988, **27**, 2718 – 2724.
26. Odisitse S., *MSc Thesis*, 2003, University of Cape Town, South Africa.
27. Bai S.K., Martell A.E., *J. Am. Chem. Soc.* 1969, **91**(16), 4412-4420.
28. Jubert C., Mohamadou A., Gerard C., Brandes S., Tabard A., Barbier J.P., *J. Chem. Soc. Dalton Trans.*, 2002, 2660-2669.
29. Jackson G.E., Linder P.W., Voyé A., *J. Chem. Soc. Dalton Trans.*, 1996, 4605-4612.
30. Nomkoko E.T., Jackson G.E., Nakani B.S., *J. Chem. Soc. Dalton Trans.*, 2004, 1432-1440.
31. Chen D., Sun Y., Martell A.E., Welch M.J., *Inorg. Chim. Acta,* 2002, **335**, 119-124.
32. Steenland M.W.A., Dierck I, Herman G.G. Devreese B., Lippens W., Van Beeumen J., Goeminne A.M, *J. Chem. Soc., Dalton Trans.*, 1997, 3637-3642.
33. Kapinos L.E., Sigel H., *Inorg. Chim. Acta*, 2002, **37**, 131-142.

34. Griesser R., Fallab S., *Chimia,* 1968, **22**, no2, 90-92.
35. Martell A.E., Smith R.M., *Critical Stability Constants*, vol2, 1975, Plenum Press, New York and London.
36. Voye A., *PhD Thesis*, 1993, University of Cape Town, South Africa.
37. Ojima H., Nonoyama K., *Coord. Chem. Rev.*, 1988, **92**, 85–111.
38. Kodama M., Yatsunami T., Kimura E., *J. Chem. Soc., Dalton Trans.*, 1979, 1783–1788.
39. de Witt G.C., May P.M., Webb J., Hetfer G., *Inorg. Chim. Acta,* 1998, **275-276,** 37-42.
40. Rowland J.M., Thornton M.L., Olmstead M.M., Mascharak P.K., *Inorg. Chem.,* 2001, **40**, 1069-1073.
41. Charez F.A., Olmstead M.M., Mascharak P.K., *Inorg. Chem.,* 1996, **35**, 1410-1412.
42. Marlin D.S., Olmstead M.M., Mascharak P.K., *Inorg. Chim. Acta,* 2001, **323,** 1-4.
43. Jackson G.E., Voye A., Kelly M., *J. Inorg Biochem.,* 2000, **79,** 147-152.
44. Chung-Sun C., Liu Si-Han., *Polyhedron*, 1984, **3**, no5, 559-566.
45. Brooker S., Dunbar G.S., Plieger P.G., *Inorg. Chim. Acta,* 2000, **304,** 204-209.
46. Williams D.R., *The Metals of Life*, 1971, van Nostrand Reinhold Company, London.
47. Steenland M.W.A., Westbroek P., Dierck I., Herman G.G., Lippens W., Temmerman E., Goeminne A.M., *Polyhedron*, 1999, **18,** 3417-3424.
48. Santos M.A., Gaspar M., Amorium M.T., *Inorg. Chim. Acta,* 1999, **284,** 20-29.
49. Koike T., Kimura E., *J. Am. Chem. Soc.,* 1991, **113**(23), 8935–8941.
50. Kimura E., Shiota T., Koike T., Shiro M., Kodama M., *J. Am. Chem. Soc.*, 1990, **112**(15), 5805–5811.
51. Fabbrizzi L., Micheloni M., Paeletti P., Poggi A., *J. Chem. Soc., Dalton Trans.*, 1981, 1438–1441.

52. Kimura E., Machida R., Kodama M., *J. Am. Chem. Soc.,* 1984, **106**, 5497–5505.
53. Machida R., Kimura E., Kushi Y., *Inorg. Chem.,* 1986, **25**, 3461-3466.
54. Brooker S., Dunbar G.S., Plieger P.G., *Polyhedron,* 1999, **18,** 679-688.
55. Alcock N.W., Clarkson G., Glover P.B., Lawrance G.A., Moore P., Napitupulu M., *J. Chem. Soc., Dalton Trans.*, 2005, 518–527.
56. Fuzerova S., Kotek J., Cisarova I., Hermann P., Binnemans K., Lukes I., *J. Chem. Soc., Dalton Trans.*, 2005, 2908–2915.
57. Damu K.V., Shaikjee M.S., Michael J.P., Howard A.S., Hancock R.D., *Inorg. Chem.,* 1986, **25,** 3879-3883.
58. Frausto da Silva J.J.R., Williams R.J.P., *The Biological Chemistry of Elements; The inorganic chemistry of life,* 1991, Clarendon Press, Oxford.

CHAPTER FOUR

SPECTROSCOPY AND MOLECULAR MODELLING

4. SPECTROSCOPY AND MOLECULAR MODELLING

4.1 NUCLEAR MAGNETIC RESONANCE

4.1.1 Introduction

Nuclear magnetic resonance (NMR) is an important tool in the investigation of chemical structures and reaction mechanisms. It has been extended to whole body imaging in medical diagnosis.[1] In this study NMR is used to determine the sequence of protonation of PrDH, PrDM and PrDPr. The presence of the proton is expected to shift the NMR signals arising from protons attached to the neighbouring carbons. It has also been used to gain some insights as to the site of metal coordination as upon complexation by Cu(II), the presence of the metal ion is expected to broaden and shift the signals arising from protons attached to neighbouring carbons being most affected.[2]

4.1.2 Experimental

In 5 cm^3 glass vials, two cm^3 portions of 0.015 mol dm^{-3} stock D_2O solution of PrDH, PrDM and PrDPr were prepared and the ^1H NMR spectra recorded on a Varian Unity Plus 400 MHz instrument. The pH of the solutions was adjusted using concentrated NaOH and HCl. Tertiary butyl alcohol was used as an internal reference. A micro-pH 2000 meter was used to measure the pH of the solutions. Solutions of 1:2 molar ratio of the metal to ligand for Cu(II)-PrDH, Cu(II)-PrDM and Cu(II)-PrDPr systems were prepared in D_2O and scanned in the pH range 1-11.

4.1.3 Results and discussion

4.1.3.1 Cu(II)-PrDH system

Figure 4.1(a) shows proton NMR spectra for the protonation of PrDH in D_2O. As the pH of the solution increases, some of the NMR signals shift up field. The shift is a result of protonation, the protons closest to the site of protonation being most affected.

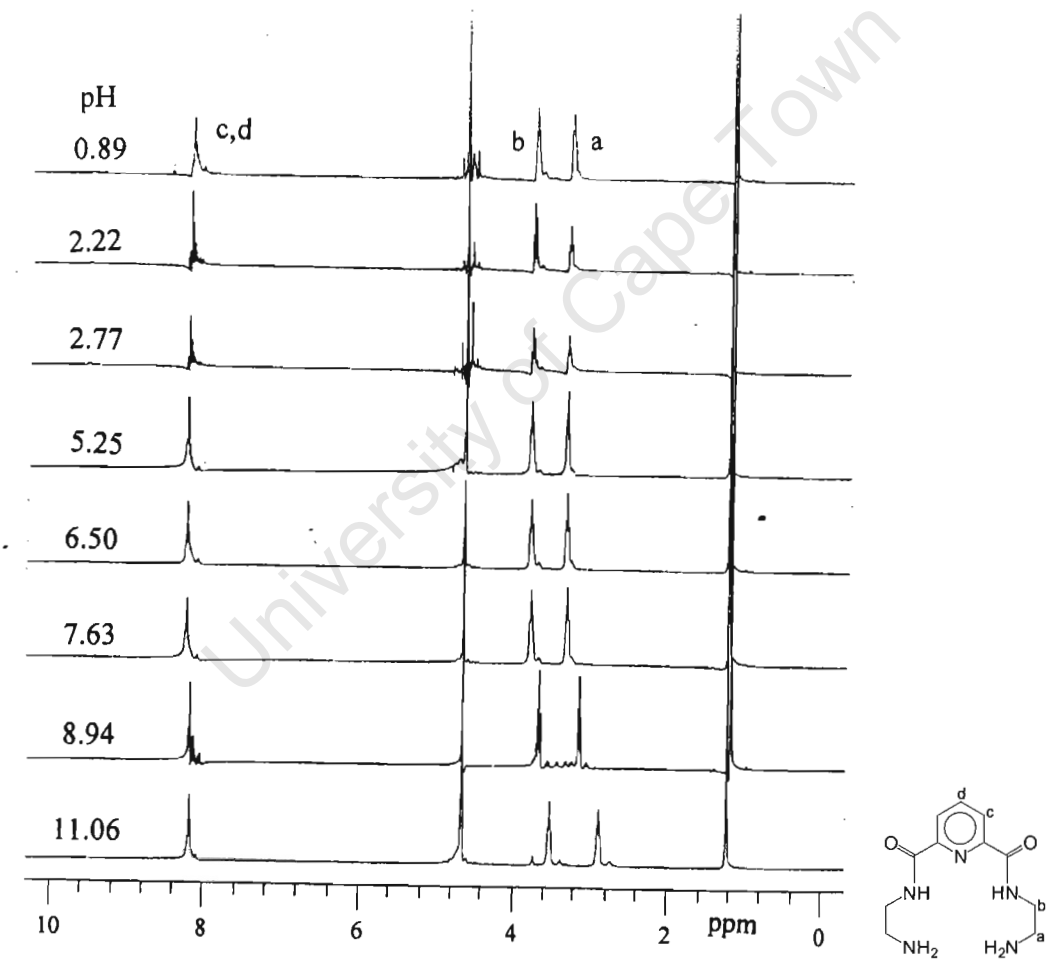

Figure 4.1(a): Proton NMR spectra of PrDH as a function of pH.

Figure 4.1(b) shows a plot of proton chemical shifts as a function of pH, where a, b and c,d refer to the chemical shifts of the protons attached to carbons next to the amine groups, amide groups and protons attached to

carbons of the pyridine ring respectively. There is a small change in the chemical shift of the c,d-protons as compared to the a- and b-protons. However, a noticeable change is observed at pH value of about 2 due to the deprotonation at the pyridyl nitrogen. The plots of change in proton chemical shift show approximate pK_a values of about 2 and 9 which are in good agreement with the values obtained from potentiometric studies.

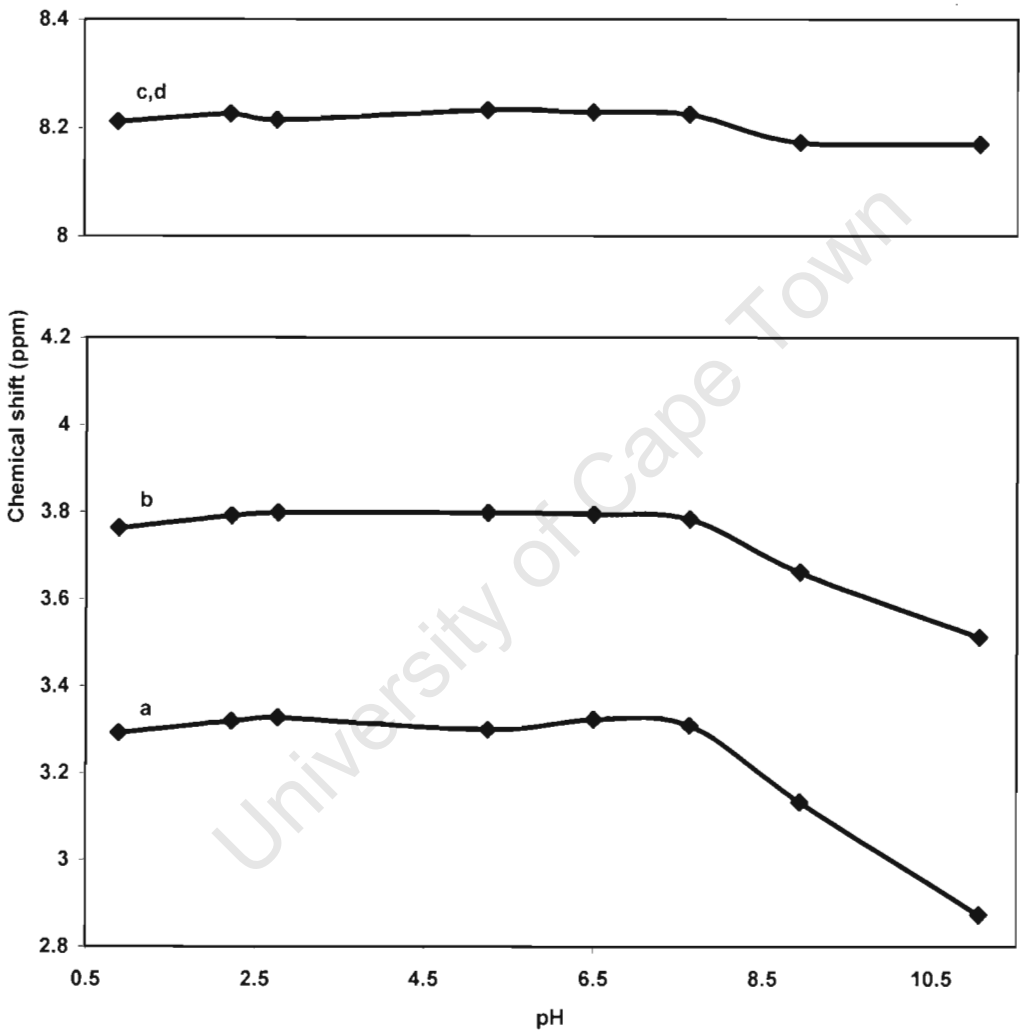

Figure 4.1(b): Change in proton chemical shift (ppm) as a function of pH for PrDH system.

Figure 4.1(c) shows the effect of Cu(II) upon the spectra of PrDH as a function of pH. Since Cu(II) is paramagnetic, it tends to broaden and shift the signals arising from protons attached to neighbouring carbons as observed in Figure 4.1(c). From the speciation graphs in Figure 3.4(c), complexation of

the free ligand starts at pH 5 and, therefore a change in NMR spectra signals is expected at pH>5. The signals a, b and c,d in Figure 4.1(c) broaden and shift as pH increases. The signal arising from protons attached to carbons next to the amine groups virtually disappear at pH 6.69 due to the closeness of the Cu(II) ion. These two possibilities cannot be distinguished as the system is in rapid chemical exchange on the NMR time scale. This indicates that either one or both amine groups are coordinated to the metal ion. The signals arising from protons attached to carbons next to the amide groups also broaden and shift to up field. This is indicative of coordination of the metal ion to at least one amide group as pH increases. It is also observed that protons (c,d) at the carbons of the pyridine ring virtually disappear due to the closeness of the Cu(II) ion coordinated to the pyridyl nitrogen. From these results it is clear that the metal coordinates to all the nitrogen centers.

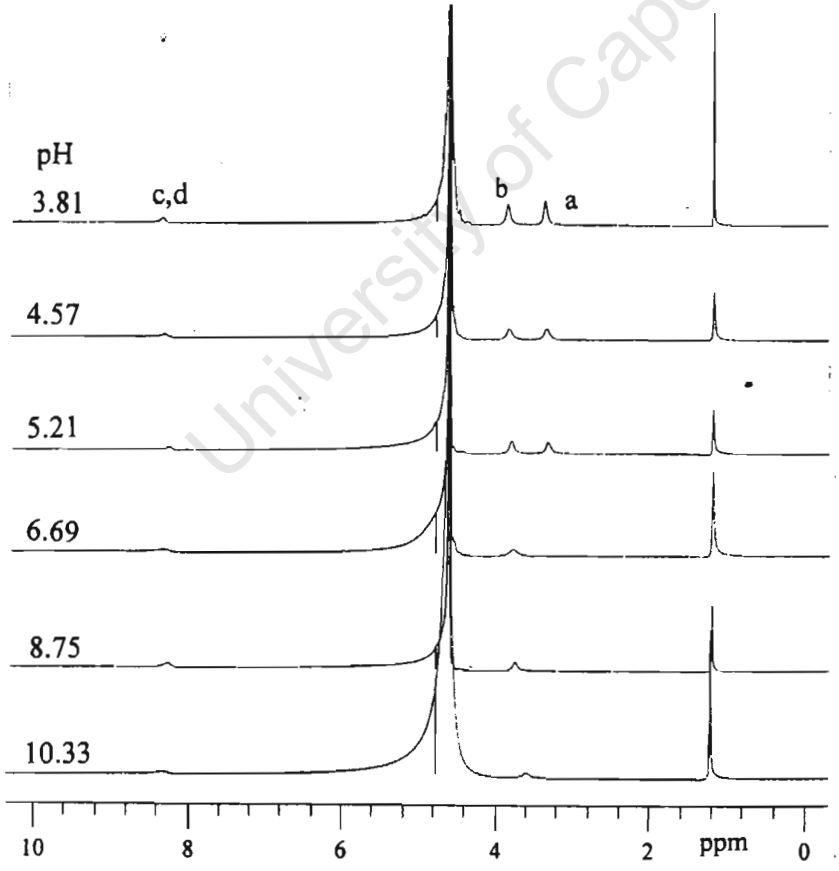

Figure 4.1(c): Proton NMR spectra for complexation of Cu(II) with PrDH as a function of pH.

4.1.3.2 Cu(II)-PrDM system

Figure 4.1(d) shows proton NMR spectra for protonation of PrDM. Like for the PrDH system, there is shift in NMR signals to up field as the pH increases due to protonation of the terminal amino and pyridyl nitrogen groups. A significant chemical shift is observed for protons attached to carbons next to the amino groups at positions, a and b. It must be noted that the signal due to a-protons has a high height such that it cuts through the spectra at the top.

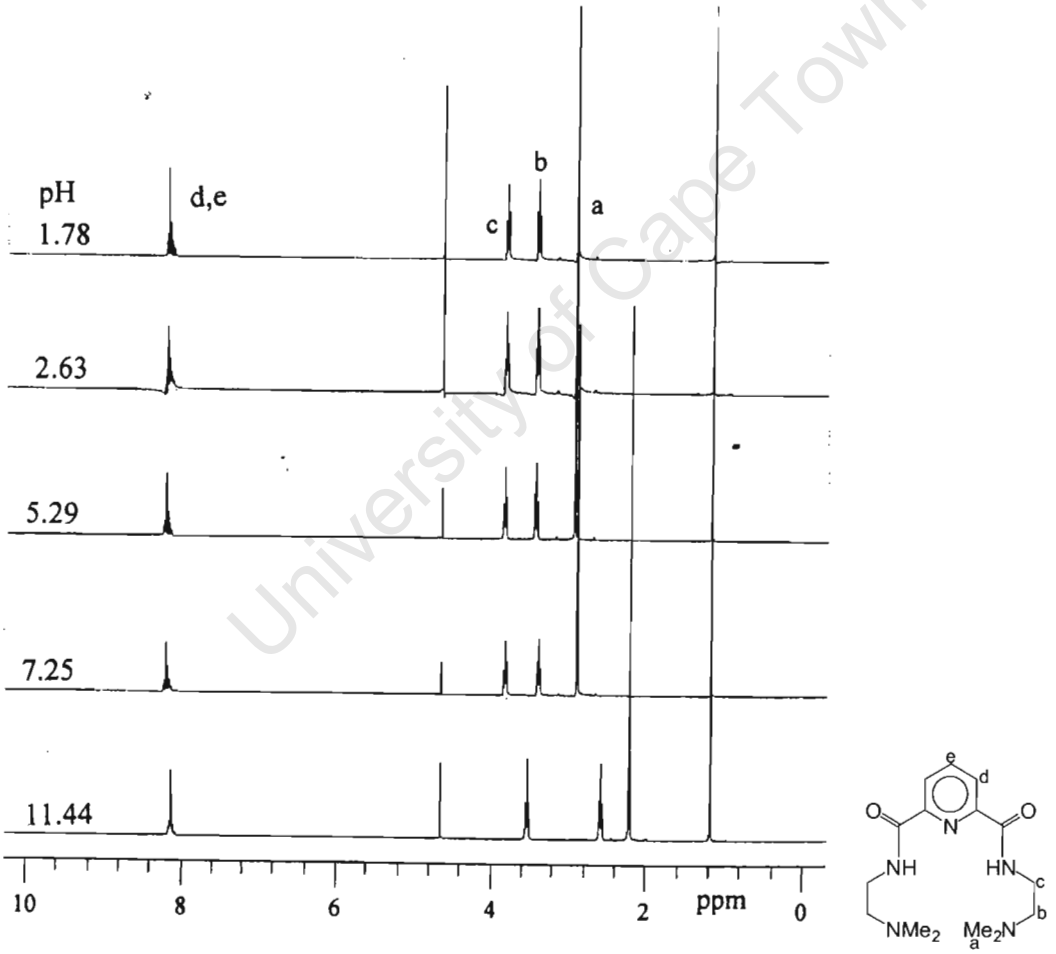

Figure 4.1(d): Proton NMR spectra of PrDM as a function of pH.

Figure 4.1(e) shows plots of proton chemical shifts as function of pH, where a, b, c and d,e refer to the protons attached to carbons on the ligand in Figure 4.1(d). The change in chemical shifts arising from protons on the

neighbouring carbons is similar to that of the PrDH system except that there is an additional signal arising from a-protons of the terminal methyl groups. The approximate pK_a value of 8.5 is in good agreement with the value of 8.647 obtained by potentiometric studies.

Figure 4.1(f) shows the spectra for complexation of Cu(II) with PrDM as a function of pH. Like for the Cu(II)-PrDH system, NMR signals arising from protons attached to neighbouring carbons broaden and shift to up field due to complexation. Complexation of the free ligand starts at pH 5 as shown by the species distribution curves in Figure 3.8(c). The change in NMR spectra signals is similar to that of the Cu(II)-PrDH system indicating that indeed complexation takes place at all the nitrogen centers.

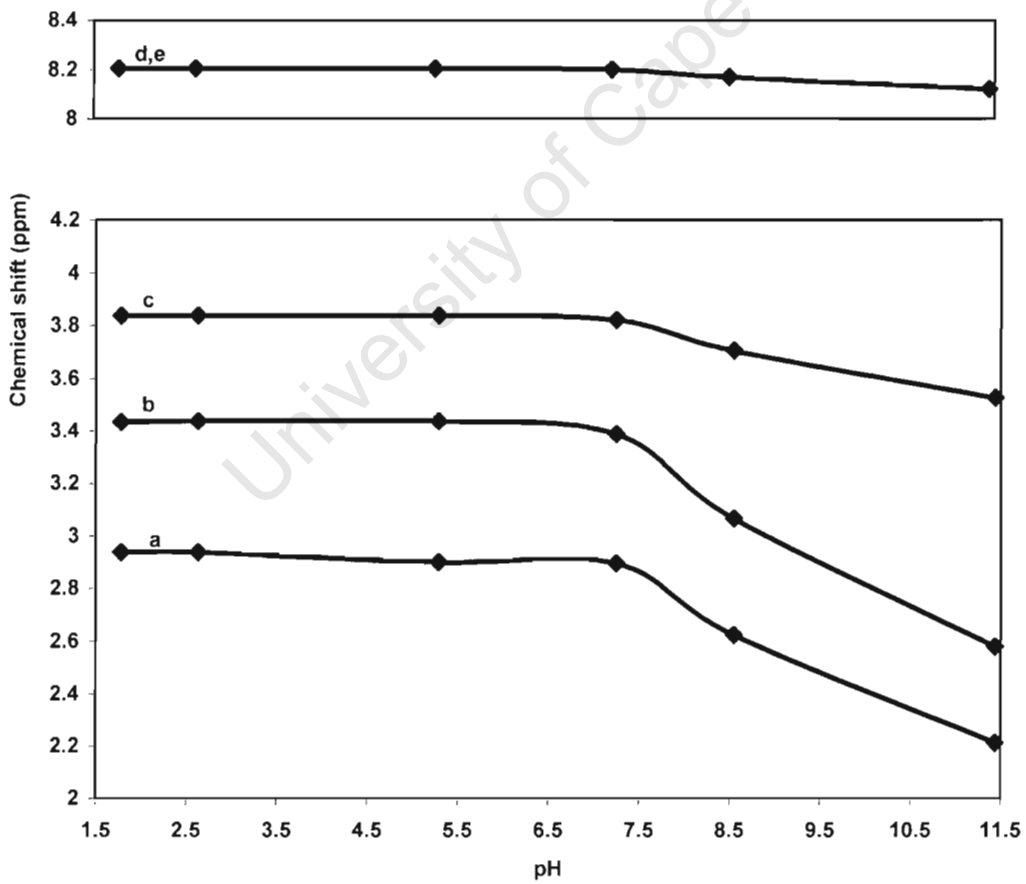

Figure 4.1(e): Change in proton chemical shift (ppm) as a function of pH for the PrDM system.

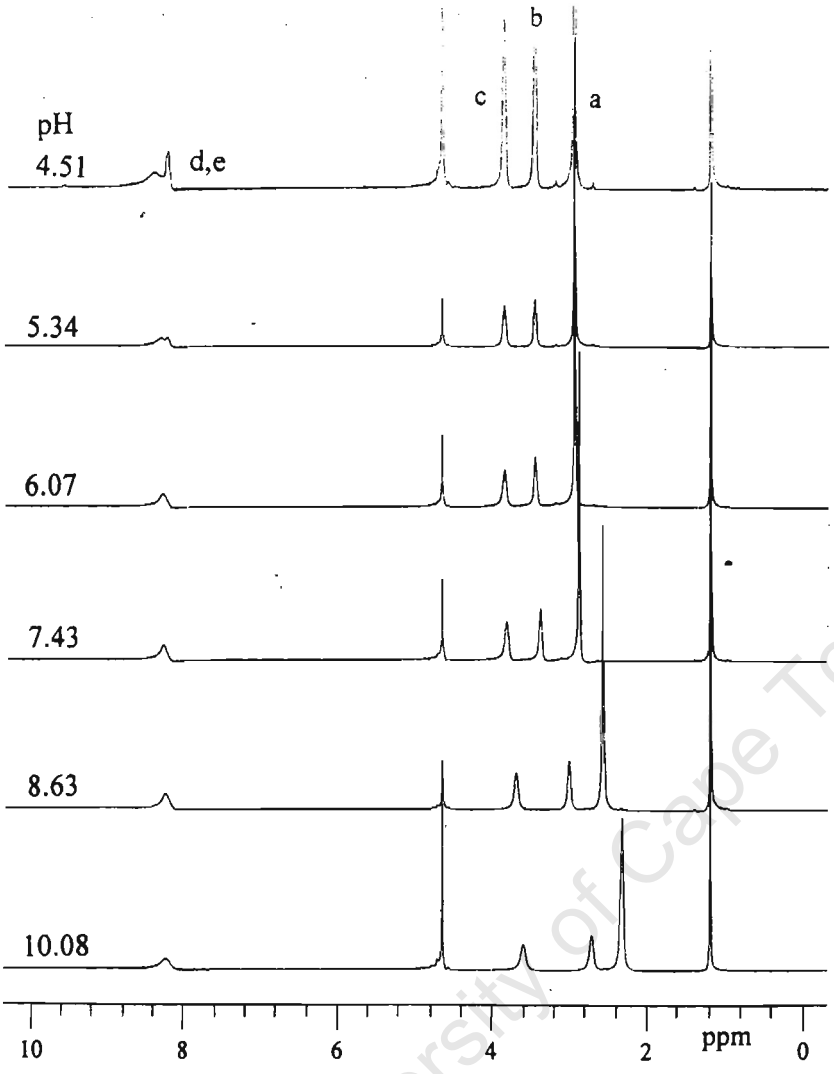

Figure 4.1(f): Proton NMR spectra for complexation of Cu(II) with PrDM as a function of pH.

4.1.3.3 Cu(II)-PrDPr system

The NMR spectra showing the protonation of PrDPr is shown in Figure 4.1(g). Unlike the other two systems, protonation of the PrDPr system begins at low pH as shown in Figure 3.3(b). The proton NMR signals show significant differences in chemical shift at pH 3.31 and 4.04 (Figure 4.1(g)) as a result of protonation of the pyridyl nitrogen.

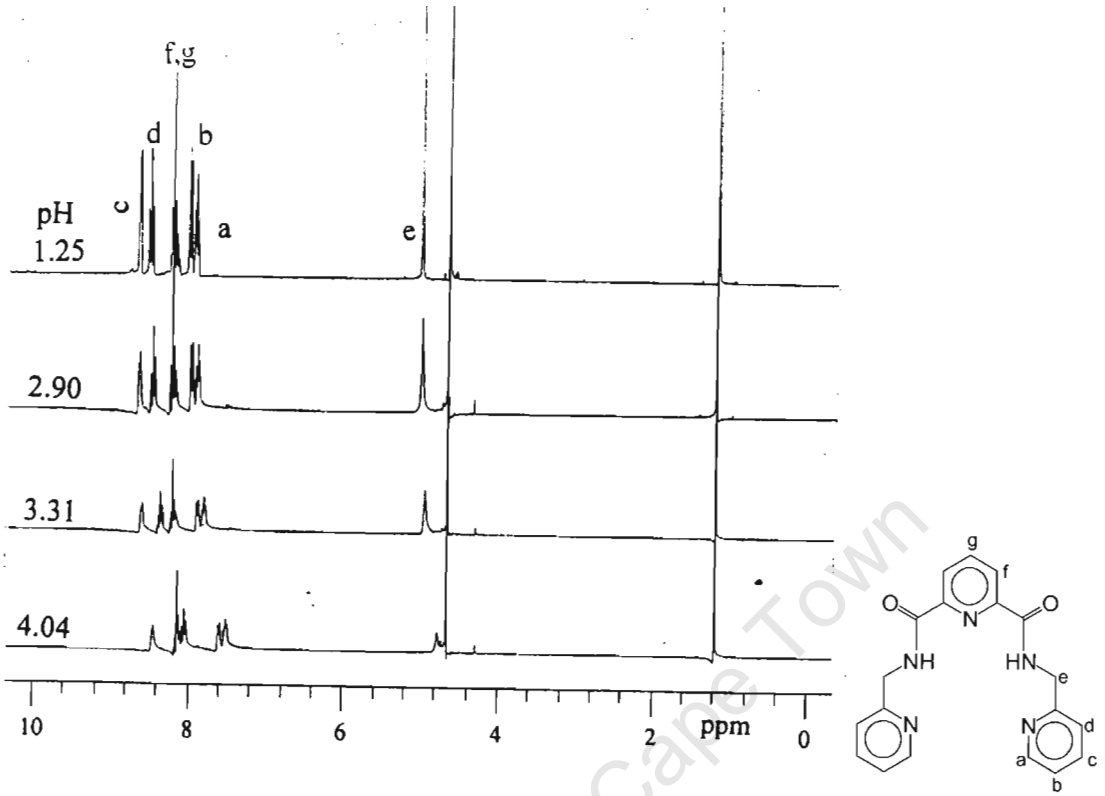

Figure 4.1(g): Proton NMR spectra of PrDPr as a function of pH.

Plots of chemical shift in Figure 4.1(h) arise from protons attached to the pyridyl nitrogens and amide groups. Like other two systems in this study, the NMR signals shift to up field as the pH increases. Figure 4.1(i) shows spectra for the complexation of Cu(II) with PrDPr. The spectra show that there is complexation at pH 1.60, and NMR signals broaden and shift to up field as the pH increases. All signals virtually disappear at pH 4.86. This is indicative of the closeness of Cu(II) to the pyridyl and amide nitrogens. The speciation graphs in Figure 3.12(c) also show that there is already complexation at pH 2.2 thus agreeing with the NMR results.

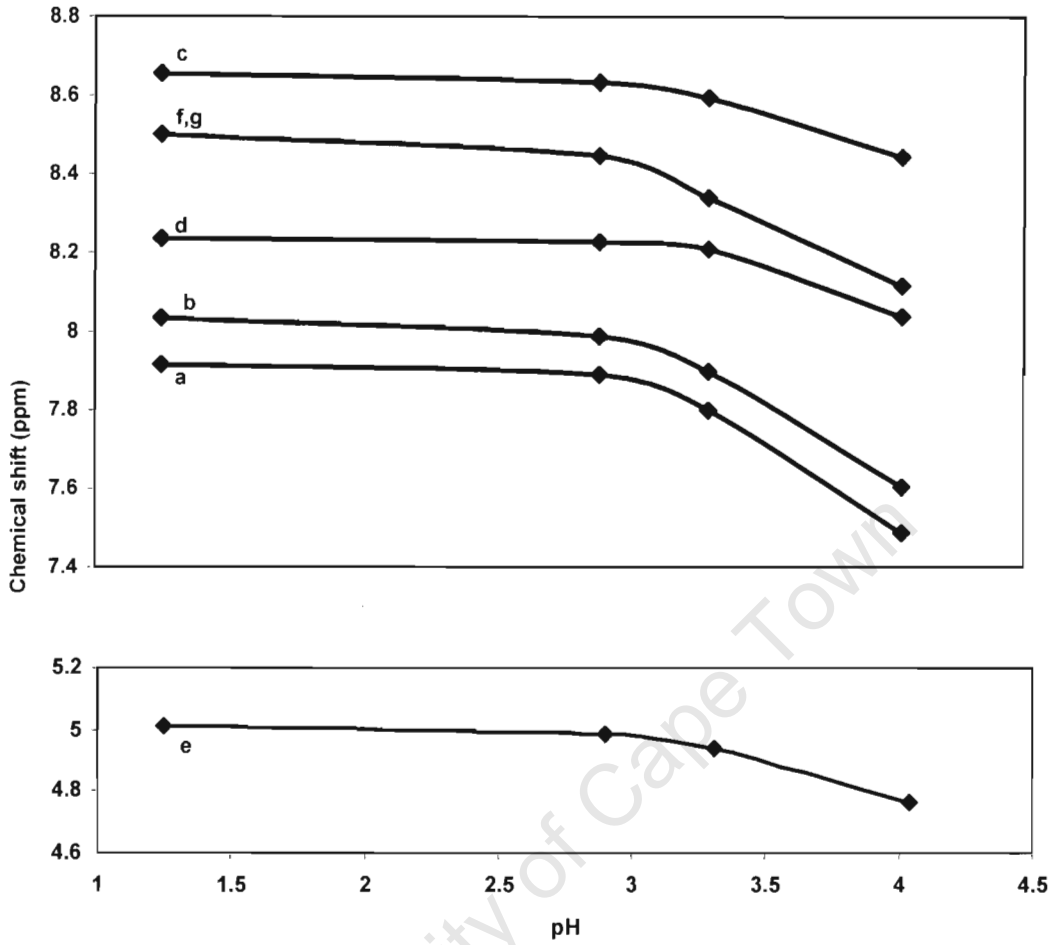

Figure 4.1(h): Change in proton chemical shift (ppm) as a function of pH for PrDPr system.

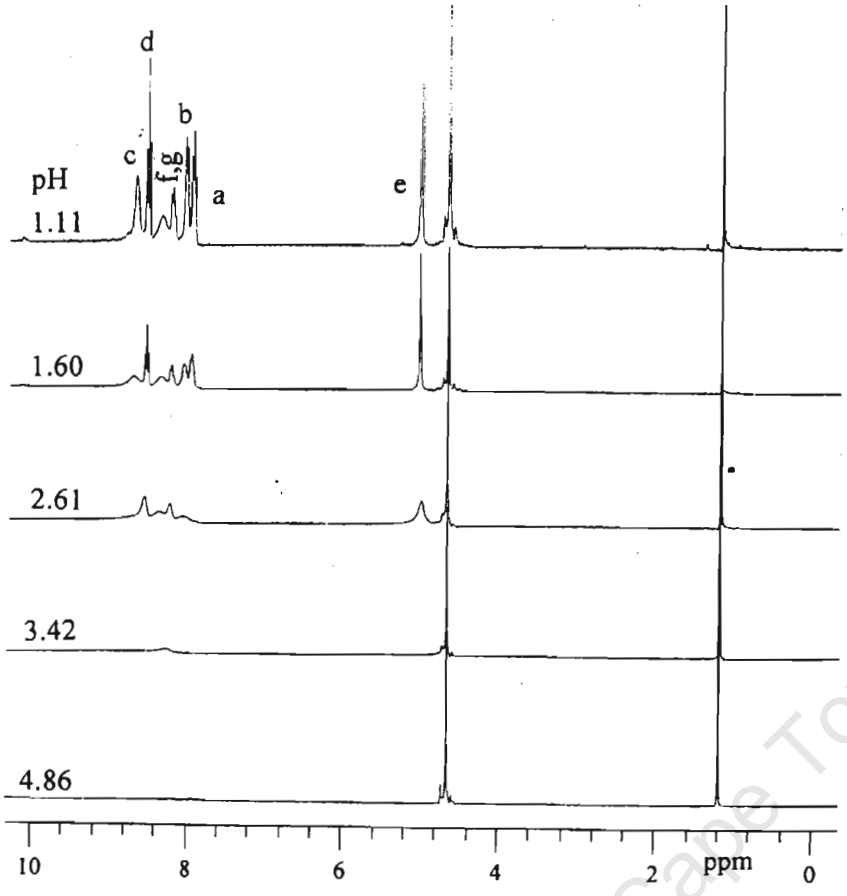

Figure 4.1(i): Proton NMR spectra for complexation of Cu(II) with PrDPr as a function of pH.

4.2 INFRARED SPECTROSCOPY

4.2.1 Introduction

Infrared (IR) is an important tool in the investigation of chemical structures. IR spectra originate from transitions between two vibrational levels of the molecule in the electronic ground state and are usually observed as absorption spectra in the infrared region.[3,4] In this study IR is used to establish the involvement of the amide oxygen or nitrogen donor in the course of the complexation process.

4.2.2 Experimental

In 5 cm^3 glass vials, two cm^3 portions of 0.1 mol dm^{-3} stock D_2O solutions of PrDH, PrDM and PrDPr were prepared and IR spectra recorded at 25 °C on a Perkin Elmer Spectra One FT-IR spectrometer (Overhead – ATR ZnSe top plate). The pH of the solutions was adjusted using NaOD and DCl. A micro-pH 2000 meter was used to measure the pH of the solutions. Solutions of 1:1 molar ratio of the metal to ligand for Cu(II)-PrDH, Cu(II)-PrDM and Cu(II)-PrDPr systems were prepared in D_2O and scanned in the pH range 1-12 in the wavenumber region 1400 and 1700 cm^{-1}.

4.2.3 Results and discussion

4.2.3.1 Cu(II)-L systems

Figure 4.2(a) shows IR spectra of PrDH in D_2O solution. The protonated ligand shows a significant absorption band at 1651 cm^{-1} which shifts to slightly lower frequency upon neutralization. This band can be assigned to the asymmetric amide carbonyl stretching vibration in the ligand. Upon complexation by Cu(II), this band broadens and almost disappears at pH 11.72 as shown in Figure 4.2(b). At pH 4.05, there are two observable bands, 1571 and 1590 cm^{-1}. The intensity of the absorption band at 1571 cm^{-1} increases with increasing pH until at pH 6.92 where it is replaced by the band at 1565 cm^{-1} at higher pH. This is indicative of loss of protons from the amide group(s) due to complexation. The band at 1590 cm^{-1} is replaced by two bands, 1582 and 1594 cm^{-1} at pH > 4.87. This shows that coordination to amide nitrogens starts at an early stage. This is also observed in the potentiometric results (section 3.5). Other bands observed in these spectra are the same as those of the ligand in the absence of Cu(II).

Figure 4.2(c) and 4.2(d) show IR spectra of PrDM and Cu(II)-PrDM in D_2O solution. Like PrDH, the absorption band at 1649 cm^{-1} is due to the carbonyl

stretching vibration in the ligand. Along with a slight shift to lower frequency, this band broadens and almost disappears at higher pH due to complexation by Cu(II). There are two absorption bands observed at 1571 and 1590 cm^{-1}. These bands behave the same way as those of the Cu(II)-PrDH system. The emergence of absorption bands at 1566, 1582 and 1594 cm^{-1} is the results of coordination of the amide nitrogens to Cu(II). Martell and co-workers[5,6] studied peptide carbonyl groups of glycine derivatives and Cu(II) using IR technique. The results showed metal-peptide nitrogen coordination for the metal chelate species in solution. It was observed that when the two peptide hydrogens are displaced from the complex, the absorption bands of the two peptide carbonyl groups shift to lower frequency due to resonance that occurs in the amide groups. The resonance is formed when a peptide proton is displaced and thus considerably lowering of carbonyl bond order occurs.

The results of the Cu(II)-PrDPr system in Figure 4.2(f) show that complexation starts at an early stage. This was also observed in the potentiometric results (section 3.5). The absorption bands at 1564, 1591, 1656 and 1679 cm^{-1} broaden and the intensity of these bands increases with pH. The observed two bands at 1565 and 1568 cm^{-1} in Figure 4.2(e) in the free ligand is replaced by one band at 1565 cm^{-1} with shoulder at 1556 cm^{-1} upon complexation by Cu(II). It was expected that complexation would commence at low pH due to the incorporation of the pyridyl groups in the PrDPr. It was also expected that the central pyridyl nitrogen would coordinate to Cu(II) first, thus enhancing ionization and coordination of the neighbouring amido groups.

In the study of Cu(II) complexes of macrocyclic ligands in aqueous solution by Steenland and co-workers[7,8], coordination of the amide to Cu(II) through the carbonyl was observed. In the present study, there were no distinct bands showing absorptions due to the coordinated carbonyl oxygens. The coordination of the carbonyl oxygen to Cu(II) in the formation of MLH and ML species is possible at low pH. However, the rigidity of the pyridine moiety and

the anchoring of the pyridyl nitrogen would induce ionization of the amide protons at low pH.

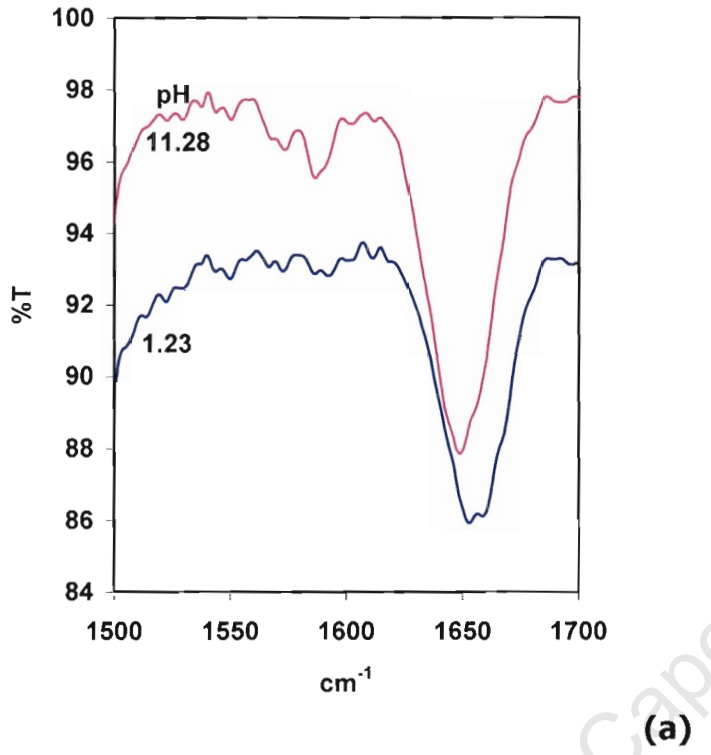

(a)

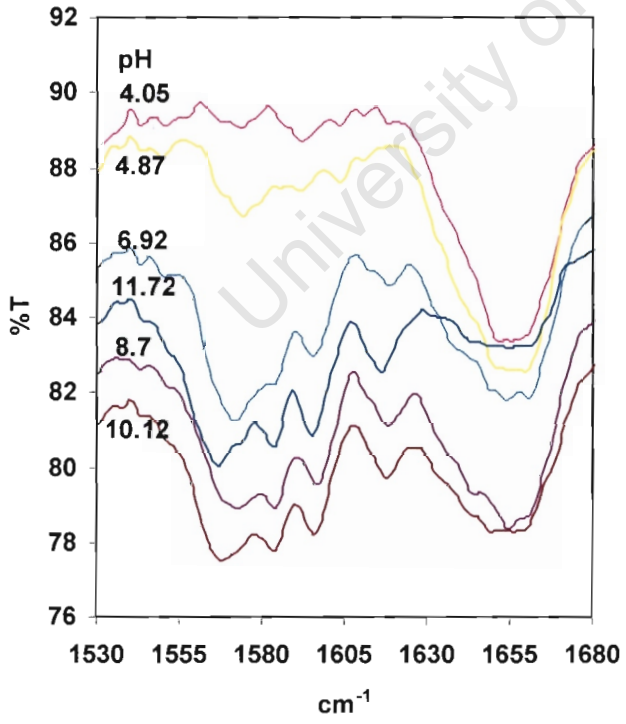

(b)

Figure 4.2 Infrared spectra of **(a):** PrDH and **(b):** Cu(II)-PrDH in D_2O as a function of pH.

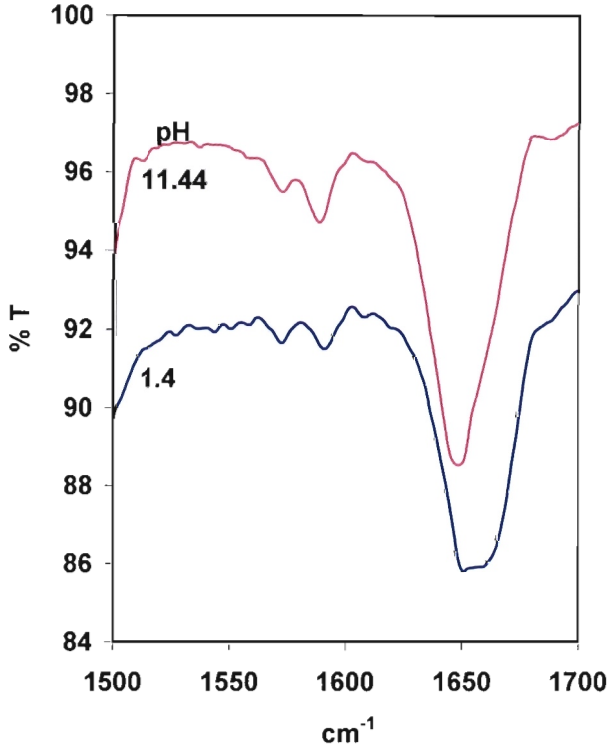

(c)

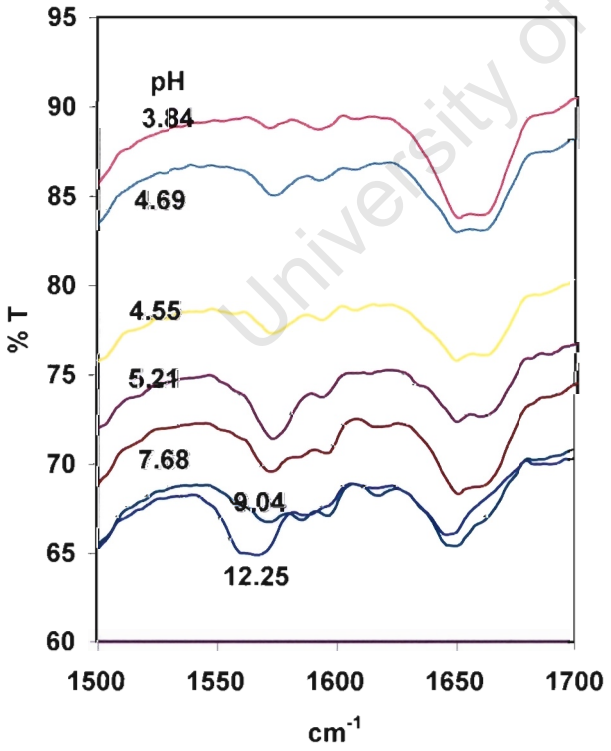

(d)

Figure 4.2 Infrared spectra of **(c):** PrDM and **(d):** Cu(II)-PrDM in D_2O as a function of pH.

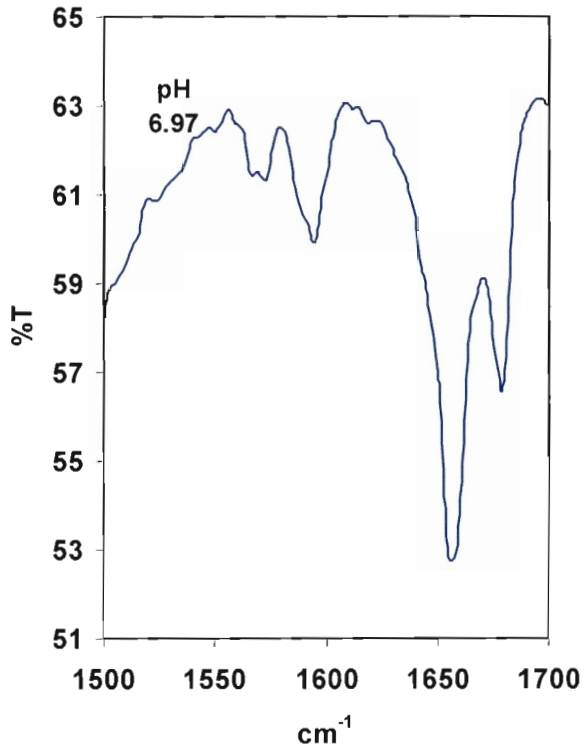

(e)

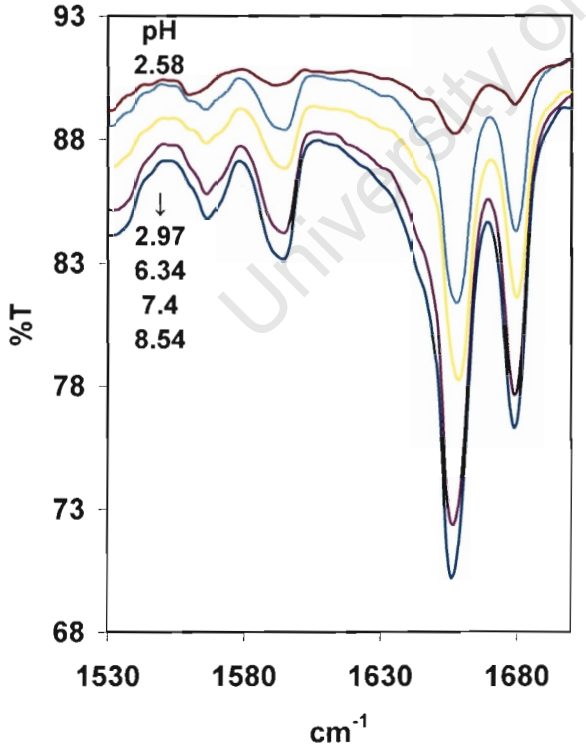

(f)

Figure 4.2 Infrared spectra of **(e):** PrDPr and **(f):** Cu(II)-PrDPr in D_2O as a function of pH.

4.3 UV - VISIBLE SPECTROSCOPY

4.3.1 Introduction

Transition metal complexes give rise to a fascinating variety of colours. These colours come from electronic transitions between energy levels whose spacings correspond to the wavelengths of visible light. In complexes, these transitions are frequently referred to as *d-d* transitions because they involve molecular orbitals that are mainly metal *d* in character. Since this spacing depends on factors such as the geometry of the complex, the nature of the ligands present, and the oxidation state of the central metal atom, electronic spectra of complexes can provide valuable information related to bonding and structure.[9] As a result, UV-visible spectrophotometry is used as a supplementary technique to glass electrode potentiometry when ionic equilibria are investigated.

UV-visible spectrophotometry provides an additional method for comparing possible chemical models not available with potentiometry. However, because the UV-visible spectra of most complexes contain broad overlapping absorption bands, parameter correlation arises and therefore, it is not usually possible to evaluate stability constants as precisely from spectrophotometric data as compared to potentiometric data. The potentiometric data may lead to a more precise analysis of the wrong model, whereas spectrophotometric data will indicate the correct model but give a less precise analysis of it. Therefore, it is necessary to combine both spectrophotometric and potentiometric data for defining the chemical model and for evaluation of the stability constants respectively.[10]

4.3.2 Electronic Spectra of Metal Complexes

The relative intensities of electronic transitions are governed by a series of selection rules. According to the Laporté rule the only allowed transitions are

those with a change of parity, *gerade to ungerade* ($g \rightarrow u$) and *ungerade to gerade* ($u \rightarrow g$) but not $g \rightarrow g$ or $u \rightarrow u$. This would mean that all *d-d* transitions in octahedral complexes are formally forbidden. Another rule states that transitions between states of different spin multiplicities are forbidden. For example, a d^2 configuration in an octahedral field would have three transitions that are spin allowed; $^3T_{1g} \rightarrow {}^3T_{2g}$, $^3T_{1g} \rightarrow {}^3A_{2g}$, $^3T_{1g} \rightarrow {}^3T_{1g}$. However, there are mechanisms by which these selection rules can be relaxed so that transitions can occur, even if only at low intensities. The bonds in transition metal complexes are not rigid but undergo vibrations that temporarily change the symmetry of the molecule. Therefore, *d-d* transitions of octahedral complexes result in low-intensity spectra. Tetrahedral complexes often absorb more strongly than octahedral complexes of the same oxidation state. The spin selection rule breaks down somewhat in complexes that exhibit spin-orbit coupling. This results in bands associated with formally spin forbidden transitions gaining enough intensity to be observed. The spin-orbit coupling and Jahn-Teller distortions often lead to more complex spectra than predicted with the spin selection rule.[9,11,12,13]

4.3.2.1 Copper complexes

Many inorganic complexes including copper complexes absorb in the visible region (400 – 700 nm). The chemistry of the copper(II) ion differs from that of the copper(I) ion in that while the latter has a closed shell configuration $(Ar)d^{10}$ and forms diamagnetic and colourless complexes, the former has an incomplete d shell configuration $(Ar)d^9$ and its complexes are predominantly paramagnetic and highly coloured.[14] The aqueous chemistry of copper is largely devoted to copper(II) compounds because copper(I) compounds are quite unstable in aqueous solution. Although Cu^{2+} can be dealt with as the equivalent of a one-electron case, the detailed interpretation of its spectra and magnetic properties can be somewhat complicated. However, copper(II) compounds show a single, broad, poorly resolved, absorption band in the visible region.

Most copper(II) complexes and compounds have a distorted octahedral structure. These compounds absorb in the region 11,000 – 16,000 cm^{-1} and show broad absorption band corresponding to the three overlapping transitions $^2A_{1g} \leftarrow {}^2B_{1g}$, $^2B_{2g} \leftarrow {}^2B_{1g}$ and $^2E_g \leftarrow {}^2B_{1g}$ which are spin-allowed. However, octahedral complexes of copper(II) are appreciably distorted due to the Jahn-Teller effect and so there is more than one peak. These peaks overlap forming a broad and unsymmetrical band. The octahedral arrangement causes crystal field splitting of the *d* orbitals on copper into lower energy e_g and high energy t_{2g} levels. The nine *d* electrons are arranged $(e_g)^3$ and $(t_{2g})^6$. Since the e_g level is not symmetrically filled, Jahn-Teller distortion occurs. Thus the complex is distorted.[11]

Aqueous Cu^{2+} forms many complexes with ammonia and ammines such as $[Cu(H_2O)_5NH_3]^{2+}$, $[Cu(H_2O)_4(NH_3)_2]^{2+}$, $Cu(H_2O)_3(NH_3)_3]^{2+}$ and $Cu(H_2O)_2(NH_3)_4]^{2+}$. It is difficult to add a fifth or sixth NH_3, though it is possible to make $[Cu(NH_3)_6]^{2+}$ using liquid ammonia as a solvent. The value of Δ_o (the d orbital ligand field splitting) for the hexammine copper(II) complex is found in the range 10,200 – 10,700 cm^{-1}. The ligand strengths of amines towards copper(II) are in the order $NH_3 > RNH_2 > R_2NH > R_3N$. In aqueous solution the Cu^{2+} ion has absorption and magnetic spectra which can be interpreted in terms of the tetragonally distorted $[Cu(H_2O)_6]^{2+}$ ion, the value of Δ_o being 12,500 cm^{-1}.[15] The ligand field strength of water compared to other donors is shown by the order Cl < H_2O < pyridine < NH_3 < 1,2-diaminoethane.

Several complexes of copper(II) with polydentate ligands containing nitrogen have been studied and the type of complex formed by copper(II) with these ligands depends on both the number of the donor atoms and the steric requirements of the ligand molecule.[15] Copper(II) peptide complexes have been studied as models for copper(II) – protein interactions. It was observed that strong copper(II) – N(peptide) bonds are formed when protons are

ionized from peptide nitrogen atoms. Other biologically important donor atoms such as N(amino), N(imidazole), O(carboxylate), O(peptide), H_2O and OH^- have been studied.[16]

The nature of electronic transitions that are brought about by chelating ligands can be inferred from the general observation of the effect of monodentate ligands on the ligand field parameter. Table 4.1 shows the guideline that is normally used for the estimation of the ligand field imposed by nitrogen-based chelating ligands. This is also relevant to the present study.

Table 4.1: Absorption maxima of the copper(II) ammine complexes[18] of the general formula $[Cu(NH_3)_n(H_2O)_{6-n}]^{2+}$

n	Absorption maximum (nm)
0	790
1	745
2	680
3	645
4	590
5	640

4.3.3 Data Analysis

A solution of metal ion and ligands will normally contain a number of different species at different concentrations. These species will contribute to the absorption spectrum and thus the final spectrum will be the sum of all the species present. It is often difficult to obtain the spectrum of a single species.

The Beer-Lambert-Bouger law, commonly called Beer's law, is the fundamental law governing the attenuation of radiation by a specific absorbing species in spectrometry. According to this law, the absorbance A of

a solution is a linear function of the concentration of the absorbing species as given by;[10]

$$A = \log(I_o/I) = \varepsilon c l \qquad (4.1)$$

where I_o and I are the intensities of the incident and emergent light beams respectively, ε the molar absorption coefficient, c the species concentration in mol dm^{-3} and l the optical path length.

For a given concentration and path length, the actual absorbance depends on the molar absorption coefficient of the absorbing species of interest. However, for the electronic absorption spectra of solutions containing more than one species the Beer-Lambert law can be expanded to give linear combination of terms for each individual species.

The absorbance A_{obs}, at wavelength λ and when n species are present, is given by:

$$A_{obs}^{\lambda} = \varepsilon_1^{\lambda} c_1 l + \varepsilon_2^{\lambda} c_2 l + \varepsilon_3^{\lambda} c_3 l + \ldots + \varepsilon_n^{\lambda} c_n l \qquad (4.2)$$

where ε_1^{λ}, ε_2^{λ} and ε_n^{λ} are molar absorption coefficients of species 1,2 and n at the same wavelength λ, and c_1, c_2 and c_n are their respective concentrations. If the path length is given in cm, ε_n^{λ} is the molar absorption coefficient of the n^{th} species in solution at wavelength λ and has the units $dm^3\ mol^{-1}\ cm^{-1}$.[17] The linear dependence of A_{obs}^{λ} on the concentrations of various species present is an important feature in the equation. If a certain species has a value of ε^{λ} equal to zero, then it does not absorb in the chosen spectral region and therefore does not influence A_{obs}^{λ}.

Complexometric titration solutions may be made up of a number of solutions of different metal and ligand concentrations, and pH. If the UV-visible spectra of these solutions are obtained at a number of wavelengths, then the spectra

of the individual species can be calculated by solving a set of linear equations (equation 4.2). It is recommended that adjustment of pH of the metal-ligand complex solution be made using strong acids and alkalis such as HCl and NaOH which do not absorb appreciably in the spectral region of interest.

Calculation of ε can be done using a specially designed computer program that requires an input file with all the information relevant to the chemical system being studied. The information includes amongst other parameters such as the concentration values of each chemical species present in the reaction. These concentration values are calculated on the basis of the stability constants obtained from glass electrode potentiometry. The values of ε are then plotted against wavelength to give a spectrum showing the absorption bands of each chemical species. Since the data is analyzed independently at each wavelength the existence of a smooth spectrum is not inherent in the data analysis and so if one is obtained it lends confidence to the experiment. If the stability constants and hence the concentrations are not correct, the spectrum will be disjointed and this is indicative of a wrong chemical model. After having electronic absorption spectral information for each of the complex species, the nature of the ligand field environment of the central metal ion can be determined.

A UV-spectra software program was developed in our laboratory in order to solve the expanded Beer-Lambert Law equation. The program deconvolutes the UV/visible titration data into the spectra of individual species.[19]

4.3.4 Experimental

Spectrophotometric titrations were performed for Cu(II) complexation with PrDH, PrDM and PrDPr ligands. An aqueous solution of 1:2 metal to ligand ratio was prepared and measured over the pH range 2-11. Small amounts of 0.1 mol dm^{-3} NaOH and 0.02 mol dm^{-3} HCl were used to adjust the pH during the titration. The solutions were kept at a temperature of 25 ^{o}C.

Spectrophotometric measurements were taken automatically at 2 nm interval in the wavelength range of 340 – 820 nm using a Cary 100 Conc spectrophotometer.

4.3.5 Results and discussion

Colour changes were noticed during the titration process of Cu(II) with PrDH, PrDM and PrDPr ligands. This was a result of the changing speciation of the solution with pH, forming different complex species with different absorption spectra. The absorption spectra were obtained in the pH range 2-11.

4.3.5.1 Cu(II)-L systems

Figure 4.3(a) shows the UV-visible electronic spectra of the Cu(II)-PrDH system as a function of pH. At pH values below 4.58, there is little complex formation and the spectrum is that of $[Cu(OH_2)_6]^{2+}$ with maximum absorption at 760 nm. As the pH increases from 4.58 to 5.34, the absorption band slightly shifts to shorter wavelengths and increases in intensity. The MLH species with maximum wavelength (λ_{max}) of 590 nm and molar extinction coefficient (ε) of 7.1 $dm^3\ mol^{-1}\ cm^{-1}$, seems to predominate at this pH range as indicated by the potentiometric results (section 3.5). Further increase in pH up to a value of 7.90 causes the absorption band to increase in intensity and shift to shorter wavelengths due to the Cu-O to Cu-N bond rearrangement. From the potentiometric results, the species formed in this region are ML and MLH_{-1}, and a 190 nm blue shift in the absorption maximum is due to the coordination of the pyridyl nitrogen, amide nitrogen and terminal amino group(s). The ML species exhibits λ_{max} = 570 nm and ε = 12.9 $dm^3\ mol^{-1}\ cm^{-1}$ whereas MLH_{-1} shows λ_{max} = 560 nm and ε = 164.9 $dm^3\ mol^{-1}\ cm^{-1}$ as shown in Figure 4.3(b). No further changes were observed in the pH range 7.90 – 10.67. The λ_{max}(=560) obtained from the calculated spectra for the MLH_{-2} species is the same as that of MLH_{-1} species. This suggests that there is no further coordination of the N-donor group. However, there is a substantial

change in extinction coefficient which indicates some change in the symmetry of the molecule. In general the more distorted the molecule the higher the extinction coefficient. Therefore, a CuN_4 type of coordination is most likely to be formed in this system.[22]

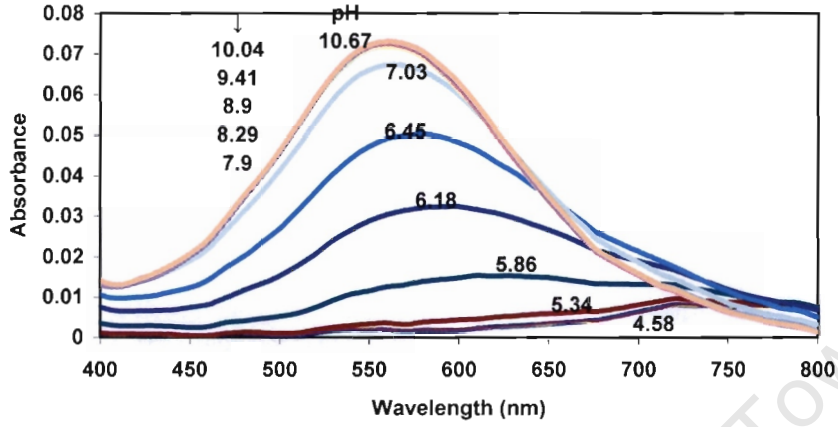

(a)

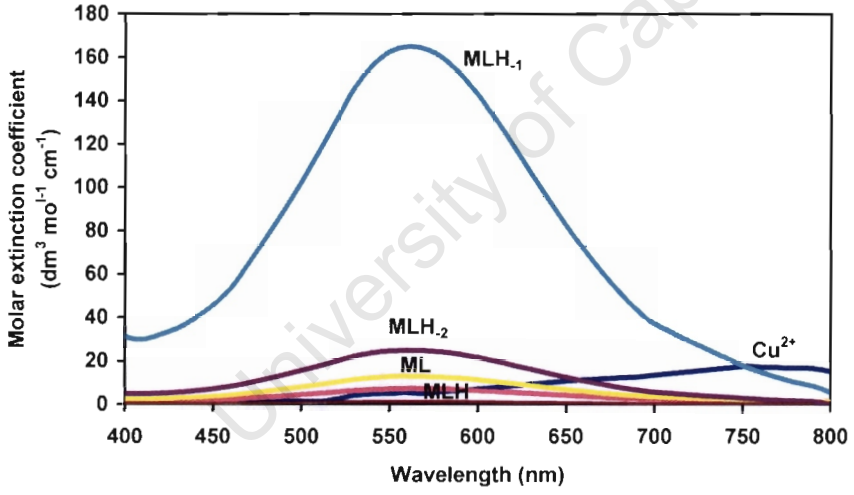

(b)

Figure 4.3 UV-visible electronic absorption spectra for **(a):** Cu(II)-PrDH [with M(0.00051 mol dm^{-3})-L(0.00109 mol dm^{-3})] and **(b):** calculated species spectra for Cu(II)-PrDH in aqueous solution

The broad absorption bands observed for the MLH, ML, MLH_{-1} and MLH_{-2} correspond to the three overlapping transitions $^2A_{1g} \leftarrow {}^2B_{1g}$, $^2B_{2g} \leftarrow {}^2B_{1g}$ and $^2E_g \leftarrow {}^2B_{1g}$ which are spin-allowed. The smoothness of the deconvoluted

spectra lends confidence to the results obtained and also supports the potentiometric model used in this system.[23]

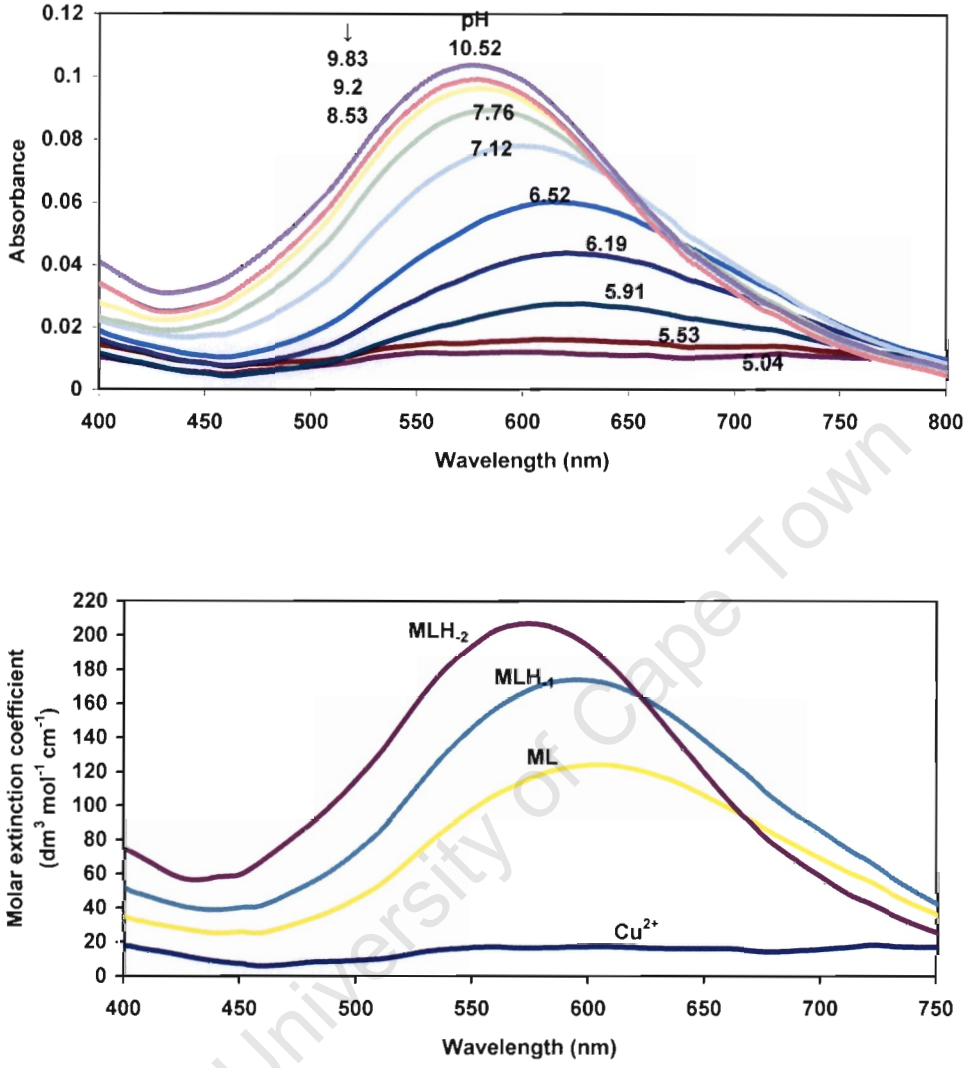

Figure 4.3 UV-visible electronic absorption spectra for **(c):** Cu(II)-PrDM [with M(0.00051 mol dm^{-3})-L(0.00107 mol dm^{-3})] and **(d):** calculated species spectra for Cu(II)-PrDM in aqueous solution.

Figure 4.3(c) shows the UV-visible electronic spectra of the Cu(II)-PrDM system as a function of pH. At pH below 5.04, the complex formation is that of the dominant CuO_6 with H_2O as ligands. At low pH(=5.04 and 5.53), the absorption band maximum increases in intensity with a slight shift to shorter wavelengths. As the pH is increased, the band maximum increases in intensity and shifts to shorter wavelength. At pH > 9.2, no further blue shift is

observed. Figure 4.3(d) shows the calculated species absorption spectra for the Cu(II)-PrDM system. A noticeable feature about these spectra is that the individual species spectra have high ε values as compared to those of the Cu(II)-PrDH system. The $\lambda_{max}(\varepsilon)$ values for the ML, MLH_{-1} and MLH_{-2} are 600(123.9), 590(173.6) and 570 nm(206.3 $dm^3\ mol^{-1}\ cm^{-1}$). According to the speciation curves (section 3.5), these species are observed to dominate at different pH regions. A difference of 160 nm for the hydrated Cu(II) and ML species is indicative of the rearrangement of ligands positioned in the coordination sphere of the Cu(II) ion. The *d-d* electronic absorption band with λ_{max} at 590 and 570 nm for the MLH_{-1} and MLH_{-2}, and slightly asymmetric at the low-frequency side is consistent with such a tetragonal coordination geometry of Cu(II).

The UV-visible electronic absorption spectra for the Cu(II)-PrDPr system are shown in Figure 4.3(e). This system shows one absorption band. Before titration by the base, the complex formation has already begun (curve at pH 2.39) and the dominant species is that of CuN_2 type of coordination with absorption maximum at 660 nm. This is in support of the speciation curves (section 3.5) which show that complexation begins at pH < 2. As the pH increases, the band maximum shifts to shorter wavelengths and increases in intensity up to a pH value of 5.81, above which a slight red shift in wavelength is observed. The calculated absorption spectra for the individual species are shown in Figure 4.3(f). These species show λ_{max} values of 660, 640, 630 and 650 nm with corresponding ε values of 23.8, 14.7, 91.6 and 94.9 $dm^3\ mol^{-1}\ cm^{-1}$ for the MLH, ML, MLH_{-1} and MLH_{-2} species respectively. Marlin and co-workers obtained a band with λ_{max} at 613 nm (ε = 220 $dm^3\ mol^{-1}\ cm^{-1}$) for this system in methanol.[24]

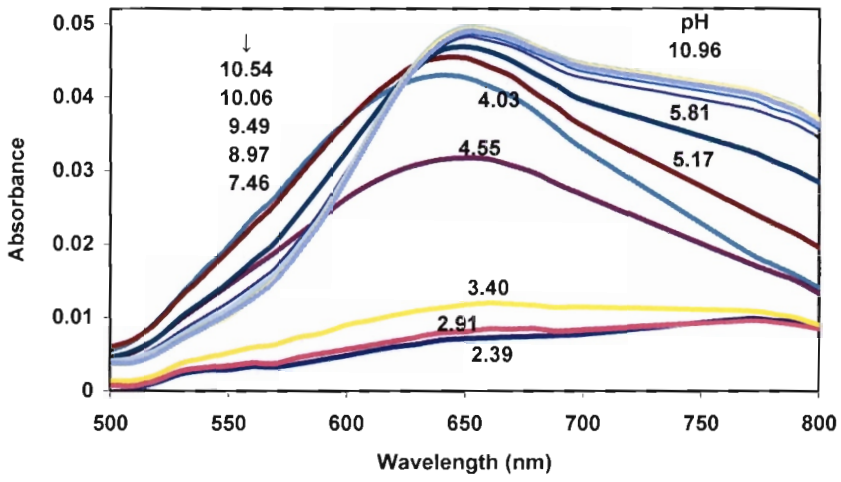

(e)

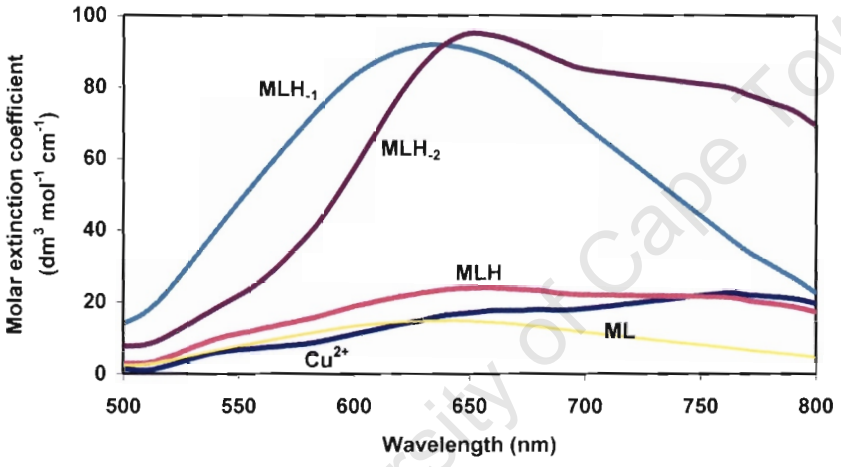

(f)

Figure 4.3 UV-visible electronic absorption spectra for **(e):** Cu(II)-PrDPr [with M(0.00051 mol dm^{-3})-L(0.00101 mol dm^{-3})] and **(f):** calculated species spectra for Cu(II)-PrDPr in aqueous solution.

The electronic spectra computed from the spectrophotometric titration data and formation constants of the different Cu(II) complexes with PrDH, PrDM and PrDPr in Figure 4.3(b,d,f) show smooth spectra. The PrDH and PrDM systems show a single broad *d-d* absorption band which is typical of a distorted tetragonal Cu(II) complex.[20] These systems are N_5O_2 type ligands capable of donating five nitrogen atoms, two amino, two amido and one pyridyl nitrogen to Cu(II). The λ_{max} of 560 nm is observed for both MLH_{-1} and

MLH_{-2} species of the Cu(II)-PrDH whereas Cu(II)-PrDM has λ_{max} of 590 and 570 nm for MLH_{-1} and MLH_{-2} respectively as shown in Table 4.2. The λ_{max} of these two species is the same for Cu(II)-PrDH whereas Cu(II)-PrDM has a difference of 20 nm for the same species. Such close agreement in λ_{max} values for these two species suggests that the metal ion has the same geometry in both species. NMR and IR studies indicate that the amide nitrogen takes part in the coordination sphere at an early stage (low pH). This is due to the incorporation of the pyridyl nitrogen functioning as an anchor for the ionization and coordination of the neighbouring amido group. Although coordination of the fifth donor atom forming a distorted square pyramidal or a distorted tetragonal complex is possible, it would be destabilized by the formation of four contigous five-membered rings. The MLH_{-2} species is most likely to be formed by coordination of one terminal amino, two deprotonated amido and pyridyl nitrogens to the Cu(II).

On the other hand, the absorption maximum for the Cu(II)-PrDPr system is somewhat red shifted as compared to those of the other two systems as shown in Table 4.2. This may be due to the relatively weak binding by the pyridyl nitrogens. There is also a red shift of 20 nm for the MLH_{-2} species which may be due to coordination by the axial nitrogen donor of the fifth nitrogen. The λ_{max} value of 650 nm is more consistent with that of $[Cu(NH_3)_5(H_2O)]^{2+}$.[18] Therefore, this suggests that all nitrogen donors are coordinated to the metal ion. This is as also supported by potentiometric and NMR studies.

Previous studies show that rearrangement of donor atoms in the coordination sphere result in the splitting or significant shift of the absorption bands.[22,25] The present study shows results similar to those obtained by Steenland and co-workers[8] for the macrocyclic pentadentate (L^{3a} and L^{3b} in Figure 4.3) analogues of PrDH and PrDM. The coordination geometry of the MLH_{-2} species in Cu(II)-PrDH, Cu(II)-PrDM and Cu(II)-PrDPr systems is likely to be overall tetragonal with only weak axial coordination of the fifth nitrogen. A

strong axial interaction from a nitrogen donor in MLH_{-2} would certainly shift its *d-d* absorption band to lower wavenumbers relative to MLH_{-1} resulting from a weakening of the in-plane ligand field by a synergic effect.[8,20] Nomkoko[26] and Mkhomta-Gama[27] also obtained similar results in the study of pentadentate diamide ligands (L^{3g} and L^{3e} in Figure 4.3).

Table 4.2: Wavelength (nm) and molar extinction coefficient values ($dm^3\ mol^{-1}\ cm^{-1}$) in brackets, corresponding to maximum absorption of various Cu(II) species formed in solution with PrDH, PrDM and PrDPr. For comparison other studied ligands have included.

	Wavelength(nm) (molar extinction coefficient($dm^3\ mol^{-1}\ cm^{-1}$))				
Ligand	**M**	**MLH**	**ML**	**MLH_{-1}**	**MLH_{-2}**
PrDH	760 (17.5)	590 (7.1)	570 (13)	560 (164.9)	560 (25)
PrDM	760 (18.0)	-----	600 (123.9)	590 (173.6)	570(206.3)
PrDPr	760 (22.4)	660 (23.8)	640 (14.7)	630 (91.6)	650 (94.9)
L^{3a} ref. 8	-----	-----	-----	580 (154)	570 (127)
L^{3b} ref. 8	-----	-----	-----	550 (99)	540 (125)
L^{3g} ref. 26	-----	620 (40)	580 (115)	560 (120)	540 (110)
L^{3e} ref. 27	-----	-----	610 (50)	550 (71)	550 (60)
NH_3 in $\|Cu(NH_3)_n(H_2O)_{6-n}\|^{2+}$	790 (n=0)	745 (n=1) 680 (n=2)	645 (n=3)	590 (n=4)	640 (n=5)

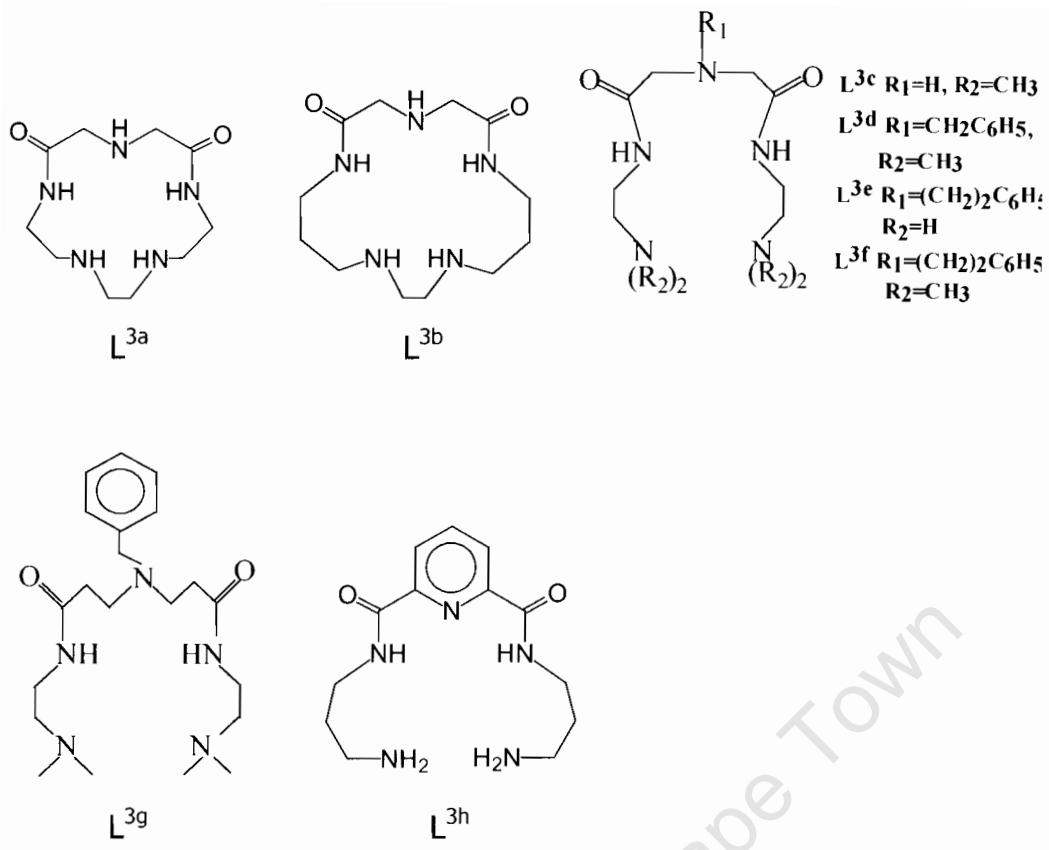

Figure 4.3: Schematic representation of ligands discussed in this section.

4.4 MOLECULAR MECHANICS

4.4.1 Introduction

Advances in computing have greatly increased the interest in computer-based molecular modelling.[29,30] Computer modelling is now widely used as an aid in the interpretation of experimental results and in the design of new materials with desirable properties. Molecular mechanics (MM) is a very popular tool for describing the structures and relative energies of many classes of molecules.[29,30,32] Its wide use is primarily due to computational simplicity and efficiency whereas quantum mechanical modelling is far more computationally intensive and until recently has been used only for rare metal complexes. Molecular mechanics in this study is used to calculate the strain energies

(internal energy) of different possible geometries for the determination of the stability of related complex species in solution.

4.4.2 Theory

The basis of the molecular mechanics method is that a good estimate of the geometry of a molecule can be obtained by taking into account all the forces between atoms, calculated using a mechanical approach.[29,30] To optimize the geometry of a molecule, the total energy that arises from these forces, or stresses, is minimized by computational methods.

Molecular mechanics studies in both inorganic and organic chemistry define strain energy U_{total} as arising from four principle energy terms,[29,30,31] the general form of which is given as;

$$U_{\text{total}} = \sum_{molecule} (E_b + E_\theta + E_\phi + E_{nb}) \qquad (4.3)$$

where $\sum E_b$ is the total bond deformation energy, $\sum E_\theta$ the total valence angle deformation energy, $\sum E_\phi$ the total torsional (or dihedral) deformation energy and $\sum E_{nb}$ the total non-bonded (van der Waals) interaction energy.

The individual energy terms are calculated using simple functions with bonds modelled as springs that obey Hooke's law;

$$E_b = \frac{1}{2} K_b (r_{ij} + r_0)^2 \qquad (4.4)$$

where K_b is the force constant or spring strength and r_0 the ideal bond length or length the spring wants to be. Valence angles are modelled in a similar way,

$$E_\theta = \frac{1}{2} K_\theta (\theta_{ijk} + \theta_0)^2 \qquad (4.5)$$

where K_θ is the strength of the spring holding the angle at its ideal value θ_0. Torsion or dihedral angles cannot be modelled in the same manner since a periodic function is required,

$$E_{\phi} = \frac{1}{2} K_{\theta}(1 + \cos(m(\phi_{ijkl} + \phi_{offset}))) \quad (4.6)$$

where K_{θ} is the height of the barrier to rotation about the torsion angle ϕ_{ijkl}, m the periodicity and ϕ_{offset} the offset of the minimum energy from a staggered arrangement. Non-bonded interactions are calculated using a function that includes a repulsive and attractive (London dispersion) component,

$$E_{nb} = Ae^{-Bd_{ij}} - Cd_{ij}^{-6} \quad (4.7)$$

where d_{ij} is the distance between the nuclei and A, B and C are atom based constants.

Additional components have been added to the calculation of the strain energy. Out-of-plane deformation energy, E_{δ}, has been included in models of aromatic or sp^2 hybridized systems,

$$E_{\delta} = \frac{1}{2} k_{\delta} \delta^2 \quad (4.8)$$

where δ is the angle between the plane defined by three atoms and the vector from the center of these atoms to a fourth bonded atom, and k_{δ} the corresponding force constant. Electrostatic interactions terms E_{ε} are modelled based on the Coulomb law,

$$E_{\varepsilon} = \frac{q_i q_j}{\varepsilon d_{ij}} \quad (4.9)$$

where q_i and q_j are partial charges on atoms i and j, ε the dielectric constant and d_{ij} the interatomic separation. Hydrogen bonding interaction terms are generally modelled using a function of the type given as;

$$E_{nb} = Fd_{ij}^{-12} - Gd_{ij}^{-10} \quad (4.10)$$

where F and G are empirically derived constants that reproduce the energy of a hydrogen bond and d_{ij} the donor-accepter distance. The addition of these terms gives rise to the revised definition of U_{total} given as;

$$U_{\text{total}} = \sum_{molecule} (E_b + E_{\theta} + E_{\phi} + E_{nb} + E_{\delta} + E_{\varepsilon} + E_{nb}) \quad (4.11)$$

The set of functions together with the collection of terms that parameterise them is referred to as the force field. In general force field terms are derived empirically with the target of reproducing experimental structures and energy distributions.[29,30] However, the goal of molecular mechanics is to find the geometry with minimum strain energy. The value of the strain energy is dependent on the force field and therefore, has little meaning in absolute terms. The choice of the force field to study molecules containing a metal is not clear-cut.[30,32]. This is due to various factors which include the partially filled d-orbitals of the transition metal ions that are responsible for multifarious structures of coordination compounds with a large variety of possible coordination numbers and geometries. Moreover, the extension of these force fields to inorganic chemistry is a more recent development.[29,30,32,33,34]

In an attempt to model metal complexes, an extensible systematic force field was designed to model inorganic and organometallic compounds as well as organic and biochemical systems.[35] It differs from existing force fields in both functional forms as well as parameterization approach. It employs semi-emperical rules to translate atomic-based parameters to parameters typically associated with a covalent valence force field. The atomic parameters depend not only on atom type, but also on internal type, thus resulting in a more accurate force field. The force field has been applied to molecular simulations of a wide variety of systems including nucleic acids, peptides, hydrocarbons, porphyrins, transition metal complexes, zeolites and organometalic compounds.

4.4.3 Simulations

The MM calculations were done on a SyncMaster 1100p computer using InsightII.[36] The Cu(II) complexes (schematic representation of proposed structures shown in Figure 4.4(1)) were constructed from fragments using the

BUILDER module. Molecular mechanics calculations were performed using the Discover_3 program which was run as an application in the InsightII package. All calculations were done in vacuum.

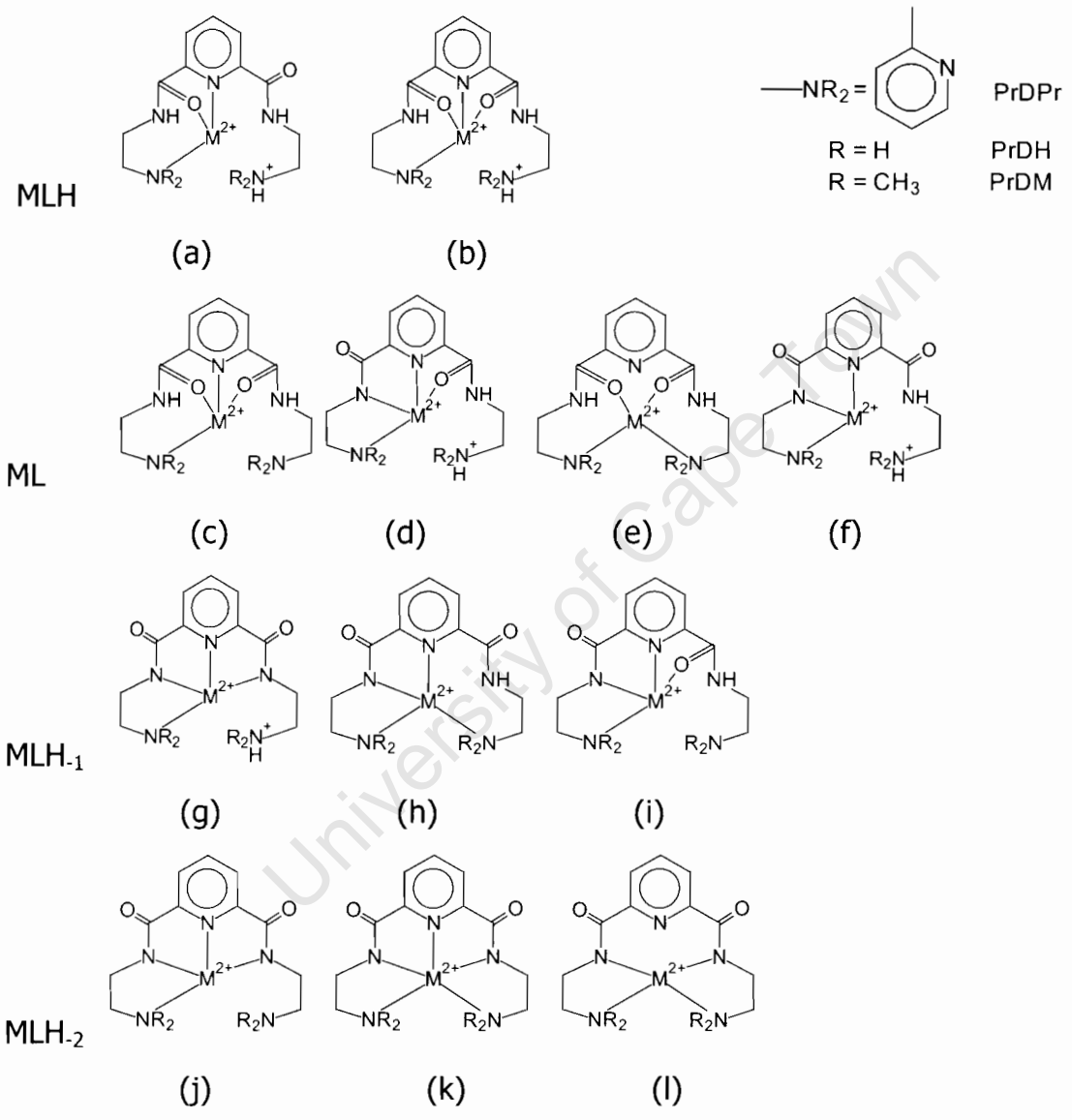

Figure 4.4(1): Schematic representation of proposed structures of the various Metal-Ligand species.

4.4.4 Results and discussion

The energy minimised structures for the Cu(II)-PrDH, Cu(II)-PrDM and Cu(II)-PrDPr systems are given in Figure 4.4(2), 4.4(3) and 4.4(4) respectively. The output data for the deformation energies including internal (strain) energy for these structures is given in Table 4.3. The energy minimised structures are compared in terms of internal energy and not potential energy. The potential energy is dependent on the number of covalent bonds in the structure and also includes a contribution from non-bonded electrostatic interactions, which is greatly influenced by the charge of the Cu(II). The internal energy which was a criterion considered for stability comparison, indicates the strain energy around the central metal ion.

MLH, (a), 7,5 **ML, (f), 5,5**

Figure 4.4(2): Energy minimised Cu(II) complexes showing equatorial plane coordination by structure (a) an amine, a pyridine nitrogen donor and a carbonyl oxygen donor atoms, giving a 7,5 chelate ring sequence (109.36 kcal mol^{-1}) and structure (f) an amine, a pyridine nitrogen donor and an amide nitrogen donor atoms, giving a 5,5 chelate ring sequence (50.75 kcal mol^{-1}) for the MLH and ML species of the Cu(II)-PrDH system.

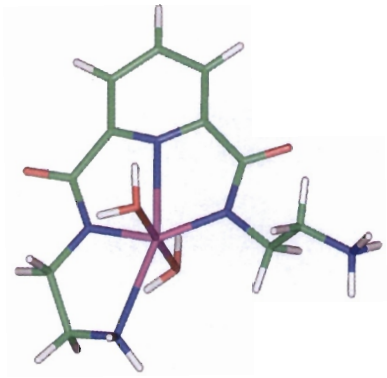

MLH_{-1}, (g), 5,5,5

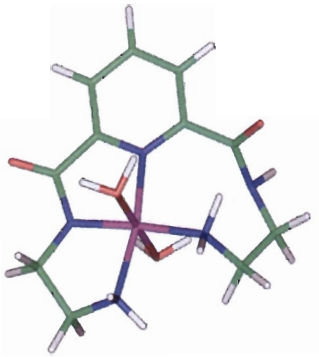

MLH_{-1}, (h), 5,5,8

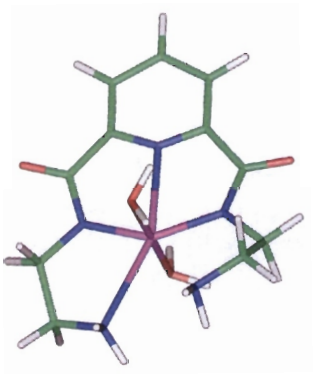

MLH_{-2}, (j), 5,5,5

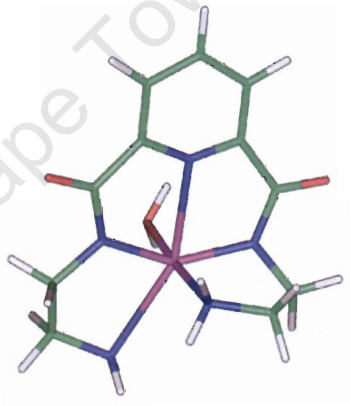

MLH_{-2}, (k), 5,5,5,5

Figure 4.4(2): Energy minimised Cu(II) complexes showing equatorial plane coordination by structure (g) an amine, a pyridine nitrogen donor and two amide nitrogen donor atoms, giving a 5,5,5 chelate ring sequence (91.21 kcal mol^{-1}), structure (h) two amine, a pyridine nitrogen donor and an amide nitrogen donor atom, giving a 5,5,8 chelate ring sequence (30.27 kcal mol^{-1}), structure (j) an amine, a pyridine nitrogen donor and two amide nitrogen donor atoms, giving a 5,5,5 chelate ring sequence (85.36 kcal mol^{-1}) and structure (k) two amine, a pyridine nitrogen donor and two amide nitrogen donor atoms, giving a 5,5,5,5 chelate ring sequence (93.12 kcal mol^{-1}) for the MLH_{-1} and MLH_{-2} species of the Cu(II)-PrDH system.

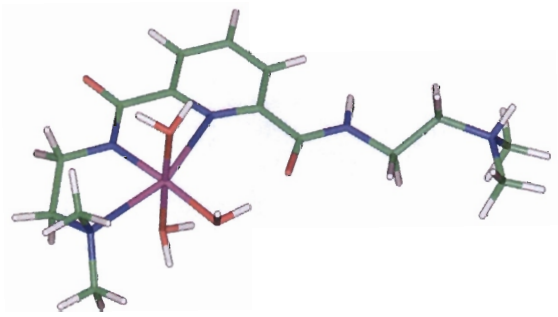

ML, (f), 5,5

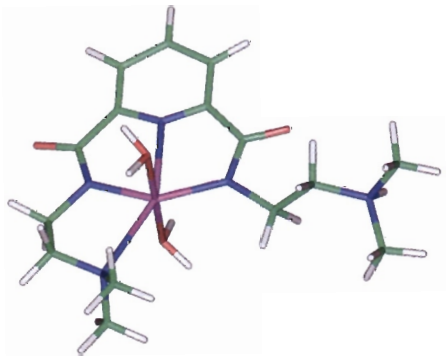

MLH_{-1}, (g), 5,5,5

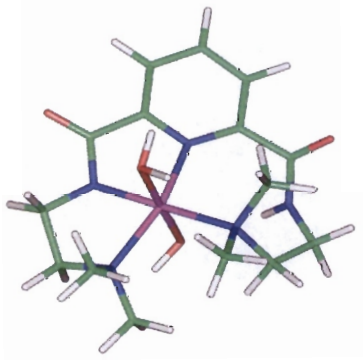

MLH_{-1}, (h), 5,5,8

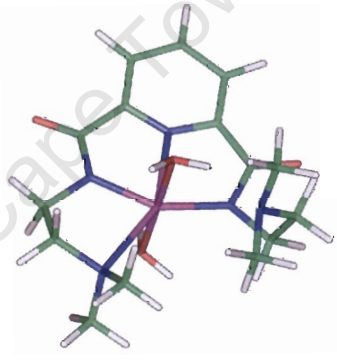

MLH_{-2}, (j), 5,5,5

Figure 4.4(3): Energy minimised Cu(II) complexes showing equatorial plane coordination by structure (f) an amine, a pyridine nitrogen donor and an amide nitrogen donor atoms, giving a 5,5 chelate ring sequence (62.94 kcal mol^{-1}), structure (g) an amine, a pyridine nitrogen donor and two amide nitrogen donor atoms, giving a 5,5,5 chelate ring sequence (120.26 kcal mol^{-1}), structure (h) two amines, a pyridine nitrogen donor and an amide nitrogen donor atoms, giving a 5,5,8 chelate ring sequence (56.94 kcal mol^{-1}) and structure (j) an amine, a pyridine nitrogen donor and two amide nitrogen donor atoms, giving a 5,5,5 chelate ring sequence (93.41 kcal mol^{-1}) for ML, MLH_{-1} and MLH_{-2} species of the Cu(II)-PrDM system.

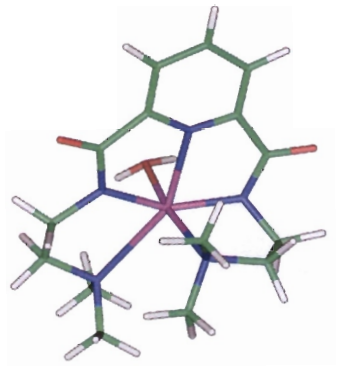

MLH_{-2}, (k), 5,5,5,5

Figure 4.4(3): Energy minimised Cu(II) complexes showing equatorial plane coordination by structure (k) two amine, a pyridine nitrogen donor and two amide nitrogen donor atoms, giving a 5,5,5,5 chelate ring sequence (102.95 kcal mol^{-1}) for the MLH_{-1} and MLH_{-2} species of the Cu(II)-PrDM system.

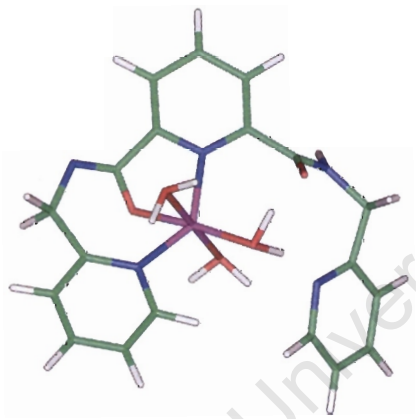

MLH, (a), 7,5

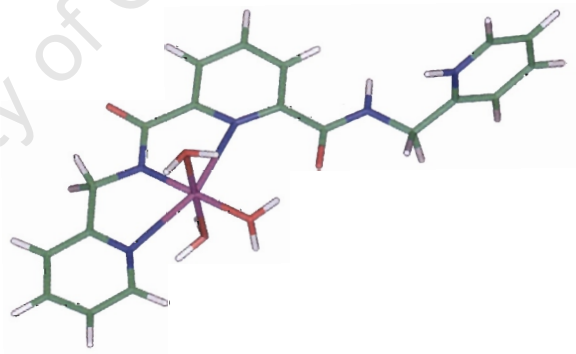

ML, (f), 5,5

Figure 4.4(4): Energy minimised Cu(II) complexes showing equatorial plane coordination by structure (a) an amine, a pyridine nitrogen donor and a carbonyl oxygen donor atom, giving a 7,5 chelate ring sequence (85.49 kcal mol^{-1}) and structure (f) an amine, a pyridine nitrogen donor and an amide nitrogen donor atom, giving a 5,5 chelate ring sequence (61.51 kcal mol^{-1}) for the MLH and ML species of the Cu(II)-PrDPr system.

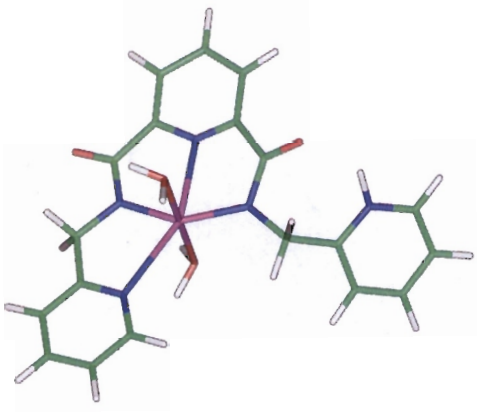

MLH_{-1}, (g), 5,5,5

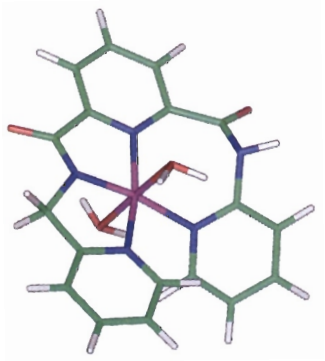

MLH_{-1}, (h), 5,5,8

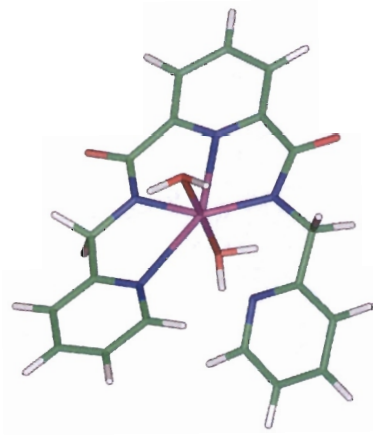

MLH_{-2}, (j), 5,5,5

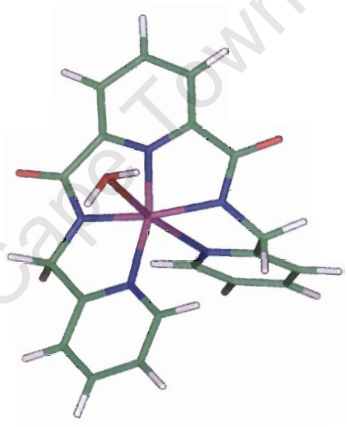

MLH_{-2}, (k), 5,5,5,5

Figure 4.4(4): Energy minimised Cu(II) complexes showing equatorial plane coordination by structure (g) an amine, a pyridine nitrogen donor and two amide nitrogen donor atoms, giving a 5,5,5 chelate ring sequence (116.07 kcal mol^{-1}), structure (h) two amine, a pyridine nitrogen donor and an amide nitrogen donor atom, giving a 5,5,8 chelate ring sequence (58.59 kcal mol^{-1}), structure (j) an amine, a pyridine nitrogen donor and two amide nitrogen donor atoms, giving a 5,5,5 chelate ring sequence (82.94 kcal mol^{-1}) and structure (k) two amine, a pyridine nitrogen donor and two amide nitrogen donor atoms, giving a 5,5,5,5 chelate ring sequence (88.54 kcal mol^{-1}) for the MLH_{-1} and MLH_{-2} species of the Cu(II)-PrDPr system.

Table 4.3: Internal energy ($E_{internal}$), bond (E_{bond}), angle (E_{angle}), torsion ($E_{torsion}$) and out-of-plane (E_{oop}) deformation energies (kcal mol^{-1}) for the different chelate ring size sequences associated with each structure for the Cu(II)-PrDH, Cu(II)-PrDM and Cu(II)-PrDPr systems.

	Cu(II)-L Structures											
PrDH	**(a) 7,5**	**(b) 7,5,5**	**(c) 7,5,5**	**(d) 7,5,5**	**(e) 7,8,7**	**(f) 5,5**	**(g) 5,5,5**	**(h) 5,5,8**	**(i) 5,5,5**	**(j) 5,5,5**	**(k) 5,5,5,5**	**(l) 5,8,5**
$E_{internal}$	109.36	126.98	111.64	107.47	150.60	50.75	91.21	30.27	42.05	85.36	93.12	49.08
E_{bond}	15.02	6.42	7.49	28.85	10.42	22.07	24.28	5.78	7.64	21.64	11.52	5.42
E_{angle}	56.29	102.87	91.58	72.44	91.07	24.27	62.87	12.43	29.93	60.63	54.33	35.09
$E_{torsion}$	35.83	17.13	12.03	5.48	45.77	4.25	3.85	11.83	4.22	2.92	24.01	8.25
E_{oop}	2.22	0.55	0.53	0.70	3.34	0.15	0.21	0.22	0.24	0.17	3.25	0.33
PrDM												
$E_{internal}$	-----	-----	87.71	131.30	96.87	62.94	120.26	56.94	38.84	93.41	102.95	58.35
E_{bond}	-----	-----	8.82	36.05	10.64	17.64	36.02	13.18	9.08	20.80	17.12	9.93
E_{angle}	-----	-----	61.51	88.19	48.93	41.09	79.70	26.02	25.01	64.28	59.50	38.90
$E_{torsion}$	-----	-----	16.85	6.77	33.77	4.16	4.40	16.89	4.56	7.19	23.39	9.13
E_{oop}	-----	-----	0.53	0.29	3.53	0.06	0.14	0.85	0.18	1.15	2.94	0.38
PrDPr												
$E_{internal}$	85.49	142.10	133.07	93.34	110.80	61.51	116.07	54.94	58.85	82.94	88.28	52.26
E_{bond}	13.64	21.97	17.94	15.39	11.75	22.29	16.09	7.21	6.38	23.52	10.18	5.77
E_{angle}	46.33	90.08	85.58	55.09	62.15	35.99	90.80	22.21	31.79	53.54	51.84	39.52
$E_{torsion}$	22.08	27.87	27.16	20.47	32.75	3.04	8.20	23.74	18.38	4.70	6.95	6.31
E_{oop}	3.43	2.17	2.39	2.38	4.15	0.18	0.98	1.78	2.29	1.18	4.57	0.66

Table 4.3 shows the molecular mechanics calculations output data of the different deformation energies including the internal energy from the complex structures. The results show that the strain energy corresponding to a chelate ring size formed by coordination of nitrogen donor atoms to the metal ion is in the order 5,5,5,5 > 5,5,5 > 5,5 > 5,8,5 > 5,5,8. It is observed that the 5,5,5,5 and 5,5,5 chelate ring systems are highly strained. In general, the 5,7 or 5,8 chelate rings tend to have unfavourable larger chelate rings. However, the 5,8,5 and 5,5,8 chelate ring systems in this study seem to be stabilized as compared to the 5,5 chelate ring system due to the pre-organization of the ligand. The results also show that structures involving carbonyl oxygen donor atoms coordinated to the metal ion are relatively more strained. The rigidity of the pyridine moiety seems to contribute to the strain energy when the carbonyl oxygen donor atom is coordinated to the metal ion. Therefore, the strain energy of these structures arises from both the sequence and the size of the rings formed around the metal ion upon different donor atom coordination.

It is worth noting that molecular mechanics has been used in this study as a simple computational tool to provide more evidence in support of the potentiometric and spectroscopic (NMR, IR, UV-visible) studies. In all calculations, no account is taken for the electronic contribution, Jahn-Teller distortion of Cu(II), entropy effects, chelate effect of the ligand and solvent effect.

4.4.5 Discussion – Proposed structures

On the basis of the selected equilibria from the potentiometric data, the proposed structures for various species have been postulated and presented in Figure 4.4(1). The proposed MLH species for the ligands are given in Figure 4.4(1) (a,b). The NMR study shows that the central pyridine nitrogen is coordinated at the beginning of complexation. Between the two structures, (a) seems a more likely coordination geometry. This is also supported by the

molecular mechanics calculations for the strain energy. This structure is formed by the Cu(II)-PrDH and Cu(II)-PrDPr systems. It is expected that as the pH increases, Cu(II) would induce ionization of the amide protons[37,38] and there would also be a transition from Cu-O to Cu-N in the coordination arrangement.[39] The ML species is formed by the deprotonation of the MLH species. Several possible arrangements exist in forming this species as shown in Figure 4.4(1) (c,d,e,f). From the molecular mechanics calculations, structure (f) has the lowest strain energy, thus being favoured over the other three structures. Moreover, IR and NMR studies show that the deprotonation of the amide group begins at an early stage (low pH). The incorporation of an anchor (central pyridyl nitrogen) would also induce ionization of the amide proton by bringing the metal ion into close proximity. The rigidity of the pyridine moiety would also destabilize the other two structures upon coordination to the carbonyl oxygens.

The possible structures for the MLH_{-1} species are shown in Figure 4.4(1) (g,h,i). Structure (i) is unlikely to be formed due to the coordination of the carbonyl oxygen to the metal ion. According to the molecular mechanics calculations, structure (h) is less strained as compared to (g). However, the amide coordination is likely, due to the close proximity of the metal ion enhanced by the coordination of the central pyridyl nitrogen. Brooker and co-workers[40] reported similar structure for Cu(II) with dioxo pentadentate ligand analogue of the ligands in this study. The IR and NMR studies show that the amide nitrogens are involved in complexation. If structure (g) is formed, the MLH_{-2} species would result from the deprotonation of the terminal amino/pyridyl nitrogen group, structure (j). However, structure (i) would result in the formation of (k). The structure (k) is highly strained by 5,5,5,5 membered chelate rings. Although structure (l) has the lowest strain energy amongst the MLH_{-2} species, the NMR study shows that the pyridyl nitrogen is coordinated to the metal ion. The UV-visible study shows that the species formed are of tetragonal geometry. The UV-visible study suggests that the MLH_{-2} species for the Cu(II)-PrDPr system has

all nitrogen donors coordinated to the metal ion. The coordination geometry of the MLH_{-2} species in both Cu(II)-PrDH and Cu(II)-PrDM systems is likely to be overall tetragonal with only a weak axial nitrogen donor for the fifth nitrogen. The proposed most likely structures formed for the Cu(II)-PrDH, Cu(II)-PrDM and Cu(II)-PrDPr systems in solution are given in Figure 4.4(5).

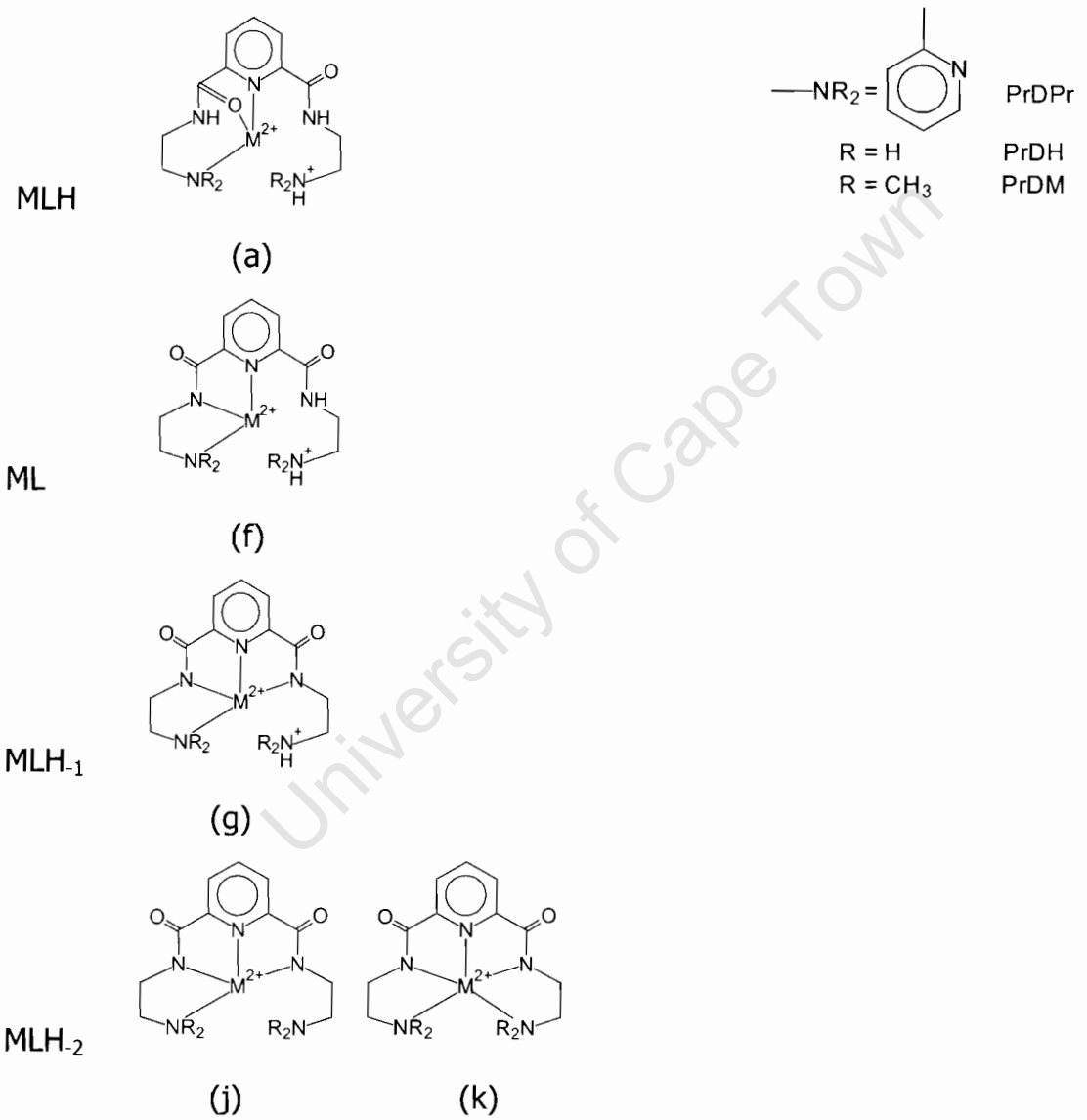

Figure 4.4(5): Schematic representation of the most likely structures formed in solution of the various Metal-Ligand species for the Cu(II)-PrDH, Cu(II)-PrDM and Cu(II)-PrDPr systems.

References:

1. Freeman R., *Magnetic resonance in chemistry and medicine,* 2003, Oxford University Press, Oxford.
2. Pregosin P.S. (Ed.), *Transition metal nuclear magnetic resonance, studies in inorganic chemistry,* 1991, Elsevier Science Publisher B.V., Amsterdam.
3. Nakamoto K., *Infrared and Raman Spectra of Inorganic and Coordination Compounds.* 3rd ed., 1970, John Wiley and Sons, New York, USA.
4. Nakamoto K., *Infrared Spectra of Inorganic and Coordination Compounds.* 2rd ed., 1970, John Wiley and Sons, New York, USA.
5. Kim M.K., Martell A.E., *J. Am. Chem. Soc.,* 1966, **88,** 914-918.
6. Motekaitis R.J., Martell A.E., *Inorg. Chem.,* 1974, **13,** 550-559.
7. Steenland M.W.A., Westbroek P., Dierck I., Herman G.G., Lippens W., Temmerman E., Goeminne A.M., *Polyhedron*, 1999, **18,** 3417-3424.
8. Steenland M.W.A., Dierck I, Herman G.G. Devreese B., Lippens W., Van Beeumen J., Goeminne A.M, *J. Chem. Soc., Dalton Trans.*, 1997, 3637-3642.
9. Huheey J.E., Keiter E.A., Keiter A.L., *Inorganic Chemistry, Principles of Strucrure and Reactivity*, 4th ed., 1993, Harper Collins College Publishers, New York.
10. Hartley F.R., Burgess C., Alcock R., *Solution Equilibria*, 1980, Ellis Horwood Ltd., West Sussex.
11. Lee J.D., *Concise Inorganic Chemistry*, 4th ed., Chapman and Hall, 1991, London.
12. Miessler G.L., Tarr D.A., Inorganic Chemistry, Prentice Hall, Inc., 1991, USA.
13. Cotton F.A., Wilkison G., *Advanced Inorganic Chemistry, A comprehensive Text*, 3rd ed., 1972, John and Wiley, Inc., London.

14. Wilkinson G., Gillard R.D., McCleverty J.A., *Comprehensive Coordination Chemistry*, 1987, **3,** Pergamon Press, Oxford.
15. Bailar J.C., Emeleus H.J., Nyholm R., Dickenson A.F.T., *Comprehensive Inorganic Chemistry*, 1973, **3,** Pergamon Press, Oxford.
16. Billo E.J., *Inog. Nucl. Chem. Letters*, 1974, **10**, 613-617.
17. Jackson G.E., Nakani B.S., *J. Chem. Soc. Dalton Trans.*, 1996, 1373-1377.
18. Jaffe H.H., Orchin M., *Theory and Applications of Ultraviolet Spectroscopy,* 1962, John Wiley & Sons, New York.
19. Jackson G.E., *UV-SPEC, Private Communication*, University of Cape Town.
20. Lever A.B.P., *Inorganic Electronic Spectroscopy*, 2nd ed., 1984, Elsevier, New York.
21. Sacconi L., Mani F., Bencini A., in; *Comprehensive Coordination Chemistry,* (Ed) Wilkinson G., Gillard R.D., McCleverty J.A., 1987, **5,** 45, Pergamon Press, Oxford.
22. Gampp H., Haspra D., Maeder M., Zuberbuehler A.D., *Inorg. Chem.,* 1984, **23,** 3724-3730.
23. Voye A., *PhD Thesis,* University of Cape Town, 1983, South Africa.
24. Marlin D.S., Olmstead M.M., Mascharack P.K., *Inorg. Chim. Acta,* 2001, **23,** 1-4.
25. Sanna D., Micera G., Kallay C., Rigo V., Sovago I., *J. Chem. Soc. Dalton Trans.*, 2004, 2702-2707.
26. Nomkoko T.E., *PhD Thesis,* University of Cape Town, 2002, South Africa.
27. Mkhomta-Gama, *PhD Thesis,* University of Cape Town, 1999, South Africa.
28. Jackson G.E., Nakani B.S., *J. Chem. Soc. Dalton Trans.*, 1996, 1373-1377.
29. Comba P., Hambley T.W., *Molecular Modeling of Inorganic Compounds,* 1995, VCH, Weinheim.

30. Comba P., Hambley T.W., *Molecular Modeling of Inorganic Compounds,* 2001, Wiley-VCH, Weinheim.
31. Hinchliffe A., *Molecular Modelling for Beginners,* 2003, Wiley & Sons Ltd, Chichester.
32. Bygott A.M.T., Sargeson A.M., *Inorg. Chem.* 1998, **37,** 4795-4806.
33. Benjamin P.H., Rustard J.R., *J. Chem. Soc. Dalton Trans.*, 1994, 6316-6326.
34. Cornell W.D., Cieplak P., Bayly C.I., Gould I.R., Merz K.M., Ferguson D.M., Spellmeyer D.C., Fox T., Caldwell J.W., Kollman P.A., *J. Chem. Soc. Dalton Trans.*, 1995, 5179-5197.
35. Shi S., Yan L., Yang Y., Fisher-Shaulsky J., Thacher T., *J. Compt. Chem.,* 2003, **24,** 1059-1076.
36. Accelrys life sciences molecular modelling software, InsightII, System Guide, Cambridge, UK, July 2005.
37. Bai S.K., Martell A.E., *J. Am. Chem. Soc.* 1969, **91**(16), 4412-4420.
38. Jubert C., Mohamadou A., Gerard C., Brandes S., Tabard A., Barbier J.P., *J. Chem. Soc. Dalton Trans.*, 2002, 2660-2669.
39. Chung-Sun C., Liu Si-Han., *Polyhedron*, 1984, **3**, no5, 559-566.
40. Brooker S., Dunbar G.S., Plieger P.G., *Inorg. Chim. Acta,* 2000, **304,** 204-209.

CHAPTER FIVE

BIO-MODELLING AND ANIMAL EXPERIMENTS

5. BIO-MODELLING AND ANIMAL EXPERIMENTS

5.1 THE BLOOD PLASMA MODEL

5.1.1 Introduction

Of importance in this study is to produce a ligand (drug) that would be able to mobilize Cu(II) in blood plasma. In biological fluids, the greater percentage of metal ions is bound to proteins. Actually, only a small fraction of these are bound to low molecular weight (l.m.w) compounds, mainly amino acids. Free (hydrated) metal ions exist in biological fluids only at extremely low concentrations, and these concentrations cannot play a significant role in physiological processes.[1] However, metals bound to l.m.w compounds play a major role in many biological and physiological processes like intestinal absorption, cell absorption and renal excretion.[1] The l.m.w complexes are believed to be involved (i) as intermediates when metal ions are inserted into or removed from certain metalloenzymes or carrier proteins, (ii) in the transfer of certain metal ions across membranes, (iii) in keeping essential metals in solution and (iv) in altering the potential of certain redox couples. Therefore, the knowledge of the equilibrium distribution of metal ions between l.m.w ligands is highly desirable.[2,3,4]

Metal ions which are considered essential to human life include calcium, magnesium, manganese, iron, cobalt, copper and zinc.[2,3] Of particular interest in this study are l.m.w. complexes of copper. In blood plasma, 90% of the copper is irreversibly bound to ceruloplasmin, 10 % is reversibly bound to serum albumen and a small amount <1% is distributed amongst l.m.w complexes, predominantly [Cu(histidate)(cystinate)].[6] In patients with inflammatory disease, elevated levels of plasma copper are found and these levels return to normal upon remission.[7] It is thought that the l.m.w fraction of copper is responsible for anti-inflammatory activity, possibly by making the copper available to superoxide dismutase.[7]

The total concentrations of Mn(II), Fe(III), Cu(II), Zn(II) and Pb(II) in normal blood plasma are between 1×10^{-7} and 5×10^{-5} mol dm^{-3}.[2,4] The corresponding minute concentrations of the respective free ions are far below the limit of detection by any analytical technique. It is also very difficult to get information from large chemical systems because of their complexity. Because of these limitations computer models simulating the complex systems have been developed.

Computer simulations of the metal-ligand equilibria in blood plasma have been performed using the general computer programs, COMICS and HALTAFALL.[8] They were both limited in respect of the way they stored data and in respect of their equation solving algorithms. They could not, therefore, treat hundreds of components and tens of thousands of complexes which might reasonably be expected to form in a complicated mixture such as blood plasma.[8]

For this reason, a specialized computer program was written in order to handle a large number of possible species. This was called ECCLES (Evaluation of Constituent Concentrations in Large Equilibrium Systems).[2] ECCLES solves the relevant mass balance equations and displays the resulting species distributions in an ordered way to enable changes in concentrations of the major complexes to be readily monitored. One of the major features of ECCLES is its preprocessor MIX which generates estimates of the equilibrium constants for the many mixed (ternary) complexes that might be important in the blood plasma.[8] Most of these complexes are mixed, ternary complexes of histidine and another amino acid.[9,10]

In order to understand the effect of the ligand (drug) on the equilibria present in this model, formation constants of the ligand and the species of interest determined in vitro, are incorporated into a database. This database, on inclusion of the drug concentration, is interrogated by the ECCLES

computer program to yield results pertaining to the influence of this drug on these equilibria.

One of the limitations of this program is that protein equilibria are not included and therefore the concept of plasma mobilizing index (p.m.i) is used. It is defined as the ratio of the total concentration of l.m.w metal complex species in the presence of the drug to that in normal blood plasma.[11] In simple terms, p.m.i is a measure of the ability of the administered ligand to move the metal ion from the protein bound fraction to the l.m.w fraction. It is based on the premise that the free concentration of the metal ion is buffered and hence held constant during any reasonable perturbation.

5.1.2 Blood plasma simulations

In investigating the copper specificity of the ligands of present study, the potentiometrically determined stability constants of Cu(II), Ni(II), Zn(II) and Ca(II) complexes were added to the updated ECCLES model[12,13] of blood plasma so as to calculate the plasma mobilizing indices. The blood plasma model consists of data for 10 metal ions and more than 5 000 ligands. This enlarged database was then interrogated by ECCLES to yield p.m.i's as a function of concentration. In the calculation, the total ligand concentration was varied over the range 10^{-5} – 10^{0} mol dm^{-3}. The results are presented in Figure 5.1(a), (b) and (c).

Figure 5.1(a) shows the Cu(II) p.m.i curves for PrDH and PrDPr as well as those of related ligands, TTDA, L^{3e}, and PCUA. One important observation from this figure is the absence of Cu(II) p.m.i for PrDM. This ligand was observed to give a log p.m.i value of 0.01 at high concentration (1 mol dm^{-3}). This indicates that PrDM has low mobilizing ability in blood plasma and thus cannot effectively increase the l.m.w Cu(II) fraction. Although the Cu(II) p.m.i curve for PrDH can be seen in the Figure 5.1(a), this ligand also shows low log p.m.i value of 0.08 at 1 mol dm^{-3} which is unreasonable for biological

systems. The reason for the low mobilizing ability of these two ligands is the stability of their complexes with Zn(II) and Ca(II). For example, in Figure 5.1(b), a 10^{-1} concentration of PrDH causes three folds increase in l.m.w Ca(II) and Zn(II), and no change in the l.m.w concentration of Cu(II).

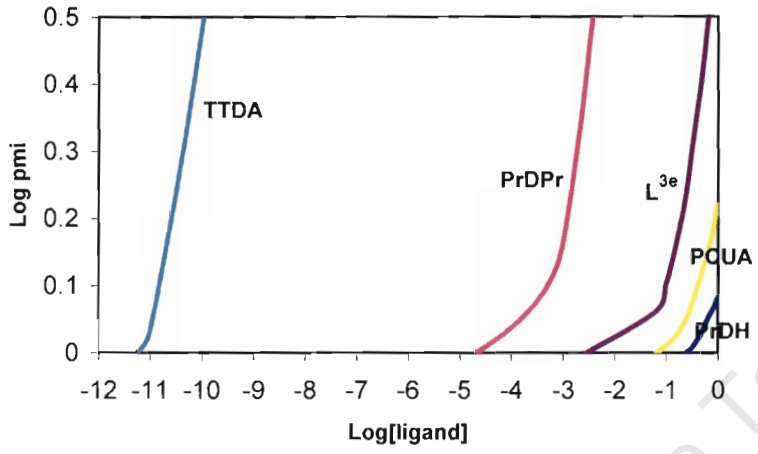

Figure 5.1(a): Logarithms of Cu(II) plasma mobilizing index as a function of logarithms of the ligand concentration for PrDH and PrDPr, and related ligands, TTDA, L^{3e}, and PCUA.

On the other hand PrDPr is 4 orders of magnitude better at mobilizing Cu(II) *in vivo* than PrDH. In comparison with related ligands, PrDPr is two to three orders of magnitude better at mobilizing Cu(II) *in vivo* than L^{3e} (N5-donor, Figure 3.17) and PCUA (N4-donor, Figure 2.1) respectively. However, TTDA (N4-donor, Figure 3.17) is about six orders of magnitude better than PrDPr. The N5-donor, L^{3g} was included in the model and it produced a log p.m.i value of 0.01 at 1 mol dm^{-3}.

Figure 5.1(b) shows p.m.i curves for Cu(II), Ni(II), Zn(II) and Ca(II) with PrDH plotted against logarithms of the concentration of the ligand. The curves indicate that the mobilizing ability of PrDH *in vivo* is in the order Ca(II) > Zn(II) > Cu(II) ≈ Ni(II). Therefore, Ca(II) and Zn(II) are good competitors of Cu(II) for PrDH in blood plasma. For the PrDPr system shown in Figure 5.1(c), this ligand is selective for Cu(II) *in vivo* relative to other metal ions. The

remarkably high mobilizing ability of this ligand is related to the stable complexes it forms with Cu(II). In addition, the predominant $CuLH_{-2}$ species of this ligand is present at the physiological pH. At a total ligand concentration of 3.1×10^{-3} mol dm^{-3} for PrDPr, the p.m.i's for Zn(II) and Ca(II) p.m.i's are very low (< 0.01). In spite of the higher concentrations of these *in vivo* competitors and the predominance of the MLH_{-2} and ML species for the two metal ions respectively, their weak binding strength with PrDPr make them less important competitors of Cu(II) *in vivo*.

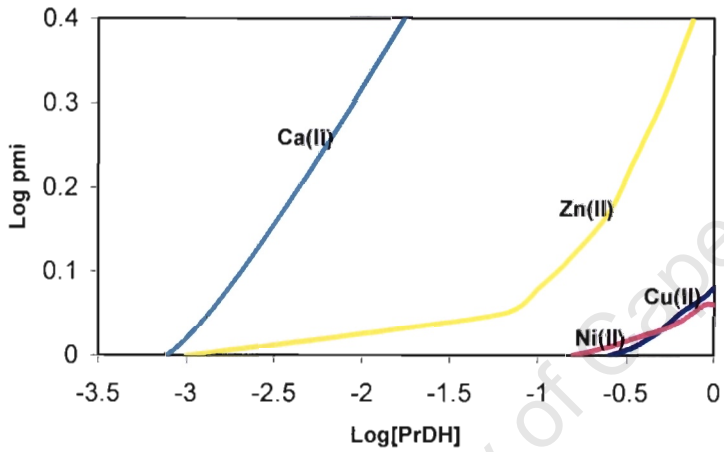

Figure 5.1(b): Logarithms of Cu(II), Zn(II), Zn(II) and Ca(II) plasma mobilizing index plotted against log[PrDH].

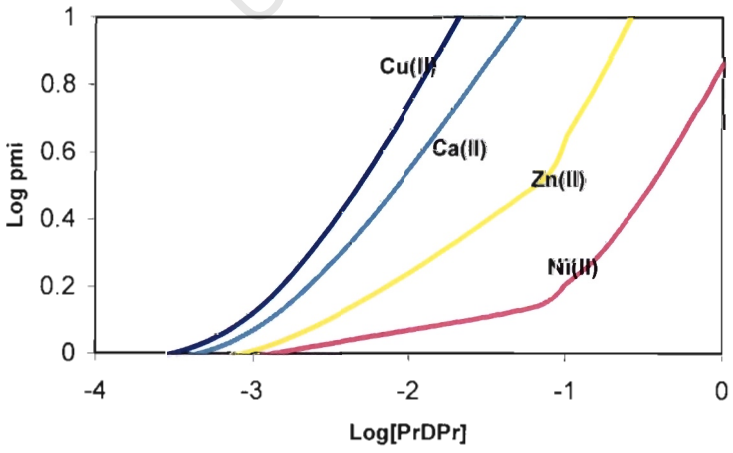

Figure 5.1(c): Logarithms of Cu(II), Zn(II), Zn(II) and Ca(II) plasma mobilizing index plotted against log[PrDPr].

5.2 SUPEROXIDE DISMUTASE MIMETIC ACTIVITY STUDIES

5.2.1 Introduction

The beneficial role of copper in minimizing inflammation has been attributed to its redox activity, particularly the ability of copper in such enzymes as superoxide dismutase (SOD) to remove the highly pro-inflammatory superoxide anion radical, $O_2^{\bullet-}$.[14,15] The superoxide anion radical is a highly reactive toxic species found in many biological systems. It is formed by the reduction of dioxygen, O_2.[14-19] Phagocytic cells appear to have specialized in such $O_2^{\bullet-}$ production due to a membrane-associated $O_2^{\bullet-}$ – producing NAD(P)H oxidase.[15] Along with hydrogen peroxide (H_2O_2) and the hydroxyl radical ($^{\bullet}OH$), superoxide has been implicated in oxidative damage phenomena related to aging, inflammation and post-ischemic injury via reperfusion.[15,17] The $O_2^{\bullet-}$ radical has also been implicated in the promotion of arthritis due to its ability to degrade hyaluronic acid and bovine synovial fluid.[20] Moreover, $O_2^{\bullet-}$ released from activated neutrophils produces a chemotaxin by reacting with a component of blood plasma.[15] This has the effect of allowing one activated neutrophil to recruit others and thus to produce local inflammation. It also inactivates catalases, peroxidases, dihydroxy acid dehydrase and other enzymes. However, the cytochrome oxidase decreases H_2O_2 and $O_2^{\bullet-}$ in the cells by direct conversion of dioxygen in respiring cell to water whereas SODs, catalases and peroxidases utilize a variety of electron donors to reduce H_2O_2 into water.[14,15,18,21,22]

Of importance in this study is copper-zinc SOD which provides cellular defence against the oxidative stress by catalyzing $O_2^{\bullet-}$ disproportionation into less toxic dioxygen and hydrogen peroxide. The CuZnSOD is found in the cytosols of eukaryotic cells.[15,17] During catalytic process, copper undergoes valence changes while zinc mainly plays a structural role. The Cu(II) and Zn(II) are ligated to a bridging imidazolate bond that plays a role in proton

conduction, which might otherwise become rate-limiting. Upon reduction of the Cu(II) by $O_2^{\bullet-}$, the Cu-imidazolate bond is broken and the imidazolate becomes protonated. Then, during reoxidation of the Cu(I) by the next $O_2^{\bullet-}$, the Cu-imidazolate bond is re-established while the proton converts the reduced $O_2^{\bullet-}$ to $HO_2^{\bullet-}$, which leaves the active site and picks up a second proton to become H_2O_2. This process has been summarized as follows;[15,16]

$$Cu(II) + O_2^{\bullet-} \leftrightarrow Cu(I) + O_2 \quad (5.1)$$

$$Cu(I) + O_2^{\bullet-} + 2H^+ \leftrightarrow Cu(II) + H_2O_2 \quad (5.2)$$

$$\text{Net } 2O_2 + 2H^+ \leftrightarrow H_2O_2 + O_2 \quad (5.3)$$

A number of Cu(II) complexes including those of polypeptides have been reported to exhibit SOD-mimic activity and thus are viewed as alternative human therapeutics to remove the pro-inflammatory superoxide anion radical *in vivo*.[14,23] In fact, low molecular weight Cu(II) complexes are capable of catalyzing the dismutation of the superoxide anion radical to dioxygen, water and/or hydrogen peroxide. [14,23]

5.2.2 Determination of Cu(II)-L SOD Mimetic Activity

Accurate measurement of the ability of a given SOD mimic to catalyze the dismutation of superoxide is essential for establishing a correlation between pharmacological effect and SOD activity. Several methods, either direct or indirect are available for SOD activity determination. UV-visible is the most widely used method. It is an indirect method which is based on two elements, a superoxide generator usually a xanthine-xanthine oxidase system and a detector, nitroblue tetrazolium (NBT).[14,24] In the absence of an SOD-mimetic agent (control experiment), the radicals react with the detector whereas in the presence of SOD-mimetic agent (inhibition experiment), this agent competes with the detector for the superoxide anion radical.

The SOD activity is measured by the degree of inhibition of the conversion process of NBT to form diformazan using UV-visible spectrophotometry at 560 nm over a period of time. The absorbance versus time curves corresponding to a control and particular concentrations of an SOD mimic (Cu(II)-L complex) are generated and slopes of these curves computed. The %Inhibition of the reduction of NBT to blue diformazan is calculated using the following equation;

$$\%\text{Inhibition} = \frac{[(S_{ces} - S_{ies})x100]}{S_{ces}} \qquad (5.4)$$

where S_{ces} and S_{ies} are slopes of the control and inhibition experimental solutions respectively. Values of %Inhibition against varying drug concentration are plotted. The inhibitory concentration (IC_{50}) defined as concentration of the drug required to reduce diformazon by 50% is read off from these plots.

These experiments are carried out in the presence of excess disodium salt of EDTA as compared to other components. This condition stimulates the competitive binding of endogenously available l.m.w ligands[24,25] and also enable complexation of small amounts of the metal ions such as Fe(III) that may be present in NBT and/or xanthine, which are known to catalyze the dismutation of superoxide anion as well.[24] It should be noted that Cu(II)-EDTA complexes are inactive as SOD mimics.

5.2.3 Experimental

The superoxide dismutase mimetic activity of Cu(II)-L (L= PrDH, PrDM, PrDPr and PCUA) complexes were determined using NBT assay.[14,24,25] Standard solutions of (i) 0.0004 M xanthine, (ii) 0.0001 M EDTA, (iii) 0.0001 g/cm^3 of catalase, (iv) 0.018 units/cm^3 xanthine oxidase and (v) 0.001 M solutions of Cu(II)-L complex in 0.05 M phosphate buffer were prepared.

In a 4 cm^3 cuvette, 0.6 cm^3 xanthine, 0.2 cm^3 EDTA, 0.2 cm^3 NBT, 0.1 cm^3 catalase and 2.9 cm^3 of phosphate buffer were added and this constituted a blank solution. In a control experiment, in addition to these compounds, 0.4 cm^3 xanthine oxidase and 2.5 cm^3 instead of 2.9 cm^3 phosphate buffer solution were added while in a test solution varying amounts of Cu(II)-L complex solutions were added prior to the addition of xanthine oxidase. The concentrations of Cu(II)-L SOD mimics ranged from 2.5×10^{-6} mol dm^{-3} to 4.5×10^{-4} mol dm^{-3}.

The absorbance readings at 560 nm were obtained at 30 seconds intervals for a total period of 10 minutes for the control and experimental SOD solutions. For each set of readings corresponding to a control and a particular concentration of SOD mimic (Cu(II)-L complex), the absorbance was plotted against time and the slopes of the resulting plots were computed. The %inhibition of the reduction of NBT to formazan was calculated using equation 5.4 and IC_{50} values similarly determined from plots of %inhibition versus concentration of the Cu(II)-L complex.

5.2.4 Results and discussion

5.2.4.1 Cu(II)-L Systems

Figure 5.2 (a), (b), (c) and (d) show the percentage inhibition as a function of the concentration of the Cu(II) complexes for the ligand systems, PrDH, PrDM, PrDPr and PCUA respectively. The concentration of the drug required to reduce diformazan formation by 50%, also known as IC_{50} can be easily read off from these graphs.

IC_{50} values of 199, 31.3, 275 and 233 μmol dm^{-3} for the Cu(II)-PrDH, Cu(II)-PrDM, Cu(II)-PrDPr and Cu(II)-PCUA complexes have been obtained as shown in Figure 5.2 (a), (b), (c) and (d) respectively. These values are associated with MLH_{-1} species for PrDH and PrDM systems and, MLH_{-2} and

MLH_{-1}/MLH_{-2} species for PrDPr and PCUA systems respectively. The IC_{50} values of the native CuZnSOD (= 0.011 μM)[26], Cu_2Zn_2SOD (= 0.006 μM)[14] and bovine erythrocyte SOD (= 0.04 μM)[27] have been reported. The IC_{50} values recorded in this work for the studied Cu(II) complexes are much higher than these values. Therefore, Cu(II) complexes of the present study have low SOD activities as compared to the native enzyme. The IC_{50} values of some Cu(II) complexes of amino acids such as tyrosine (= 45 μM) and lysine (= 86 μM) and, non-steroidal anti-inflammatory drugs (NSAIDs) such as salicylates (= 2-28 μM) have been reported.[28,29] These values are reasonably or rather relatively close to those obtained in this study. Moreover, Mkhonta-Gama[30] reported IC_{50} values for the related dioxo N5-donor ligands (L^{3c}-L^{3f}, Figure 3.17) in the range 131 – 195 μM whereas Nomkoko[31] reported a value of 11.7 μM for the dioxo N5-donor ligand (L^{3g}, Figure 3.17).

An important observation in the results of the present study is the fact that the IC_{50} values correlate with the corresponding p.m.i values. The Cu(II)-L system with low log p.m.i value or rather low mobilizing ability in blood plasma is observed to possess relatively high SOD mimetic activity. In this case it is the Cu(II)-PrDM system which shows relatively high SOD mimetic activity whereas the Cu(II)-PrDPr system which showed relatively high mobilizing ability in blood plasma shows low SOD mimetic activity. The low IC_{50} value exhibited by the Cu(II)-PrDM system can be interpreted in terms of the possible replacement of coordinated water molecule by the superoxide anion radical. Moreover, the presence of the protonated ligand's sites of the MLH_{-1} species should also contribute to the dismutation of the superoxide anion radical through hydrogen bonding. On the other hand, the high IC_{50} value may be due to the unavailability of the binding sites for the superoxide anion radical to coordinate to the metal ion. Important requirements for SOD-like activity are a medium donor power and the flexibility of the ligands, in order to facilitate the reduction and the accommodation of Cu(I), which is known to prefer tetrahedral or linear environments.[27] The coordination

geometry of the native SOD enzyme is distorted square-pyramidal for Cu(II) and distorted tetrahedral for Zn(II).

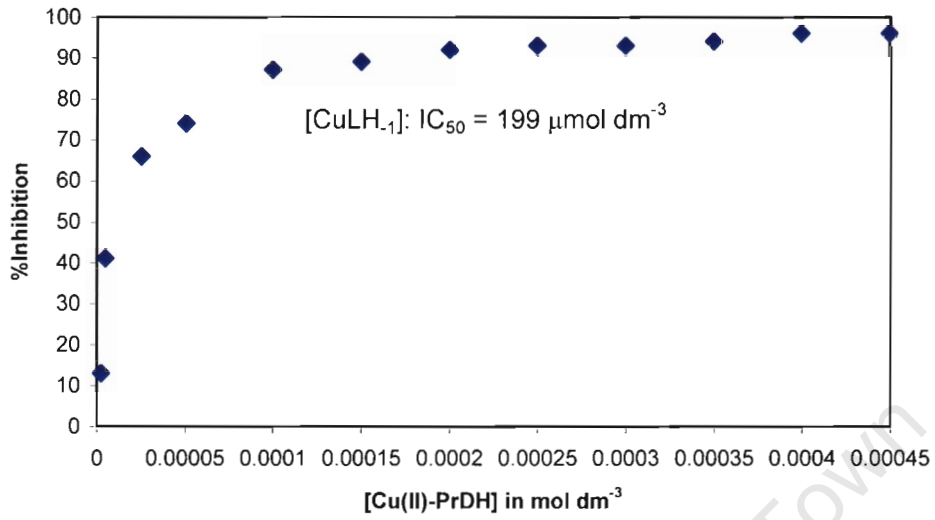

(a)

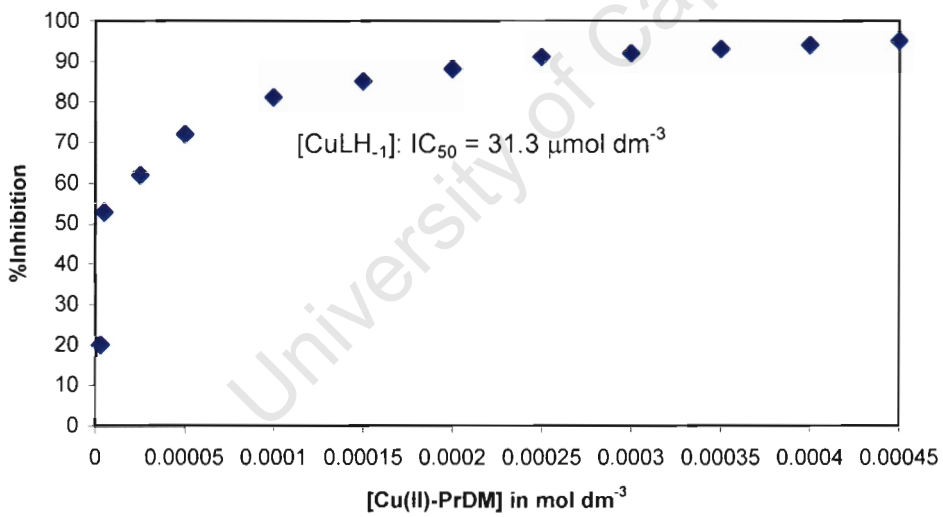

(b)

Figure 5.2 %Inhibition as a function of concentration of MLH_{-1} species for the **(a):** Cu(II)-PrDH and **(b):** Cu(II)-PrDM systems.

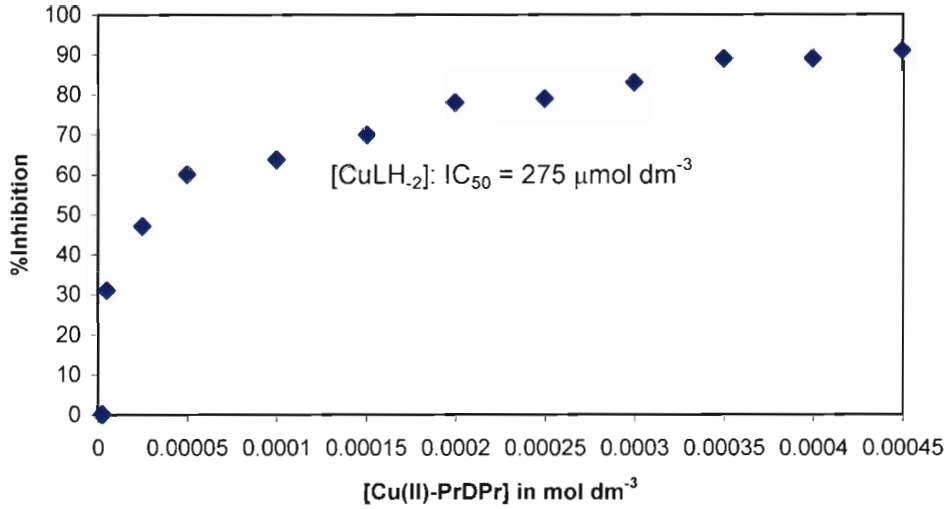

(c)

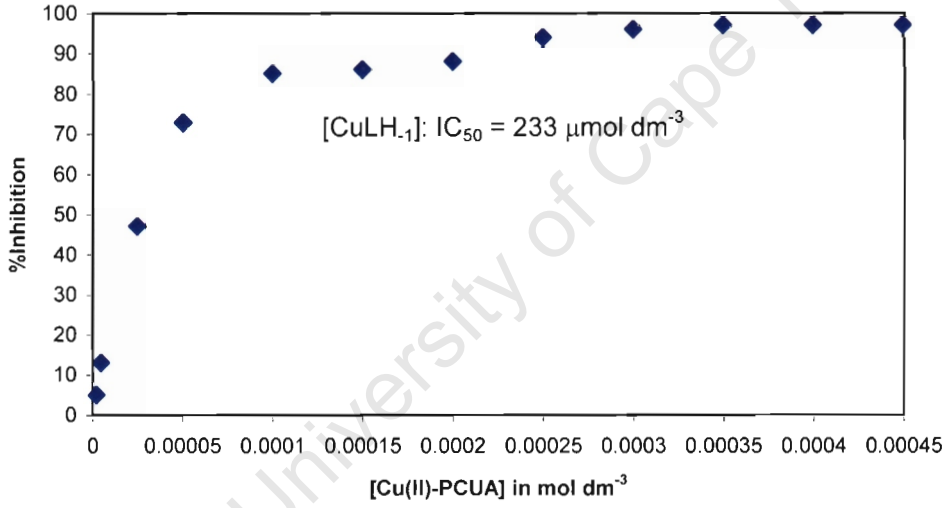

(d)

Figure 5.2 %Inhibition as a function of concentration of MLH_{-2} and MLH_{-1} species for the **(c):** Cu(II)-PrDPr and **(d):** Cu(II)-PCUA systems respectively.

5.3 OCTANOL/WATER PARTITION COEFFICIENTS

5.3.1 Introduction

One important aspect upon which biological activity depends is the ability of the drug to reach the target area of action. In the human body, drugs have to traverse a number of body tissues before they can impart their therapeutic effect. Transport across the skin and bio-membranes in general is a process of limited diffusion governed by the drugs' chemical and physical properties such as lipophilicity and protein binding.[32,33]

Partition coefficients measurements can be used as reference parameter for hydrophobicity in biochemical and pharmacological systems. The measure of hydrophobicity can be expressed as the logarithm of the partition coefficient between 1-octanol and an aqueous phase.[38] For Cu(II)-complex as a drug, this may be given as;

$$\text{Log}P_{\text{oct/water}} = \text{Log}\left(\frac{[Cu^{2+}]_{org}}{[Cu^{2+}]_{aq}}\right) \qquad (5.5)$$

where $[Cu^{2+}]_{org}$ and $[Cu^{2+}]_{aq}$ are the concentrations of Cu(II) in the organic and aqueous phases respectively.

An investigation of a biphasic system at varying pH values interestingly shows the role that speciation plays in the determination of the partition coefficients. The amount of Cu(II) transferred from aqueous solution to organic layer changes with pH because speciation changes with pH and the different species have different partition coefficients. Moreover, the change in charge in successive complex formation is accompanied by a change in the solubility of the solutes (species) in the two phases.[36]

Partition coefficients are usually employed as criteria in quantitative structure-activity relationship studies in biomedical chemistry.[34,35] They can also be

used in the estimation of bioaccumulation in animals and plants, and in the prediction of toxicity and drug absorption.[38]

5.3.2 Experimental

The commonly used experimental (traditional) method for the determination of partition coefficients ($logP_{oct/aq}$) is the shake-flask method, which is adopted as the standard OECD (Organisation for Economic Cooperation and Development) method.[37] However, for compounds having higher hydrophobicity, this method cannot be used because of the formation of octanol emulsions in water.[38]

In this study partition coefficients were determined using the shake-flask.[39,40] 100 cm^3 of Cu(II) (0.001 mol dm^{-3}) – L (0.002 mol dm^{-3}) solutions were prepared. Into fifteen 20 cm^3 glass vials, 5 cm^3 portions of the metal-ligand solutions were pipetted. The first vial was left at pH 3.0 while the rest of the vials were adjusted in 0.5 pH increments apart using 0.1 mol dm^{-3} of NaOH. These solutions were then spiked with $^{64}CuCl_2$ solution of activity 5 – 7.5 mCi. To each vial containing the spiked metal-ligand solution, 5 cm^3 portions of water saturated 1-octanol were added. These were then stoppered and shaken for 5 minutes, swirled to collect droplets from sides of the vials and set aside to allow the two phases to separate at a constant temperature of 25 ^oC. 1 cm^3 of each phase was pipetted into radioactive counting vials using a microlitre pipette and activity of each phase counted for 5 minutes in a Minaxi Auto gamma counter (5000 Series-Packard) using a window set at 340 – 540 eV.

5.3.3 Results and discussion

5.3.3.1 Cu(II)-L systems

Figure 5.3(a), (b), (c) and (d) show the partition coefficients ($logP_{oct/aq}$) of Cu(II)-PrDH, Cu(II)-PrDM, Cu(II)-PrDPr and Cu(II)-PCUA systems as a function of pH respectively. These $logP_{oct/aq}$ values were determined at 25 ^{o}C and an ionic strength of 0.15 mol dm^{-3} $(Cl^{-})Na^{+}$.

Observed in Figure 5.3(a), (b), (c) and (d) is the fact that all $logP_{oct/aq}$ values are negative. The negative values of $logP_{oct/aq}$ indicate that these complexes are largely hydrophilic. The $logP_{oct/aq}$ values -2.35, -2.11, -0.58 and -1.65 for the Cu(II)-PrDH, Cu(II)-PrDM, Cu(II)-PrDPr and Cu(II)-PCUA systems have been obtained at physiological pH (7.4) respectively. The low values in the acidic pH range for the complex species is indicative of the presence of hydrated $[Cu(OH_2)_6]^{2+}$ species. This would be highly expected for PrDH and PrDM systems for which Cu(II) complexation commences at pH>4.

The speciation graphs show that Cu(II) complexation commences at approximately pH 4.5 for PrDH (Figure 3.5(c)) and pH 5 for PrDM (Figure 3.8(c)) systems and therefore, high concentrations of hydrated $[Cu(OH_2)_6]^{2+}$ species are expected below these pH values. There is an increase in $logP_{oct/aq}$ values as pH increases due to various species formed from Cu(II) with PrDH and PrDM (Figure 5.3(a) and (b)). The $logP_{oct/aq}$ value of -2.23 at pH 6.5 is associated to the ML species for the PrDM system whereas the value of -2.51 at pH 6.0 is associated with the MLH/ML species for PrDH system. These species are tri/di-positively charged, a factor that could enhance their association with the aqueous solution. At physiological pH, MLH_{-1} is the predominant species for both systems and it is observed that approximately 0.43% of the Cu(II)-PrDH and 0.83% of the Cu(II)-PrDM complexes are extracted into the organic phase of the octanol-water mixture used as a bio-phase model of the membrane. There is rapid increase in

$logP_{oct/aq}$ values as pH is increased from 8-10 due to the formation of MLH_{-2} with maximum $logP_{oct/aq}$ values of -1.72 and -0.83 for the PrDH and PrDM systems respectively. Formation of the neutral MLH_{-2} species enhances extraction into the organic phase. The relatively hydrophilic nature of these two ligands in addition to the charge distributions, explains the complexes' preference for the aqueous layer resulting in negative values of $logP_{oct/ag}$.

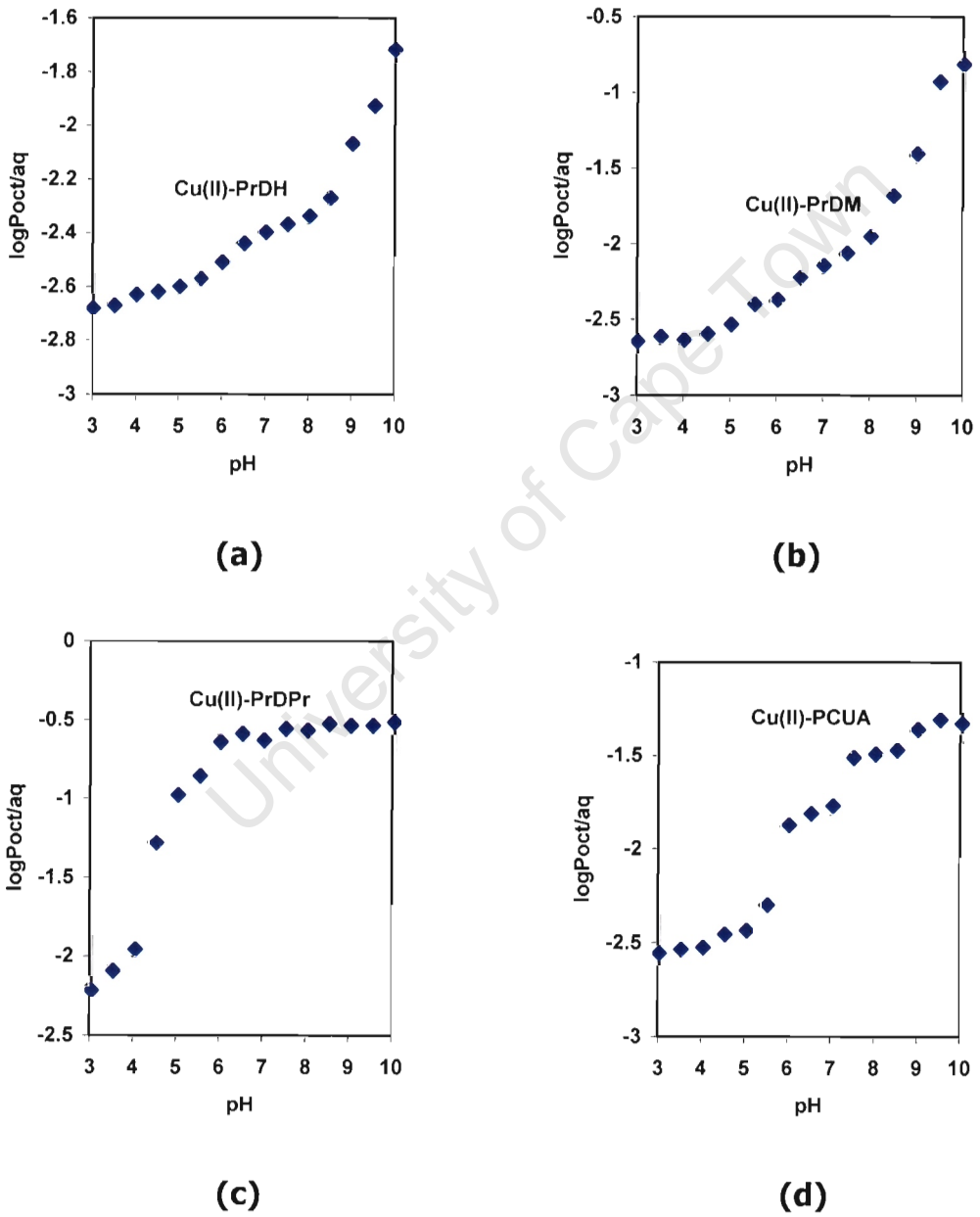

Figure 5.3 Logarithms of octanol-water partition coefficients as functions of pH for **(a):** Cu(II)-PrDH, **(b):** Cu(II)-PrDM, **(c):** Cu(II)-PrDPr and **(d):** Cu(II)-PCUA systems.

For the Cu(II)-PrDPr system the $logP_{oct/aq}$ values are higher than those of the other three systems in this study as shown in Figure 5.3(c). For this system Cu(II) complexation begins at low pH (= 2.2, Figure 3.12(c)) by the formation of the MLH species which predominates at pH 3.2. Therefore, $logP_{oct/aq}$ of -2.21 is assigned to this species. On the other hand, complexation of Cu(II) with PCUA begins at pH 2.5 with formation of the MLH species predominating at pH 5.1, giving a $logP_{oct/aq}$ value of -2.44 (Figure 5.3(d)). Unlike the PCUA system for which the ML species predominates at pH 6.5 ($logP_{oct/aq}$ = -1.82), the ML species of the Cu(II)-PrDPr system overlaps or rather coexists with both MLH and MLH_{-1} species. However, MLH_{-1} species of the PrDPr system predominates at pH 4.8 thus being assigned to $logP_{oct/aq}$ value of -0.98. The positively charged species would be expected to result in negative $logP_{oct/aq}$ values due to the ability of water to stabilize charges. At physiological pH the MLH_{-2} and MLH_{-1} are the predominant species for PrDPr and PCUA respectively and it is observed that 19% of Cu(II)-PrDPr and 2.9% of Cu(II)-PCUA complexes are extracted into the organic phase of the octanol-water mixture. Although these complexes are relatively hydrophilic by virtue of having negative $logP_{oct/aq}$ values, they are more lipophilic than PrDH and PrDM systems. The amount of the Cu(II)-PrDPr complex (19%) extracted into the organic phase of the octanol-water mixture is reasonably good for transport across bio-membranes. The relatively high amount of this complex extracted into the organic phase is due to the presence of the bulky groups and this suggests the essential role of such groups in percutaneous drug administration. It was therefore, expected that the incorporation of the benzyl group would enhance lipophilicity of the complex.

Jackson and coworkers[41] reported $logP_{oct/aq}$ values for the related Cu(II) complexes of dioxo N5-donor ligands in the range -3.70 to -6.63 for the MLH, ML, MLH_{-1} and MLH_{-2} species. Nomkoko and coworkers[42] also reported $logP_{oct/aq}$ value of -1.25 at physiological pH (7.4) for the related dioxo N5-donor ligand. Positive $logP_{oct/aq}$ values (0.618 – 4.128) of some anti-

inflammatory drugs have been reported.[40] Therefore, for a drug (complex) to be reasonably lipophilic the $logP_{oct/aq}$ value must be at least 0.618. The value of $logP_{oct/aq}$ = -0.58 for the Cu(II)-PrDPr system shows that this complex is relatively lipophilic. Mathias and coworkers[43,44] have reported positive $logP_{oct/aq}$ values for the positively charged complexes thus indicating that the electrostatic interactions are not the sole factor governing octanol-water partition.[45] Rothwell and coworkers[46] have recently reported the octanol-water partition coefficients of Quercetin and related flavonoids in the range -1.11 to 3.22. The consumption of flavonoids has been associated with protection against coronary heart disease and cancer. Several workers[47-49] studied ^{64}Cu-labeled complexes of $logP_{oct/aq}$ values in the range -1.60 to -3.02 for potential use as attaching copper radionuclides to biological molecules for diagnostic imaging and targeted radiotherapy. Therefore, the results obtained in this study are encouraging considering that they fall in the above range and also that the Cu(II)-PrDPr complex is reasonably lipophilic at physiological pH (7.4).

In general, neutral species (complexes) take part in the partition equilibrium between the aqueous and organic phases while charged species remain in the aqueous phase. The contributing factors to the hydrophilicity of the present complexes are; a) the presence of coordinated water molecules, b) hydrogen bonding between charged groups in these species and the solvent molecules, c) the overall charge of the MLH, ML, MLH_{-1} complex and d) hydrogen bonding between carbonyl oxygen atoms and the bulk of the water molecules.

5.4 BIO-DISTRIBUTION STUDIES

5.4.1 Introduction

As an essential element, copper plays an important role in all living organisms including humans.[50] Biologically active oxidation states of copper, I, II and III, are found in copper complexes that act to transport copper to body sites where it is required.[50] Free copper may be toxic and therefore, copper exists mostly in complexed forms, bound to macromolecules and low molecular weight ligands in body fluids.[51] Dietary copper is readily absorbed in the stomach and small intestine, from which it is transported to the liver by the blood as a serum albumin complex. It is in the liver that copper is processed and stored as a metallothionein complex or converted into ceruloplasmin which is released into the blood to meet normal metabolic needs.[52-54]

The body of a healthy, 70 kilogram, human adult contains approximately 110 milligrams of copper, much of it in the liver (10 mg), brain (8.8 mg), blood (6 mg), skeleton (including the bone marrow; 46 mg), and muscle (26 mg).[29,55] The daily intake of copper in the human body is approximately 1.5 - 3 mg.[29] In humans copper absorption varies inversely with dietary copper intake[56] and absorption occurs primarily in the small intestine[57] after digestion of food in the stomach and duodenum.[58] Once absorbed, approximately 70 - 80% of plasma copper is in non-exchangeable forms, bound to ceruloplasmin. The remainder is bound to albumin, transcuprein, metallothionein and low molecular weight complexes as the exchangeable copper fraction in blood.[58,59] A summary of the nutritional biochemistry and metabolism of copper for adult humans presented by Linder and Hazegh-Azam[58] is shown in Figure 5.4(a). Values for copper indicate average daily amounts of copper ingested, absorbed and secreted via various routes. Concentrations of copper in fluids are also shown as well as total amounts of copper in various tissues. Percentages refer to absorbed or percentage of total body copper in specific tissues.

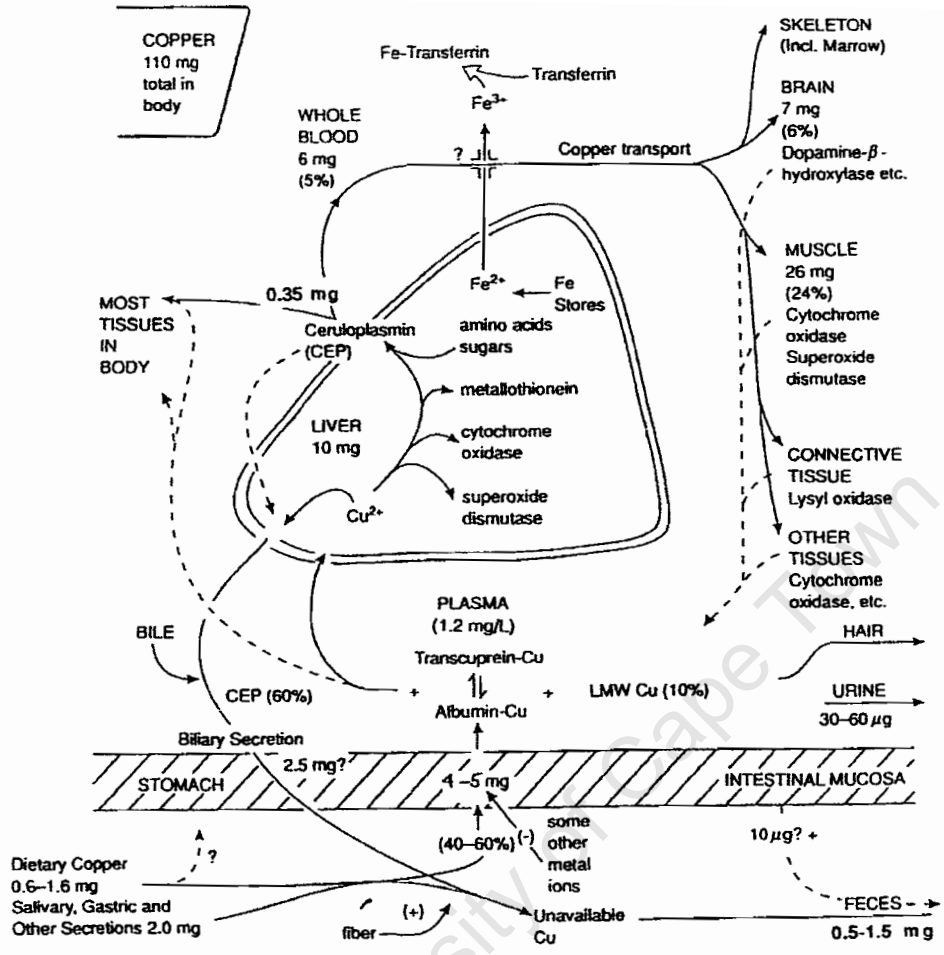

Figure 5.4(a): A summary of the nutritional biochemistry and metabolism of copper for adult humans.[58]

It was observed after intraperitoneal injection of tracer amounts of ^{67}Cu in mice that all of the copper rapidly left the blood and entered the liver and kidney before re-emerging in the plasma.[55] The uptake of the administered isotope by other tissues and organs such as heart and brain appeared to take place mainly during the re-emerging of copper in the plasma. The present study investigates copper bio-distribution in mice using $^{64}Cu(II)$ as a radiotracer for the copper chelating agents. This allows the determination of the changed bioavailability and efficacy of these agents in transporting Cu(II) through the body to possible sites of inflammation as well as determining the ligands' *in vivo* stability. The bio-distribution studies results are also compared

with potentiometric (section 3.5), blood plasma model (section 5.1.2) and octanol-water partition coefficients (section 5.3.3) results.

5.4.2 Experimental

Bio-distribution studies on mice were approved by the Research Animals Ethics Committee of the University of Cape Town (permission number 005/039). The authority to possess and use the radioactive nuclide $^{64}Cu(II)$ (half-life = 12.7 hours) was granted by the University of Cape Town's radiation protection and health safety committee in conjunction with the Department of Health (authority number 33/01/0327). The procedures for carrying out experiments were done in compliance with the guidelines set by the University of Cape Town Research Animals Ethics Committee.

The experimental approach adopted for these animal experiments was similar to the approach of Jackson and co-workers[60] and, other workers[48,49] in the field of nuclear medicine. Solutions of Cu(II)(0.001 mol dm^{-3}) - L(0.003 mol dm^{-3}) complexes of PrDH, PrDM, PrDPr and PCUA were prepared in sterile saline solution at pH 7.40. These prepared complex solutions (20 cm^3) were spiked with 10-14 mCi $^{64}CuCl_2$(aq) (radiochemical purity > 98 %)

A total of 48 female Balb/c mice of age 7-8 weeks weighing 19-23 grams were used in these experiments. The mice were housed in groups of three (3) mice per cage and were given food and water *ad libitum* during the investigation period. These groups of three mice were injected intravenously with 0.2 cm^3, [^{64}Cu]Cu(II)-L solution (containing 6.5 μg Cu), of 5 μCi activity via the tail vein. Another group of mice was injected with [^{64}Cu]$CuCl_2$ as a control experiment. The mice were kept individually in polycarbonate cages containing paper towelling for urine absorption.

At 1, 6 and 24 hour post-injection time points, groups of mice (three at a time) were sacrificed by carbon dioxide inhalation and aliquots of blood taken

from the heart. Various samples (liver, muscle, tail, heart, lung, kidney, spleen, head, intestines, and carcass) were removed, rinsed with NaCl (0.9 %), dried and then weighed. The urine impregnated towelling was extracted with 100 cm^3 of 10 % v/v HCl. The radioactivity in these samples as well as a 10 cm^3 aliqouts of the urine extract were counted using a Minaxi Autogamma 5000 Series γ counter, with the window set at 340-540 KeV. Control samples were counted alongside with the experimental samples. All readings were corrected for background noise by subtracting the activity of an empty sample bottle and also adjusted to activity at time zero according to the half-life of ^{64}Cu(II) using the exponential decay law given in equation 5.6.

$$N = N_o e^{-\lambda t} \quad (5.6)$$

where t is the time elapsed, λ is the decay constant, N is the amount of activity after time t and N_o is the amount of activity at time t = 0. The percentage injected dose per organ (%dose/organ) and percentage injected per gram (%dose/g) were calculated from the corrected activity counts.

Although low activity ^{64}Cu(II) ($t_{1/2}$ = 12.7) of 10 – 14 mCi was used in these experiments, precautionary measures were taken against possible exposure to the high penetrating abilities of high energy positrons and gamma radiation. During these experiments, disposable gowns, gloves and radiation badges were worn. The preparation of [^{64}Cu]Cu(II)-L complexes as well as injection of mice were performed behind lead brick walls. The aqueous solution of the radiolabeled [^{64}Cu]Cu(II) complexes and [^{64}Cu]$CuCl_2$ were kept in closed containers under refrigeration. After all experiments, the materials including syringes, needles, disposables, the sacrificed animals and their respective excised organs were initially kept in a refrigerator for at least four weeks. This allowed the radioactivity to decay below safe levels before incineration.

5.4.3 Results and discussion

Based on the aforementioned *in vitro* results, it was deemed necessary to perform bio-distribution experiments. Since the body is a dynamic system, the biodistribution was measured as a function of time. The results given in Table 5.1 show %dose per organ and %dose per gram for [^{64}Cu]Cu(II)-PrDH, [^{64}Cu]Cu(II)-PrDM, [^{64}Cu]Cu(II)-PrDPr and [^{64}Cu]Cu(II)-PCUA as well as [^{64}Cu]$CuCl_2$ (control) at 1 hour time point. High activity in the carcass resulted in further excision of other organs but now at 6 and 24 hour post-injection. The excision of other organs was done in order to investigate the localization of this activity. The results are given in Table 5.2 and Table 5.3 including those of control experiments ([^{64}Cu]$CuCl_2$).

The bio-distribution results for the control, [^{64}Cu]$CuCl_2$, show that there is rapid clearance from the blood with less than 1 %dose remaining 1 hour post-injection. The clearance is due to the high uptake by the liver with 61.57 %dose after 1 hour and 63.69 %dose after 6 hours found in this organ. The activity dropped to 11.32 %dose 24 hour post-injection due to excretion through urine. The carcass, which is left after removing head and liver, recorded a high activity uptake of 31.51 %dose after 1 hour. After further excision of organs at time point 6 and 24 hours, the activity in carcass increased from 7.85 %dose 6 hour post-injection to 11.35 %dose after 24 hours. Like the liver and carcass, intestines and kidney show increase in [^{64}Cu]Cu(II) activity as shown in Table 5.1, thus suggesting that excretion is via hepatobiliary and renal routes. These results are in good agreement with those reported by Nomkoko and co-workers[60] for [^{64}Cu]$CuCl_2$. The biodistribution pattern of the control experiments follows that of the normal metabolic pathway of copper reported by Linder and co-workers.[55]

The bio-distribution for the [^{64}Cu]Cu(II) complexes of PrDH, PrDM, PrDPr and PCUA at 1 hour post injection is generally similar to those of the control. High activity is observed in the blood for the different complexes compared to the

control as shown in Table 1. This indicates that clearance from the blood system is slower for these complexes than for the control. However, the uptake by the liver (58.18 – 63.89 %dose) is approximately the same as that of the control (61.57 %dose). Like the control, [^{64}Cu]Cu(II) complexes show high activity in the carcass after 1 hour with activity of 34.02, 36.04, 31.32 and 29.16 %dose for PrDH, PrDM, PrDPr and PCUA systems respectively.

Table 5.1: Bio-distribution of [^{64}Cu]Cu(II) in mice for various ligands 1 hour post-injection (%dose per organ and %dose per gram, mean ± std.dev., n=3).

Organ	[^{64}Cu]Cu(II) complex, % dose per organ % dose per gram				
	PrDH	**PrDM**	**PrDPr**	**PCUA**	**$CuCl_2$**
Blood	1.61 ± 0.15 1.31 ± 0.07	1.39 ± 0.20 1.04 ± 0.18	2.89 ± 0.56 2.37 ± 0.38	1.38 ± 0.39 1.18 ± 0.25	0.80 ± 0.08 0.63 ± 0.07
Carcass	34.02 ± 4.68 2.23 ± 0.35	36.04 ± 9.95 2.14 ± 0.71	31.32 ± 3.78 2.02 ± 0.10	29.16 ± 2.87 1.84 ± 0.21	31.51 ± 7.29 2.00 ± 0.43
Head	2.05 ± 0.02 0.69 ± 0.06	3.20 ± 0.54 1.06 ± 0.18	3.63 ± 0.35 1.30 ± 0.11	3.42 ± 0.10 1.09 ± 0.06	2.54 ± 0.17 0.78 ± 0.01
Liver	60.03 ± 5.18 57.37 ± 9.66	58.18 ± 6.00 50.67 ± 2.30	59.53 ± 2.69 52.81 ± 4.38	63.89 ± 2.25 57.65 ± 5.38	61.57 ± 6.91 52.94 ± 6.18
Urine	2.30 ± 0.40	1.18 ± 0.52	2.64 ± 0.70	2.04 ± 0.89	3.58 ± 0.48

Table 5.2: Bio-distribution of [^{64}Cu]Cu(II) complexes of PrDH, PrDM, PrDPr and PCUA (%dose per organ, mean ± std.dev., n=3)

	[^{64}Cu]Cu(II)-PrDH		[^{64}Cu]Cu(II)-PrDM		[^{64}Cu]Cu(II)-PrDPr		[^{64}Cu]Cu(II)-PCUA		[^{64}Cu]$CuCl_2$	
Organ	6 hr	24hr	6 hr	24hr	6 hr	24hr	6 hr	24hr	6 hr	24hr
Blood	1.02 ± 0.13	2.81 ± 0.83	0.89 ± 0.05	2.24 ± 0.22	1.22 ± 0.33	2.08 ± 0.20	1.07 ± 0.17	1.86 ± 0.14	0.80 ± 0.23	0.86 ± 0.24
Carcass	8.10 ± 1.39	16.26 ± 3.83	7.43 ± 0.79	18.81 ± 3.52	7.08 ± 1.54	12.02 ± 0.29	6.94 ± 0.79	13.25 ± 2.87	7.85 ± 1.87	11.35 ± 1.77
Head	1.94 ± 0.08	4.41 ± 1.21	1.99 ± 0.20	4.72 ± 0.31	1.61 ± 0.10	3.40 ± 0.11	2.00 ± 0.26	3.72 ± 0.21	1.94 ± 0.04	7.56 ± 2.74
Heart	0.28 ± 0.04	0.60 ± 0.18	0.20 ± 0.03	0.55 ± 0.14	0.21 ± 0.02	0.46 ± 0.05	0.28 ± 0.04	0.44 ± 0.04	0.19 ± 0.02	0.21 ± 0.07
Intestines	14.55 ± 1.74	23.51 ± 4.00	19.66 ± 1.23	26.03 ± 3.56	12.23 ± 0.99	30.25 ± 4.18	16.80 ± 4.97	25.34 ± 5.61	22.17 ± 2.87	11.61 ± 6.94
Kidney	1.24 ± 0.16	2.75 ± 0.62	1.15 ± 0.08	2.72 ± 0.28	2.21 ± 0.90	2.31 ± 0.34	1.15 ± 0.09	1.94 ± 0.01	1.04 ± 0.15	0.96 ± 0.42
Liver	70.70 ± 0.81	40.25 ± 5.11	66.99 ± 1.31	38.98 ± 6.99	64.31 ± 2.89	35.56 ± 9.26	67.89 ± 5.42	33.57 ± 7.56	63.69 ± 5.06	11.39 ± 7.11
Lung	0.29 ± 0.25	1.34 ± 0.59	0.54 ± 0.21	1.30 ± 0.14	0.45 ± 0.14	1.00 ± 0.03	0.61 ± 0.07	0.96 ± 0.04	0.53 ± 0.08	0.44 ± 0.18
Muscle	0.05 ± 0.01	0.09 ± 0.01	0.05 ± 0.02	0.14 ± 0.06	0.06 ± 0.03	0.12 ± 0.03	0.07 ± 0.01	0.15 ±0.09	0.06 ± 0.04	0.04 ± 0.03
Spleen	0.17 ± 0.06	0.54 ± 0.23	0.23 ± 0.01	0.68 ± 0.18	0.14 ± 0.03	0.30 ± 0.13	0.28 ± 0.05	0.44 ± 0.11	0.23 ± 0.04	0.12 ± 0.02
Urine	1.65 ± 0.22	7.43 ± 1.39	0.85 ± 0.46	3.61 ± 0.88	10.48 ± 2.31	12.52 ± 4.42	2.89 ± 1.08	18.34 ± 2.52	1.50 ± 1.29	55.44 ± 8.72

Table 5.3: Bio-distribution of [^{64}Cu]Cu(II) complexes of PrDH, PrDM, PrDPr and PCUA (%dose per gram, mean ± std.dev., n=3)

	[^{64}Cu]Cu(II)-PrDH		[^{64}Cu]Cu(II)-PrDM		[^{64}Cu]Cu(II)-PrDPr		[^{64}Cu]Cu(II)-PCUA		[^{64}Cu]$CuCl_2$	
Organ	6 hr	24hr	6 hr	24hr	6 hr	24hr	6 hr	24hr	6 hr	24hr
Blood	0.76 ± 0.10	2.12 ± 0.54	0.73 ± 0.03	1.77 ± 0.11	1.02 ± 0.35	1.62 ± 0.27	0.87 ± 0.10	1.49 ± 0.25	0.62 ± 0.17	0.71 ± 0.22
Carcass	0.66 ± 0.09	1.24 ± 0.21	0.63 ± 0.05	1.40 ± 0.17	0.60 ± 0.09	1.11 ± 0.17	0.61 ± 0.05	1.16 ± 0.35	0.63 ± 0.17	0.95 ± 0.20
Head	0.66 ± 0.04	1.46 ± 0.35	0.65 ± 0.04	1.44 ± 0.14	0.55 ± 0.05	1.11 ± 0.11	0.63 ± 0.08	1.13 ± 0.17	0.59 ± 0.02	2.60 ± 1.09
Heart	1.84 ± 0.40	5.62 ± 0.46	1.70 ± 0.22	3.99 ± 0.26	1.80 ± 0.15	3.56 ± 0.74	1.78 ± 0.19	3.55 ± 0.38	1.56 ± 0.15	1.73 ± 0.43
Intestines	3.93 ± 0.80	8.27 ± 0.89	7.24 ± 0.16	8.79 ± 1.00	4.21 ± 0.73	9.18 ± 2.13	5.84 ± 2.00	9.09 ± 4.09	8.14 ± 1.12	3.95 ± 1.86
Kidney	3.03 ± 0.33	8.75 ± 0.62	3.32 ± 0.19	7.61 ± 0.59	6.33 ± 0.90	6.16 ± 0.44	3.18 ± 0.17	5.10 ± 0.20	3.09 ± 0.41	3.03 ± 1.03
Liver	54.59 ± 8.15	37.77 ± 5.18	66.54 ± 9.31	31.00 ± 6.13	58.52 ± 3.70	30.48 ± 9.36	56.36 ± 1.65	30.69 ± 7.56	56.20 ± 0.45	11.32 ± 0.64
Lung	2.24 ± 0.67	8.90 ± 0.77	3.22 ± 0.72	4.79 ± 0.85	4.01 ± 0.59	6.23 ± 0.45	3.33 ± 0.41	5.74 ± 0.81	1.85 ± 0.25	2.27 ± 0.34
Muscle	0.23 ± 0.04	1.05 ± 0.40	0.44 ± 0.04	1.02 ± 0.14	0.43 ± 0.17	0.79 ± 0.22	0.44 ± 0.10	0.90 ±0.18	0.42 ± 0.13	0.25 ± 0.10
Spleen	0.31 ± 0.13	9.18 ± 0.53	2.03 ± 0.31	5.22 ± 0.90	2.02 ± 0.51	2.92 ± 0.93	2.30 ± 0.13	3.86 ± 0.38	1.73 ± 0.13	1.32 ± 0.11

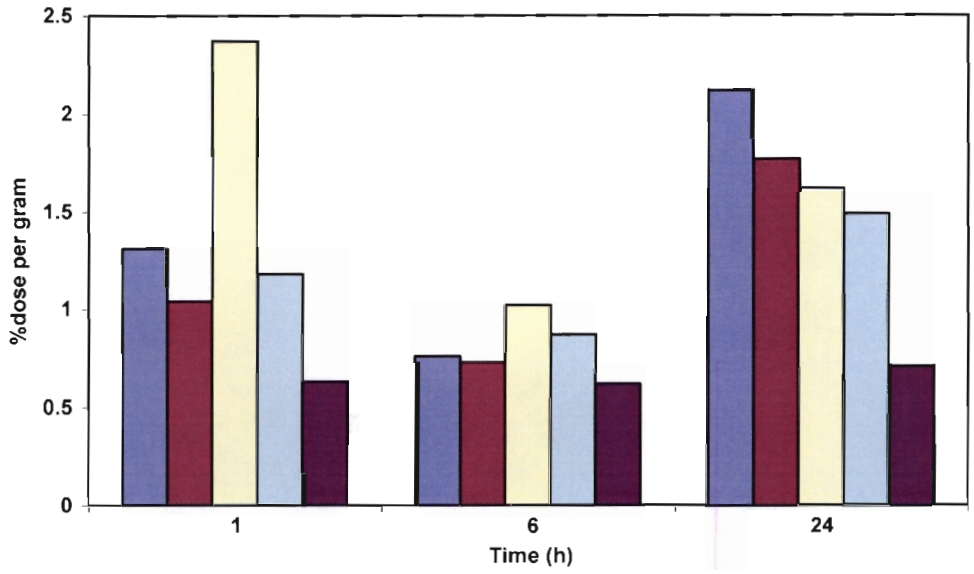

Figure 5.4(b): %dose per gram for [^{64}Cu]Cu(II)-PrDH, [^{64}Cu]Cu(II)-PrDM, [^{64}Cu]Cu(II)-PrDPr, [^{64}Cu]Cu(II)-PCUA and [^{64}Cu]$CuCl_2$ in blood 1, 6 and 24 hour post-injection.

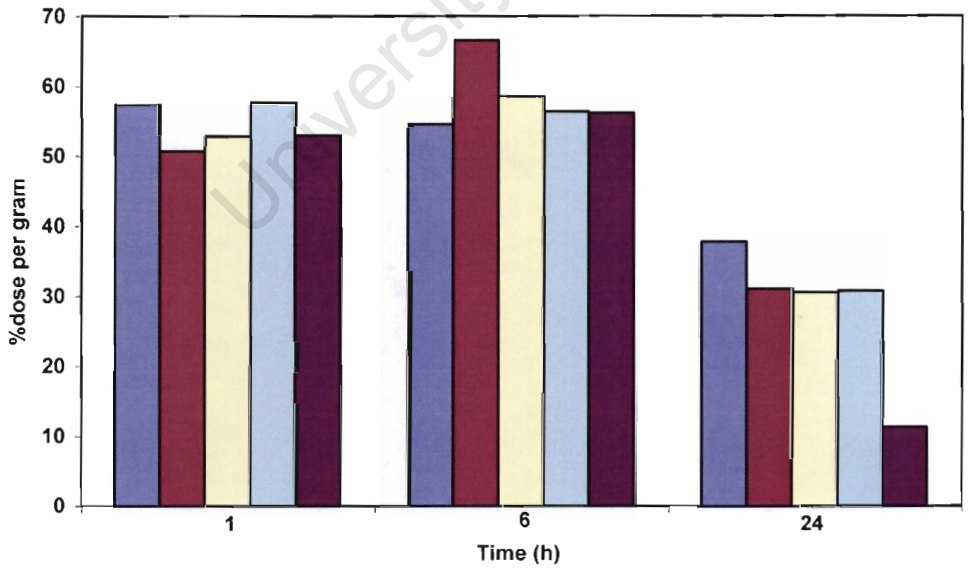

Figure 5.4(c): %dose per gram for [^{64}Cu]Cu(II)-PrDH, [^{64}Cu]Cu(II)-PrDM, [^{64}Cu]Cu(II)-PrDPr, [^{64}Cu]Cu(II)-PCUA and [^{64}Cu]$CuCl_2$ in liver 1, 6 and 24 hour post-injection.

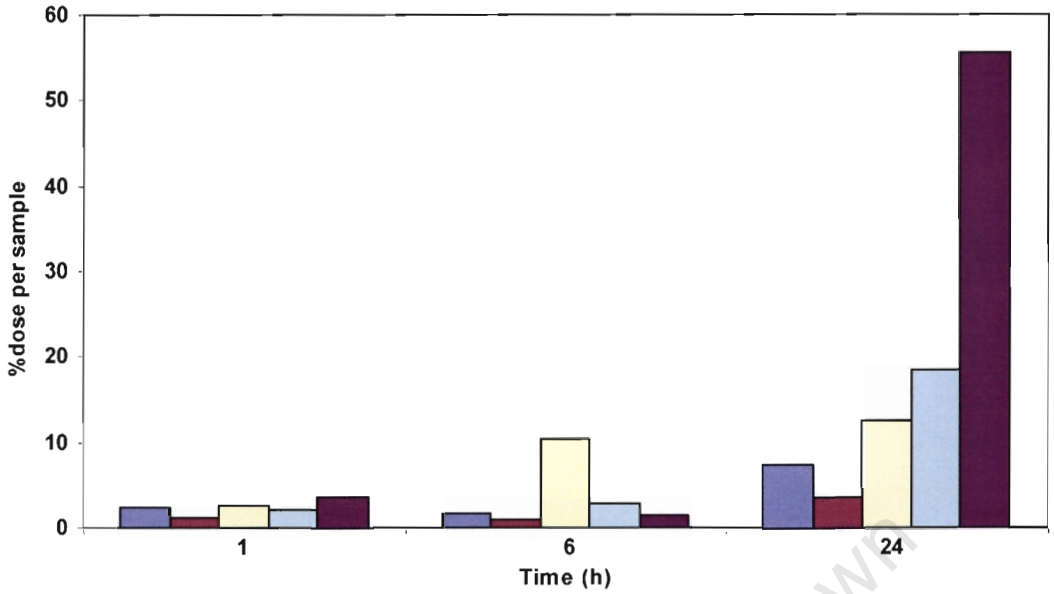

Figure 5.4(d): %dose per sample for ■ [^{64}Cu]Cu(II)-PrDH, ■ [^{64}Cu]Cu(II)-PrDM, ■ [^{64}Cu]Cu(II)-PrDPr, ■ [^{64}Cu]Cu(II)-PCUA and ■ [^{64}Cu]$CuCl_2$ in urine 1, 6 and 24 hour post-injection.

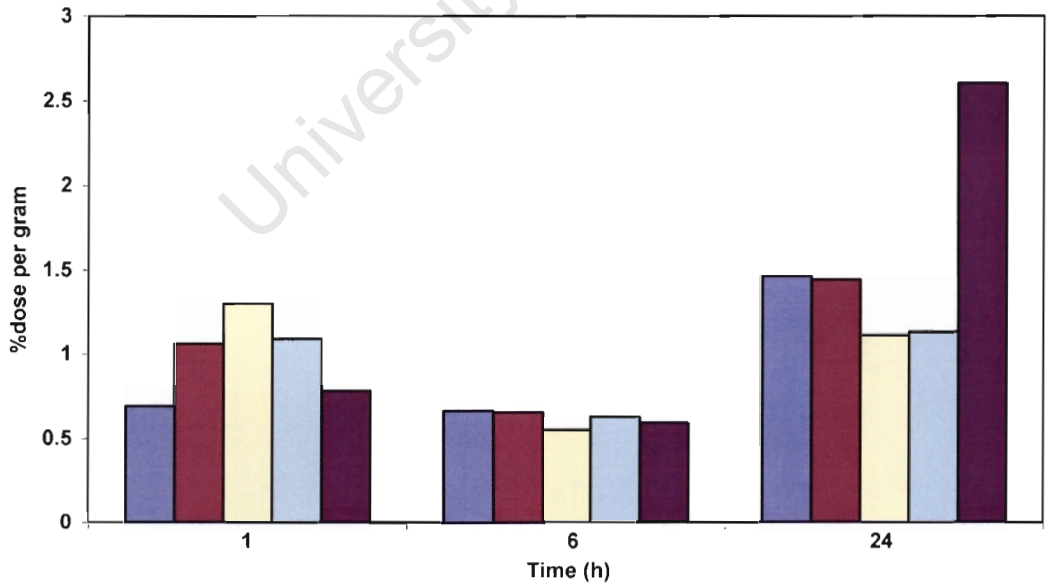

Figure 5.4(e): %dose per gram for ■ [^{64}Cu]Cu(II)-PrDH, ■ [^{64}Cu]Cu(II)-PrDM, ■ [^{64}Cu]Cu(II)-PrDPr, ■ [^{64}Cu]Cu(II)-PCUA and ■ [^{64}Cu]$CuCl_2$ in head 1, 6 and 24 hour post-injection.

At 6 and 24 hours post-injection redistribution of the [^{64}Cu]Cu(II) complexes' activity occurs resulting in activity accumulation in the major organs as shown in Table 5.2 and 5.3. The results show that there is slow clearance from the blood after 24 hours for all four complex systems. This is clearly seen in Figure 5.4(b) for which the %dose per gram in the blood for the [^{64}Cu]Cu(II) complexes is more than twice that of the control 24 hour post-injection. The liver shows high activity after 6 hours before activity slowly clears after 24 hours. This is demonstrated in Figure 5.4(c) which shows %dose per gram in the liver for [^{64}Cu]Cu(II) complexes including the control. The activity retention in the liver is in the range 33 – 40 %dose for these complexes 24 hour post-injection whereas that of the control is about 11 %dose. The clearance from the liver results in accumulation in other organs as shown in Table 5.2. The high activity uptake of these complexes in the intestines suggests excretion into the intestine via the biliary route. The activity uptake in the intestine is in the range 23 – 30 %dose 24 hour post-injection as compared to 12 – 19 %dose 6 hour post-injection. The kidney shows activity after 6 hours which is increased 24 hour post-injection. This suggests possible excretion of these complexes via the renal route. However, rapid clearance via the renal route is observed for the control experiments as shown in Figure 5.4(d) which shows %dose per sample in the urine for [^{64}Cu]Cu(II) complexes. Of interest in these results is the fact that [^{64}Cu]Cu(II)-PrDH, [^{64}Cu]Cu(II)-PrDM, [^{64}Cu]Cu(II)-PrDPr and [^{64}Cu]Cu(II)-PCUA complexes are retained in the body as compared to the control ([^{64}Cu]$CuCl_2$) which is rapidly excreted via the hepatobiliary and renal routes. The activity retention in the body for these systems is about 50 %dose compared to 20 %dose for the control.

There is also activity in other organs such as head, heart, lung, muscle and spleen as well as carcass. The relatively high accumulation of these complexes in these organs suggests that these complexes are more lipophilic as compared to the control. It was expected that the incorporation of the

pyridyl groups would enhance the lipophilicity of these complexes *in vivo*. Moreover, mono-positively charged and neutral species are formed at this pH thus increasing the uptake by tissues. Although, it was earlier observed from octanol-water partition and blood plasma model results that the PrDPr system is more lipophilic than PrDH, PrDM and PCUA, the results show that the [^{64}Cu]Cu(II) complexes of PrDH, PrDM, PrDPr and PCUA have more or less the same retention for these complexes *in vivo*. Therefore, it is important to compare bio-modelling (computer simulations) results with the experimental.

In contrast to earlier observations, under the same conditions, by Jackson and co-workers[41] for [^{64}Cu]Cu(II) complexes of polyamino ligands, the presently investigated complexes have been found to be retained significantly by most of the organs. The aforementioned polyamino systems were observed to be rapidly excreted, unchanged via the renal route because they were too hydrophilic and stable such that the complex was excreted intact in the urine. Nomkoko and co-workers[42,60,61] also studied poly(amine)amide ligands which showed that some of their systems were reasonably retained in the body under the same conditions. One of the noticeable features in their study and the present study is the fact that these systems have initial rapid and high uptake by the liver. The high uptake is to be expected in view of the fact that copper storing and metabolism occur in this organ. It has been suggested that the high uptake of [^{64}Cu]Cu(II) by the liver is due to transchelation of the radioisotope by albumin and histidine, and these *in vivo* proteins and l.m.w ligands bind Cu(II) strongly.[45]

Several studies have been performed by researchers using ^{64}Cu-labeled species for different purposes. Anderson and co-workers[45,62] have investigated thermodynamically and kinetically stable macrocyclic complexes with different formal charges as biofunctional chelators. All the complexes were observed to be rapidly cleared from circulation and positively charged complexes had higher liver uptake and slow clearance. The bio-distributions of these complexes were found to be dependent on both the macrocycle

backbone and the formal charge on the complex thus suggesting that there are potentially many factors that control clearance and also that charge plays an important role. Further investigations on macrocyclic ligands as biofunctional chelators were carried out for attaching copper radionuclides to biological molecules for diagnostic imaging and target of radiotherapy.[47,48] It was observed that positively charged ^{64}Cu complexes of the studied ligands exhibited rapid uptake in the liver and kidneys with slow clearance, whereas the negatively charged and neutral complexes cleared rapidly from all tissues. Packard and co-workers also reported similar renal elimination for negatively charged ^{64}Cu-labeled complexes.[49]

In summary, the presently studied ligands have shown relatively improved absorption and retention over 24 hours in the body. Such activity accumulation and retention in the body is encouraging and therefore merits evaluation of these copper chelating agents for possible use as anti-inflammatory agents. However, these complexes are unlikely to penetrate the blood-brain barrier in view of their octanol-water partition coefficients.

5.5 DERMAL ABSORPTION STUDIES

Although Cu(II) complexes, when administered orally and intravenously do increase available copper, it is difficult to move this coordinated metal ion through a series of body compartments without protein binding.[63] Of all the various classical ways of drug administration, percutaneous absorption offers the advantage of being a less painful method, and therefore, tolerable to patients. However, the percutaneous drug administration relies on the lipophilicity and molecular weight of the drug.

5.5.1 Introduction

The dermal absorption studies on mice were approved by the Research Animals Ethics Committee of the University of Cape Town (permission number 005/039). The procedures for carrying out these experiments were done in compliance with the guidelines mentioned in the bio-distribution studies (section 5.4). Preparations of solutions of Cu(II) complexes of PrDH, PrDM, PrDPr and PCUA were also done the same way as in bio-distribution studies.

5.5.2 Experimental

The experimental approach adopted for the dermal absorption experiments was similar to that of Scott and co-workers.[64] Solutions of Cu(II)(0.001 mol dm^{-3}) - L(0.003 mol dm^{-3}) complexes of PrDH, PrDM, PrDPr and PCUA were prepared the same as in the bio-distribution studies. A total of 20 female Balb/c mice of age 7-8 weeks weighing 20-23 grams were used in these experiments. Groups of four mice per ligand system including control were dermally dosed with 0.2 cm^3, [^{64}Cu]Cu(II)-L solution (containing 6.5 μg Cu), of 5 μCi activity on the enclosed skin of the anterior dorsal side of the test animals.

The application site was prepared by clipping an area of approximately 2 x 2 cm on the anterior dorsal side of all test animals 15 hours prior to dosing. Care was taken to avoid nicking the skin. The animals were anaesthetized with saline solution of ketamine/xylazine following clipping and a small tubing ring (1.2 cm diameter and 0.5 cm height) was fixed to their backs using cyanoacrylate adhesive. On application of dosing solutions to the enclosed skin, a polyethylene screen was glued to the top of the ring to prevent access to the application site. The mice were kept individually in cages. At the 24 hour post-dosing time point, groups of mice (four at a time) were sacrificed by carbon dioxide inhalation, aliquots of blood taken from the inferior vena

cava. Various samples (liver, kidney, ring with application site skin, etc) were removed and counted to determine distribution of radioactivity.

5.5.3 Results and discussion

The bio-distribution study results for the Cu(II) complexes of PrDH, PrDM, PrDPr and PCUA ligands indicate that these complexes survive *in vivo*. Based on these results, it was deemed necessary to perform dermal absorption experiments.

Table 5.4: %Dose unabsorbed and %dose absorbed for the dermal absorption study of [^{64}Cu]Cu(II) complexes of PrDH, PrDM, PrDPr and PCUA 24 hour post-dosing.

	%dose unabsorbed (ring + enclosed skin) and %dose absorbed (body + urine) in brackets for a given mouse 24 hour post-dosing				
[^{64}Cu]Cu(II) complexes of	Mouse 1	Mouse 2	Mouse 3	Mouse 4	Average %dose (per mouse)
PrDH	95.72 (4.28)	77.77 (22.23)	97.00 (3.00)	85.15 (14.85)	88.21 (11.09)
PrDM	95.06 (4.94)	62.89 (37.11)	89.93 (10.07)	82.75 (17.25)	82.66 (17.34)
PrDPr	82.32 (17.68)	64.05 (35.95)	55.42 (44.58)	79.94 (20.06)	70.43 (29.57)
PCUA	91.88 (8.12)	87.66 (22.34)	94.33 (5.67)	65.71 (34.39)	84.90 (15.10)
$CuCl_2$	77.57 (22.43)	87.55 (12.45)	95.66 (4.44)	73.63 (26.27)	83.60 (16.40)

The results for the dermal absorption studies are presented in Table 5.4. The most striking feature of these results is their high variability. The variation in absorption may be due to a number of reasons. After preparing the application site by clipping the area on the anterior dorsal side, the animal skin was not cleaned to remove the skin oil. This may have resulted in the applied dose being unable to 'wet' the skin. Another contributing factor could

be the glue which spread over the absorption area and also that the vehicle (water) may have not adequately induced absorption. The bio-distribution results of the dermally absorbed Cu(II) complexes of PrDH, PrDM, PrDPr and PCUA given in Table 5.5 differ from those of the bio-distribution by injection through the tail vein. This is not unusual in the sense that it is found that bio-distribution depends on a route of administration. Because of the variability of the results it is difficult to comment further on these results. What is clear however, is that the copper is more widely distributed in the body.

In conclusion, the presently studied ligands are dermally absorbed using water as a vehicle. The vehicles such as acetone would do better than water. This was demonstrated by Mathew and co-workers[65,66] who administered approximately 7% of 1,3-Diphenyl-1-triazene dermally on rats and mice over 72 hours and 25-60% of 2,2'-iminodiethanol on mice over a period of 48 hours.

Table 5.5: Bio-distribution of the dermally absorbed [^{64}Cu]Cu(II) complexes of PrDH, PrDM, PrDPr and PCUA (%dose per organ or gram, mean ± std.dev., n=4) 24 hour post-dosing.

	[^{64}Cu]Cu(II)-PrDH		[^{64}Cu]Cu(II)-PrDM		[^{64}Cu]Cu(II)-PrDPr		[^{64}Cu]Cu(II)-PCUA		[^{64}Cu]$CuCl_2$	
Organ	per organ	per gram	per organ	per gram	per organ	per gram	per organ	per gram	per organ	per gram
Blood	0.53 ± 0.05	0.45 ± 0.26	1.95 ± 0.12	1.28 ± 0.32	0.34 ± 0.02	0.32 ± 0.10	0.21 ± 0.03	0.19 ± 0.05	2.25 ± 0.08	1.50 ± 0.23
Carcass	2.60 ± 1.27	0.22 ± 0.11	27.81 ± 12.7	1.84 ± 0.81	9.69 ± 5.72	0.92 ± 0.56	10.50 ± 2.88	0.96 ± 0.27	14.20 ± 10.2	0.89 ± 0.59
Head	9.21 ± 8.17	3.35 ± 2.97	7.88 ± 2.78	2.29 ± 0.79	18.09 ± 8.30	6.90 ± 3.16	8.63 ± 2.66	3.08 ± 0.91	3.34 ± 0.67	1.02 ± 0.20
Heart	0.11 ± 0.02	1.14 ± 0.22	0.37 ± 0.02	2.01 ± 0.11	0.07 ± 0.01	0.62 ± 0.12	0.04 ± 0.02	0.48 ± 0.26	0.37 ± 0.07	2.10 ± 0.43
Intestines	13.29 ± 4.56	4.18 ± 1.73	12.11 ± 1.73	3.21 ± 0.52	15.99 ± 6.24	6.47 ± 2.47	10.83 ± 6.80	4.00 ± 2.59	20.92 ± 2.53	6.27 ± 0.70
Kidney	0.35 ± 0.05	1.02 ± 0.15	1.84 ± 0.10	3.51 ± 0.18	0.30 ± 0.03	0.94 ± 0.11	0.22 ± 0.17	0.85 ± 0.60	1.74 ± 0.27	3.61 ± 0.63
Liver	2.32 ± 0.44	2.00 ± 0.44	19.96 ± 1.27	12.47 ± 0.51	2.14 ± 0.35	2.04 ± 0.18	1.57 ± 1.00	1.52 ± 1.05	18.48 ± 3.16	13.80 ± 2.52
Lung	1.17 ± 0.02	0.89 ± 0.24	0.63 ± 0.04	3.96 ± 1.01	0.10 ± 0.03	0.63 ± 0.06	0.08 ± 0.06	0.81 ± 0.50	0.67 ± 0.12	3.04 ± 0.52
Muscle	0.06 ± 0.02	0.52 ± 0.31	0.56 ± 0.20	2.91 ± 0.16	0.02 ± 0.01	0.10 ± 0.03	0.04 ± 0.02	0.52 ±0.53	0.13 ± 0.03	0.58 ± 0.27
Spleen	0.07 ± 0.01	0.77 ± 0.70	0.21 ± 0.02	2.34 ± 0.58	0.03 ± 0.01	0.34 ± 0.13	0.06 ± 0.03	0.79 ± 0.42	0.19 ± 0.02	2.11 ± 0.35
Urine	71.29 ± 16.7		26.67 ± 5.58		53.27 ± 12.3		67.82 ± 9.39		37.80 ± 13.4	

References:

1. Faure H., Favier A., in; *Handbook of Metal-Ligand Interactions in Biological Fluids, Bioinorganic Chemistry*, (Ed) Berthon G., 1995, **2**, pp1163-1169 Marcel Decker, Inc., New York.
2. May P.M., Linder P.W., Williams D.R., *J. Chem. Soc. Dalton Trans.*, 1977, 588-595.
3. Perrin D.D., Agarwal R.P., in; *Metal ions in Biological Systems, Inorganic Drugs in Deficiency and Disease*, (Ed), Sigel H., 1973, **2**, pp168, Mercel Decker, Inc, New York
4. Williams D.R., *The Metals of Life*, 1971, Van Norstrand Reinhold, London.
5. Williams D.R., (Ed), *An Introduction to Bioinorganic Chemistry*, 1976, Charles C. Thomas Publisher, USA.
6. Jackson G.E., Kelly M.J., J. *Inorganic Chimica Acta*, 1988, **152**, 215-217.
7. Sorenson J.R.J., in; *Metal ions in Biological Systems, Inorganic Drugs in Deficiency and Disease*, (Ed), Sigel H., 1982, **14**, chpt.4., Mercel Decker, Inc, New York
8. May P.M., in; *Handbook of Metal-Ligand Interactions in Biological Fluids, Bioinorganic Chemistry*, (Ed) Berthon G., 1995, **2**, 1184-1194, Marcel Decker, Inc., New York.
9. Jackson G.E., in; *Handbook of Metal-Ligand Interactions in Biological Fluids, Bioinorganic Chemistry*, (Ed) Berthon G., 1995, **2**, 1228-1239, Marcel Decker, Inc., New York.
10. Brumas V., Alliey N., Berthon G., *J. Inorg. Biochem.* 1993, **52**, 287-296.
11. May P.M., Williams D.R., *FEBS Letters,* 1977, **78**(1), 134-138.
12. Jackson G.E., Kelly M.J., *J. Chem. Soc. Dalton Trans.*, 1989, 2429-2433.
13. Jackson G.E., Kelly M.J., *J. Chem. Soc. Dalton Trans.*, 1990, 1889-1893.
14. Gonzalez-Alvarez M., Alzuet G., Borras J., Agudo L.C., Montego-Bernado J.M., *J. Biol. Inorg. Chem.*, 2003, **8**, 112-120.
15. Fridovich I., *J. Biol. Chem.*, 1989, **264**(14), 7761-7764.
16. Fridovich I., *J. Expt. Chem.*, 1998, **201**, 1203-1209.

17. Pelmenschikov V., Siegbahn P.E.M., *Inorg. Chem.*, 2005, **44**(9), 3311-3320.
18. Kuo C.F., Mashino T., Fridovich I., *J. Biol. Chem.*, 1987, **262**, 4724-4727.
19. Kono Y., Fridovich I., *J. Biol. Chem.*, 1983, **258**, 13646-13648.
20. McCord J.M., *Science*, 1974, **185,** 529-531.
21. Steinkuhler C., Saporo O., Carri M.T., Nagel W., Marcocci L., Ciriolo M.R., Weser U., Rotilio G., *J. Biol. Chem.*, 1991, **266**, 24580-24587.
22. Petrovic N., Comi A., Ettinger M.J., *J. Biol. Chem.*, 1996, **271**, 28331-28334.
23. Patel R.N., Pandega K.B., *J. Inorg. Biochem.,* 1998, **72**, 109-114.
24. Auclair C., Voisin E., in; *CRC Handbook of Methods for Oxygen Radical research,* ed. R.A. Greenwald, 1985, CRC Press, Boca Raton, Fla.
25. Fridovich I., in; *CRC Handbook of Methods for Oxygen Radical research,* ed. R.A. Greenwald, 1985, CRC Press, Boca Raton, Fla.
26. Zhu H-L, Zheng L-M, Fu D-G, Huang X-Y, Wu M-F, Tang W-X, *J. Inorg. Biochem.,* 1998, **70**, 211-218.
27. Tabbi G., Driessen W.L., Reedijk J., Bonomo R.P., Veldman N., Spek A.L., *Inorg. Chem.,* 1997, **36**, 1168-1175.
28. Dillion C.T., Hambley T.W., Kennedy B.J., Lay P.A., Zhou Q., Davies N.M., Biffin J.R., Regtop H.L., *Chem. Res. Toxicol.,* 2003, **16,** 28-37.
29. Weder J.E., Dillion C.T., Hambley T.W., Kennedy B.J., Lay P.A., Zhou Q., Davies N.M., Biffin J.R., Regtop H.L., Davies N.M., *Coord. Chem. Rev.,* 2002, **232,** 95-126.
30. Mkhonta-Gama L., *PhD Thesis*, 1999, University of Cape Town, South Africa.
31. Nomkoko E.T., *PhD Thesis*, 2002, University of Cape Town, South Africa.
32. Poole S.K., Poole C.F., *J. Chrom., B*, 2003, **797,** 3-19.
33. Klopman G., Zhu H., *Mini-Rev. Med. Chem.,* 2005, **5,** 127-133.
34. Mailhot H., Peters R.H., *Envir. Sci. Tech.,* 1988, **22,** 1479-1488.
35. Essex J.W., Reynolds C.A., *J. Am. Chem. Soc.,* 1992, **114,** 3634-3639.
36. Beck M.J., Nagypal I., *Chemistry of Complex Equilibria,* 1990, Ellis Horwood Ltd, Chichester.

37. Anderson J.T., Schrader W., *Anal. Chem.,* 1999, **71,** 3610-3614.
38. Kong X.Q., Shea D., Gebreyes W.A., Xia Xin-Rui, *Anal. Chem.,* 2005, **77,** 1275-1281.
39. Leo A., Hansch C., Elkins D., *Chem. Rev.,* 1971, **71,** 525-554.
40. Pehourcq F., Matoga M., Jarry C., Bannwarth B., *J. Liq. Chrom. & Rel. Technol.,* 2001, **24**(14), 2177-2186.
41. Jackson G.E., Mkhomta-Gama L., Voye A., Kelly M., J. *Inorg. Biochem.,* 2000, **79**, 147-152.
42. Nomkoko T.E., Jackson G.E., Nakani B., *Inorg. Chem Comm.,* 2003, **6,** 335-338.
43. Sri-Aran M., Mathias C.J., Lim J.K., Green M.A., *Nucl. Med. & Bio.* 1998, **25,** 107-110.
44. Ackerman L.J., West D.X., Mathias C.J., Green M.A., *Nucl. Med. & Bio.* 1999, **26**, 551-554.
45. Jones-Wilson T.M., Deal K.A., Anderson C.J., McCarthy D.W., Kovac Z., Motekaitis R.J., Sherry A.D., Martell A.E., Welch M.J., *Nucl. Med. & Bio.* 1998, **25**, 523-530.
46. Rothwell J.A., Day A.J., Morgan M.R.A., *J. Agric. Food Chem.,* 2005, **53,** 4355-4360.
47. Sun X., Wuest M., Kovacs Z., Sherry A.D., Motekaitis R., Wang Z., Martell A.E., Welch M.J., Anderson C.J., *J. Biol. Inorg. Chem.,* 2003, **8,** 217-225.
48. Sun X., Wuest M., Weisman G.R., Wong E.H., Reed D.P., Boswell C.A., Motekaitis R., Martell A.E., Welch M.J., Anderson C.J., *J. Med. Chem.*, 2002, **45**, 469-477.
49. Packard A.B., Kronauge J.F., Day P.J., Treves S.T., *Nucl. Med. & Bio.* 1998, **25**, 531-537.
50. Delves H.T., in; *Biological role of copper*, 1980, pp5-22, Ciba Foundation Symposium 79, Excerpta Medica, Armsterdam.
51. Gulumian M., Hancock R.D., Rollin H.B., in; *Handbook of Metal-Ligand Interactions in Biological Fluids, Bioinorganic Chemistry*, (Ed) Berthon G., 1995, **1**, 93-107, Marcel Decker, Inc., New York.
52. Lewis A.J., *Agents Actions*, 1984, **15**, 513.

53. Bremner I., in; *Biological role of copper*, 1980, pp23-48, Ciba Foundation Symposium 79, Excerpta Medica, Armsterdam.
54. Sorenson J.R.J., *Prog. Med. Chem.*, 1989, **26**, 437-547.
55. Linder M.C., Wooten L., Cerveza P., Cotton S., Shulze R., Lomeli N., *Am. J. Clin. Nutr.,* 1998, **67**(suppl), 965S-971S.
56. Turnlund J.R., Keyes W.R., Peiffer G.L., Scott K.C., *Am. J. Clin. Nutr.,* 1998, **67**, 1219-1225.
57. Wapnir R.A., *Am. J. Clin. Nutr.,* 1998, **67**(suppl), 1054S-1060S.
58. Linder M.C., Hazegh-Azam M., *Am. J. Clin. Nutr.,* 1996, **63**(suppl), 797S-811S.
59. Harford C., Sarkar B., in; *Handbook of Metal-Ligand Interactions in Biological Fluids, Bioinorganic Chemistry*, (Ed) Berthon G., 1995, **1**, 405-410, Marcel Decker, Inc., New York.
60. Nomkoko E.T., Jackson G.E., Nakani B.S., *J. Chem. Soc. Dalton Trans.*, 2004, 1432-1440.
61. Nomkoko E.T., Jackson G.E., Nakani B.S., Werner K.A., Zeevaart J.R., *J. Chem. Soc. Dalton Trans.*, 2004, 741-749.
62. Cutler C.S., Wuest M., Anderson C.J., Reichert D.E., Sun Y., Martell A.E., Welch M.J. *Nucl. Med. & Bio.* 2000, **27**, 375-380.
63. Jackson G.E., May P.M., Williams D.R., *J. Inorg. Nucl. Chem.,* 1978, **40**, 1227-1234.
64. Scott W.T., Waechter J.M., Rick D.L., Mendrala A.L., *Food and Chem. Toxicology,* 2000, **38,** 1043-1051.
65. Mathews J.M., De Costa K.S., *Drug Metabolism & Disposition,* 1999, **27,** 1499-1504.
66. Mathews J.M., Garner C.E., Black S.L., Matthews H.B., *Xenobiotica*, 1997, **27**, 733-746.

CHAPTER SIX

GENERAL DISCUSSION AND CONCLUSION

6. GENERAL DISCUSSION AND CONCLUSION

The role of Cu(II) in biological systems and processes is well known.[1,2] The elevation of Cu(II) complex species in plasma and synovial fluids of rheumatoid arthritis patients is known.[3,4] It was also found that a number of Cu(II) chelates exhibit anti-inflammatory activity. Therefore, several studies have been carried out in designing chemically stable, Cu(II) complexes, for use as anti-arthritic agents.[5,6,7] The present study has been designed to develop Cu(II) complexes for their end use as anti-inflammatory human pharmaceutical agents. However, the suitable ligand must be able to complex Cu(II) and enhance the transportation across a bio-membrane.

The present study investigated the solution equilibria of H^+, Cu^{2+}, Ni^{2+}, Zn^{2+} and Ca^{2+} with PrDH, PrDM and PrDPr ligands at 25 ^oC and in 0.15 mol dm^{-3} $Cl^-(Na^+)$ using glass electrode potentiometry. These ligands have been found to take up to three protons in the pH range 2-11. The observed protonation constants agree with those of their analogues and the protonation constants of PrDH agree with those reported in the literature.[8] On the basis of the complex formation and deprotonation functions, the models which best describe the solution thermodynamics of the M(II)-L systems were chosen. Moreover, the reasonably low standard deviations in $\log\beta_{pqr}$'s and Hamilton R-factors further confirm the validity of the models used in data analysis. The Cu(II) complexes showed general formation of MLH, ML, MLH_{-1} and MLH_{-2} species. The formation equilibria for Ni(II), Zn(II) and Ca(II) show that these metal ions form relatively stable complexes with PrDH, PrDM and PrDPr However, it is observed that Cu(II) forms more stable complexes than these metal ions. It is also observed that the stability of the M(II)-L complexes is in the order M(II)-PrDH > M(II)-PrDM > M(II)-PrDPr. This is due to the different basicities of the terminal groups which is in the order $-NH_2$ > $-N(CH_3)_2$ > -Py. The calculated selectivity factors indicate that the studied ligands are more selective for Cu(II) by 3-11 orders of magnitude relative to Ni(II), Zn(II) and Ca(II).

The elucidation of the chemical structures of Cu(II) complexes of these ligands have been determined by using NMR, IR and UV-visible spectroscopy as well as molecular mechanics calculations. The results of the protonation constants determined by NMR study are in good agreement with values obtained from potentiometric studies. The results show that the central pyridyl nitrogen and amide nitrogen(s) as well as the terminal amino/pyridyl groups coordinate to the metal ion in solution. This is indicated by the broadening of the proton resonances and shifting of the NMR signal arising from protons attached to neighbouring carbons upon complexation by Cu(II). The results from the IR study show a band due to the asymmetric carbonyl stretching vibration in these ligands. This band broadens and almost disappears at higher pH upon complexation by Cu(II). The involvement of the amide nitrogen in the coordination sphere is shown by the increase in intensity and shifting of the bands at low frequencies. The UV-visible study gave smooth deconvoluted spectra for the individual species of the Cu(II)-PrDH, Cu(II)-PrDM and Cu(II)-PrDPr systems in support of the potentiometric results. The three studied ligands form tetragonally distorted octahedral MLH_{-1} and MLH_{-2} species with Cu(II) due to the utilization of the ligand field Jahn-Teller effect. It is indeed worth noting that the incorporation of the central pyridyl nitrogen from the pyridine-2,6-dicarboxamide moiety in these ligands which is the first one to be coordinated to the metal ion, induces amide coordination. Molecular mechanics was used to calculate the strain energies (internal) of the different possible geometries for the complexes. A comparison of these energies was used to rationalise the different stabilities of these complexes.

Zn(II) and Ca(II) ions, being present in blood plasma in large concentrations are regarded as potential competitors of Cu(II) *in vivo*. The results of the blood plasma simulations show that these metal ions are good competitors of Cu(II) for PrDH, PrDM and PCUA in blood plasma whereas PrDPr is relatively selective for Cu(II). In fact, the selectivity and mobilizing ability of these

ligands is in the order PrDPr > PCUA > PrDH > PrDM. The results also show that these ligands are better mobilizers of Cu(II) as compared to the previously studied pentadentate donor ligand.[7] The superoxide mimetic activity studies show that the ligand system with low Cu(II) mobilizing ability has relatively high SOD mimetic activity. The relatively low IC_{50} of the Cu(II)-PrDM system can be interpreted in terms of the possible replacement of coordinated water molecule by the superoxide anion radical. The presence of the protonated ligand's sites of the MLH_{-1} species should also contribute to the dismutation of the superoxide anion radical through hydrogen bonding. The ligands PrDH, PrDM, PrDPr and PCUA were designed with the hope that the dominant Cu(II) complex at pH 7.4 would be the neutral $[CuLH_{-2}]^0$ species. However, the species distribution diagrams from the potentiometric results show that the negatively charged MLH_{-1} species dominates at the physiological pH (7.4) except for the Cu(II)-PrDPr system which forms MLH_{-2} at this pH. In general, methyl and aryl groups are known to increase the lipophilicity of molecules. Having this fact in mind, the present ligands were designed. The octanol-water partition coefficients ($logP_{oct/aq}$) were determined as a measure of hydrophobicity. It is observed that 0.43, 0.83, 2.9 and 19% of Cu(II)-PrDH, Cu(II)-PrDM, Cu(II)-PCUA and Cu(II)-PrDPr complexes are extracted into the organic phase of the octanol-water mixture used as a bio-phase model. It is indeed observed that the ligand system with bulky groups as well as forming neutral complex species has an enhanced extraction into the organic phase.

Based on the aforementioned *in vitro* results, it was necessary to perform biodistribution and dermal absorption experiments. Since the body is a dynamic system the biodistribution was measured as a function of time. The biodistribution results revealed an initial rapid clearance of $[^{64}Cu]$Cu(II)-PrDH, $[^{64}Cu]$Cu(II)-PrDM, $[^{64}Cu]$Cu(II)-PCUA and $[^{64}Cu]$Cu(II)-PrDPr complexes from the blood and initial rapid and high uptake by the liver. The high uptake in the liver is due to the fact that copper storing and metabolism occur in this organ. In contrast to earlier observations, under the same conditions, by

Jackson and co-workers[6] for [^{64}Cu]Cu(II) complexes of polyamino ligands, the presently investigated complexes were found to be significantly retained by most of the organs. The aforementioned polyamino systems were observed to be rapidly excreted unchanged via the renal route because they were too hydrophilic and stable such that the complex was excreted intact in the urine. Nomkoko and co-workers[7,9,10] also studied poly(amine)amide ligands which showed that some of their systems were reasonably retained in the body under the same conditions. Indeed the presently studied ligands have shown relatively improved absorption and retention over 24 hours in the body. Such activity accumulation and retention in the body is encouraging and therefore merits evaluation of these copper chelating agents for possible use as anti-inflammatory agents. Dermal absorption results also showed that at least 5 %dose of the applied dose on the enclosed skin was absorbed over a period of 24 hours. Therefore, these ligands' systems seem to be dermally absorbed using water as a vehicle.

The overall results in this study are encouraging and merit further evaluation for the use of Cu(II) complexes in chemotherapy and diagnosis. It is hoped that this study has contributed to the knowledge and understanding of some factors involved in the development of copper chelating agents for the alleviation of inflammation associated with RA. The proposed ligands for future studies are shown in Figure 6.1.

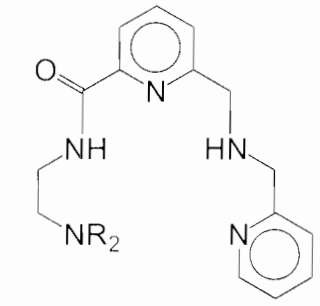

R = -H, -CH3

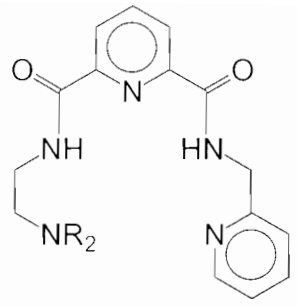

R = -H, -CH3

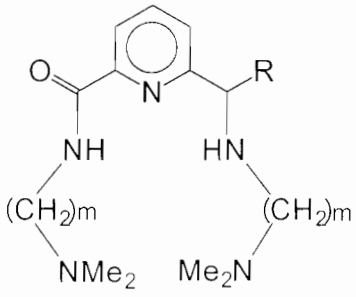

m = 2,3

R = -COOH,-CONHMe,

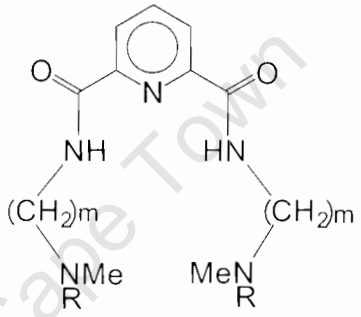

R = biofunctional group

Figure 6.1: Schematic representation of structures of ligands for future studies.

References:

1. Reichert D.E., Lewis J.S., Anderson C.J., *Coord. Chem. Rev.,* 1999, **184**, 3-66.
2. Weder J.E., Dillion C.T., Hambley T.W., Kennedy B.J., Lay P.A., Biffin J.R., Regtop H.L., Davies N.M., *Coord. Chem. Rev.,* 2002, **232**, 95-126.
3. Sorenson J.R.J., in; *Metal ions in biological systems, inorganic drugs in deficiency and disease*. (Ed) Sigel H., Marcel Dekker, Inc., 1982, **14**, pp77-113.
4. Bonta I.L., Parnham M.J., Vincent J.E., Bragt P.C., in: Ellis G.P., West G.B. (Eds), *Prog. Med. Chem.*, 1980, **17**, 186-260.
5. Jackson G.E., Nakani B.S., *J. Chem. Soc. Dalton Trans.*, 1996, 1373-1377.
6. Jackson G.E., Mkhomta-Gama L., Voye A., Kelly M., *J. Inorg. Biochem.,* 2000, **79**, 147-152.
7. Nomkoko E.T., Jackson G.E., Nakani B.S., *Inorg. Chem. Comm.,* 2003, **6,** 335-338.
8. Motekaitis R.J., Martell A.E., *Inorg. Chem.*, 1988, **27**, 2718 – 2724.
9. Nomkoko E.T., Jackson G.E., Nakani B.S., *J. Chem. Soc. Dalton Trans.*, 2004, 1432-1440.
10. Nomkoko E.T., Jackson G.E., Nakani B.S., Werner K.A., Zeevaart J.R., *J. Chem. Soc. Dalton Trans.*, 2004, 741-749.

APPENDIX

LIST OF FIGURES

LIST OF TABLES